

A-20 Chimera

Austere Field Light Attack Aircraft
Delft University of Technology













A-20 Chimera

2021 Design Competition - Team Aircraft Design - Undergraduate Team

by

Delft University of Technology

Group Chimera

Name	Email	AIAA #	Signature
Jarem M. Hinsenveld	j.m.hinsenveld@gmail.com	1230452	
Milan Jansens	milan_jansens@hotmail.com	1230454	
Mitchell T. de Keijzer	m.t.dekeijzer@student.tudelft.nl	1240993	
Felix A. Kuhnert	felix.kuhnert@outlook.de	1207102	
Luuk van der Mark	l.vandermark@student.tudelft.nl	1240988	
Amirsadra Moghaddam	sadramoghaddam@gmail.com	1230392	
Sebastiaan P. van Oosterhout	sebastiaan_paul@hotmail.com	1230453	
Tom H. Y. Tom	tomtomtiger08@gmail.com	1241010	
Douwe G. Velds	douwevelds@gmail.com	1230451	
Yuki Watabe	y.watabe@student.tudelft.nl	1230455	

Project Advisers

Name	Email
Dr. Ir. R. Vos	R.Vos@tudelft.nl
Dr. S. J. de Vet	S.J.deVet@tudelft.nl
G. B. L. Tosti Balducci	G.B.L.TostiBalducci@tudelft.nl



Acknowledgement

This report is the result of the education we have received in the Bachelor courses at the Aerospace Engineering Faculty of the Delft University of Technology. As a group we have learned a lot during our years as Bachelor students and will learn much more on the path we will take after this report. Therefore, we would like to thank every employee of the Aerospace Engineering Faculty whom have made this Bachelor program available.

A special thank goes out to Dr. Ir. Roelof Vos, Dr. Sebastiaan J. de Vet and Giorgio B. L. Tosti Balducci for their help and guidance throughout the process of designing this aircraft. With their insights and feedback, they helped us bring this design to a higher level. They also provided us with guidance where ever needed during the design phase.

We also want to thank Maj. ret. Richard *Hiker* Helsdingen, former F-16 pilot of the Royal Netherlands Air Force and former head of the European F-16 Weapons school. Furthermore, we want to thank Maj. Pascal *Smiley* Smaal, current F-35 pilot of the Royal Netherlands Air Force. Both helped us tremendously with their insight in the pilot's view on flying fighter aircraft and their experience from numerous combat missions. They aided us in making choices based on real-life feedback, which we believe was a great help to our project.

Group *Chimera*

Delft, February 2021

Contents

List of Symbols	1	6 Fuselage Design	30
Executive Overview	2	6.1 Design Overview	30
1 Introduction	4	6.2 Cockpit	30
2 Requirements, Missions and Threats	5	6.3 Fuselage	32
2.1 Key and Driving Requirement	5	7 Wing Design	34
2.2 Flight Profile	6	7.1 Design Overview	34
2.3 Mission analysis	6	7.2 Design Approach	34
2.4 Threat Analysis	8	8 Empennage Design	39
2.5 Mission Environment and Encountered Threats	10	8.1 Design Overview	39
2.6 Missions, Armament and Counter Mea- sures	10	8.2 Design Approach	40
3 Market Analysis	13	8.3 Sensitivity Analysis	43
3.1 Stakeholder list	13	8.4 Verification and Validation	43
3.2 Market Size	14	9 Propulsion Unit Design	46
3.3 Competition	14	9.1 Design Overview	46
3.4 Segment Analysis	15	9.2 Design Approach	46
4 Design Approach and Concept Trade-off	17	10 Landing Gear Design	48
4.1 Design Approach	17	10.1 Design Overview	48
4.2 Trade-Off	21	10.2 Design Approach	48
4.3 Trade-Off Result	23	10.3 Sensitivity Analysis	49
5 Weight Estimations	26	11 Additional Subsystems	50
5.1 Class I Weight Estimation	26	11.1 Fuel System	50
5.2 Class II Weight Estimation	26	11.2 Hydraulic System	51
5.3 Mass Moment of Inertia	28	11.3 Electrical System	51
5.4 Verification and Validation	28	11.4 Environmental Control System	52
		11.5 Avionics and Sensors	53
		12 Drag Analysis	55
		12.1 First Order Drag Analysis	55

12.2	Second Order Drag Analysis	55	14.5	Verification and Validation	75
12.3	Results	56	15	Operations & Logistics Plan	77
12.4	Verification and Validation	57	15.1	Operations	77
13	Stability and Control Analysis	59	15.2	Logistics Plan	77
13.1	Longitudinal Static Stability	60	16	Production Quantity and Cost Analysis	79
13.2	Lateral Static Stability	60	16.1	Production Quantity	79
13.3	Longitudinal Dynamic Stability.	61	16.2	Cost Analysis	80
13.4	Lateral Dynamic Stability	63	17	Next Design Steps	83
13.5	PID Controller for Aperiodic Spiral.	66	17.1	Work Flow Diagram for future steps	83
13.6	Control Derivatives due to Elevator, Aileron and Rudder.	68	18	Compliance to User Requirements & Future Recommendations	85
13.7	Sensitivity Analysis	69	18.1	User Requirements Compliance Table	85
13.8	Verification and Validation	69	18.2	Future Recommendations.	86
14	Aircraft Performance Analysis	70	19	Conclusion	87
14.1	Range Diagrams	70	References	88	
14.2	Gust and Manoeuvre Load Diagram	71	Appendix A	91	
14.3	Specific Excess Power Diagrams	73			
14.4	Turn Rate Diagrams	74			

List of Symbols

Abbreviations

AA	Anti-Aircraft
AR	Aspect Ratio
c.g.	Centre of Gravity
CBR	California Bearing Ratio
CD	Cockpit Distributor
CMF	Composite Metal Foam
CPI	Consumer Price Index
DAPCA	Development And Production Costs Of Aircraft
ECS	Environmental Control System
EHA	Electro-Hydrostatic Actuation
EHA-CPU	EHA Processor
FCC	Flight Control Computer
FLIR	Forward-Looking Infrared
HUD	Head-up display
LiDAR	Light Detection and Ranging
MAC	Mean Aerodynamic Chord
MANPADS	MAN-Portable Air-Defense Systems
MAW	Missile Approach Warning
MMOI	Mass Moment of Inertia
MNS	Mission Need Statement
MTOW	Maximum Take Off Weight
OEW	Operational Empty Weight
PD	Power Delivery system
PID	Proportional Integral Derivative
POS	Project Objective Statement
QDF	Quantity Discount Factor
RFP	Request for Proposal
ROI	Return On Investment

S.M.	Stick fixed stability margin
S/G	Starter-Generator
SAM	Surface-to-Air Missile
TBO	Time Between Overhauls
TRL	Technology Readiness Level

Greek symbol

δ_a	Aileron deflection	[°]
δ_a	Aileron deflection	[°]
δ_{ac}	Actuator commanded aileron deflection	[°]
Γ	Dihedral	[°]
λ	Taper ratio	[-]
$\Lambda_{\text{hinge line}}$	Sweep angle of hinge line	[°]
$\Lambda_{c/4}$	Quarter-chord sweep angle	[°]
ϕ	Roll angle	[°]
τ	Time constant	[s ⁻¹]
τ_a	Aileron efficiency	[-]

Nomenclature

T_2	Time to double	[s]
b_1	Inboard span position	[m]
b_2	Outboard span position	[m]
\bar{c}	MAC length	[m]
$c(y)$	Chord function, describing the chord length as a function of span, y	[m]
C_{fe}	Skin friction coefficient	[-]
C_{D_0}	Zero lift drag coefficient	[-]
C_{d_0}	Zero drag coefficient of the airfoil	[-]
C_{l_β}	Rolling moment due to sideslip derivative	[rad ⁻¹]
$C_{L_{\alpha_{A-h}}}$	Lift rate coefficient aircraft less tail	[-]

$C_{L_{\alpha_h}}$	Lift rate coefficient horizontal tail	[-]	$C_{y_{\delta_a}}$	Sideforce due to aileron deflection	[-]
$C_{l_{\delta_\alpha}}$	Control derivative with respect to δ_α , describing rolling moment	[-]	$C_{y_{\delta_r}}$	Sideforce due to rudder deflection	[-]
$C_{l_{\delta_a}}$	Rolling moment due to aileron deflection	[-]	C_{y_p}	Sideforce due to roll rate derivative	[rad ⁻¹]
$C_{l_{\delta_r}}$	Rolling moment due to rudder deflection	[-]	C_{y_r}	Sideforce due to yaw rate derivative	[rad ⁻¹]
$C_{L_{A-h}}$	Lift coefficient of the aircraft less tail	[-]	C_{Z_u}	Lift coefficient due to the airspeed	[-]
C_{L_h}	Lift coefficient of the horizontal tail	[-]	e	Oswald efficiency factor	[-]
$C_{L_{max}}$	Maximum lift coefficient	[-]	l_h	Tail length	[m]
C_{l_p}	Rolling moment due to roll rate derivative	[rad ⁻¹]	M	Mach number	[-]
C_{l_r}	Rolling moment due to yaw rate derivative	[rad ⁻¹]	m	Mass	[kg]
C_L	Lift coefficient	[-]	p	Roll rate	[°/s]
$C_{m_{ac}}$	Moment coefficient about the aerodynamic center	[-]	P_s	Specific Excess Power	[W/N]
C_{m_u}	Pitching moment coefficient due to the airspeed	[-]	S	Surface area of the wing	[m ²]
C_{n_β}	Yawing moment due to sideslip derivative	[rad ⁻¹]	S_h	Surface area of the horizontal tail	[m ²]
$C_{n_{\delta_a}}$	Yawing moment due to aileron deflection	[-]	S_{wf}	Wing area effected by flaps	[m ²]
$C_{n_{\delta_r}}$	Yawing moment due to rudder deflection	[-]	t	Time	[s]
C_{n_p}	Yawing moment due to roll rate derivative	[rad ⁻¹]	$\left(\frac{V_h}{V}\right)$	Tail/wing speed ratio	[-]
C_{n_r}	Yawing moment due to yaw rate derivative	[rad ⁻¹]	W_E	Empty Weight	[-]
C_{X_α}	Drag coefficient due to the angle of attack	[-]	W_F	Fuel Weight	[-]
C_{X_u}	Drag coefficient due to the airspeed	[-]	W_{OE}	Operational Empty Weight	[-]
C_{y_β}	Sideforce due to sideslip derivative	[rad ⁻¹]	W_{TO}	Take off weight	[N]
			\bar{x}_{ac}	Aerodynamic center position relative to the MAC	[%MAC]
			x_{cg}	Longitudinal position of the center of gravity	[m]
			x_{LEMAC}	Longitudinal position of the leading edge MAC	[m]
			x_{LEMAC}	Position of the leading edge of the MAC	[m]

Executive Summary

The A-20 *Chimera* shall perform Close Air Support, or CAS, reconnaissance, and armed patrol missions. During those missions, encountered threats include handheld weapons, anti aircraft guns, and shoulder launched missiles like heat-seeking missiles. A market analysis indicates that 830 units can be sold, leading to a profit of \$830 million with a selling price of \$11.0 million per aircraft.

The aircraft was designed by first performing a Class I sizing for four concept aircraft. A trade-off was performed, and all four concepts were merged into one final concept. This entered the Class II sizing process. From the Class II weight estimation, an Operational Empty Weight, OEW, of 7.0 t, and a Maximum Take Off Weight, MTOW, of 13.1 t was estimated.

This weight was used to size the aircraft, taking into account the required payload of 3 000 lbs, and austere field performance. The wing has an Aspect Ratio, AR, of 7, a quarter-chord sweep angle of 0° , a taper ratio of 0.4, and a dihedral of 3° . The wing span is 18.5 m, the Mean Aerodynamic Chord, MAC, is 2.8 m, and the wing area is 49 m^2 . The aircraft features two engines, which generate 21 kN of thrust each. The engines are placed high on the fuselage between the wing and tail. The fuselage is 15 m long, and was sized to fit the two crew members, and two integrated guns. The pilots are protected from incoming fire by a Composite Metal Foam structure around the cockpit. The aircraft features an H-tail, which was sized using a static stability analysis. The horizontal tail is unswept and untapered. Its surface is 10.3 m^2 , with a span of 7.7 m. The two vertical tails have a quarter-chord sweep angle of 20° , a taper ratio of 0.5, and a span of 2.7 m. This results in a surface area of 2.7 m^2 for each vertical tail. The landing gear was sized to accommodate a 13° pitch at a bank angle of 8° at take off and landing. The main landing gear is stored in a wing fairing at the leading edge, and the nose landing gear is stored in the fuselage. Wheels were sized to meet the California Bearing Ratio, CBR, 5 requirement. All electrical, and control systems were designed with redundancy in mind. The airframe achieves level 1 handling qualities for the Short Period Motion, Phugoid, Dutch Roll and Aperiodic Roll in all flight conditions. For the spiral in loiter and landing conditions it does not, hence a Proportional Integral Derivative, PID, Controller was designed.

The airplane has a modular design for easy maintenance and transport. It shall enter service in 2025. [Figure 1](#) gives an impression of the aircraft design.



Figure 1: The A-20 *Chimera* on a mission

1 Introduction

As warfare has changed from symmetrical to mostly asymmetrical, also the utilization of available aircraft has changed significantly. This results in an A-10 *Thunderbolt* performing CAS missions against terrorist groups, while it was originally designed to assault heavily armored vehicles. The F-35, which is currently one of the most advanced aircraft, is used for the same type of CAS missions. These aircraft are overdesigned for the task at hand. The A-20 *Chimera*, which is presented in this report, aims to combine everything that works on the currently used aircraft. In order to achieve this goal, a mission need statement, MNS, and project objective statement, POS, were set-up to solve the need of the stakeholder.

MNS: To provide close air support to ground forces from short, front-line, austere fields at short notice, while being affordable.

POS: To design an affordable light attack aircraft, within 10 weeks by 10 students, which can operate from short austere fields close to the front lines.

The purpose of this report is to present the reader with the process followed for the conceptual design of the A-20 *Chimera*. The report is build up in three main parts. First, in [chapter 2](#) the mission obtained from the request for proposal, RFP, is analyzed. This discussion entails a thorough threat analysis, combined with a function breakdown of the aircraft system and its key and driving requirements. Afterwards, a market analysis is performed in [chapter 3](#) to examine the feasibility of a light attack aircraft on the market. After this, the design approach to the aircraft is discussed in [chapter 4](#), followed by a trade-off between the obtained concepts. These three chapters conclude the first part of the report.

[Chapter 5](#) discusses both the first and second order weight estimations, combined with a technical drawing of the obtained aircraft. Followed by a more detailed discussion on the design of the subsystems presented in [chapter 6](#) to [chapter 11](#). Then the detailed drag analysis, [chapter 12](#), stability & control, [chapter 13](#), and performance, [chapter 14](#), are executed. These chapters present the aerodynamic characteristics, handling, and performance qualities, which concludes the second part.

The final part of the report starts with a discussion on the operations and logistics of the aircraft in [chapter 15](#). The results of the market analysis are used in [chapter 16](#) to get a selling quantity and breakdown for the cost. This is followed by [chapter 17](#), where the phases after this project to realize the aircraft are described. The final chapter, [chapter 18](#), shows the reader the compliance of the aircraft to the user requirements set at the beginning of the report and presents the reader with a number of future recommendations.

2 Requirements, Missions and Threats

In this chapter, the driving requirements for the design of the A-20 Chimera are listed. A mission and threat analysis was performed in order to get a better understanding of the types of missions and threats the aircraft will be able to do or encounter during operations. To get an overview, past and possible future war scenarios are examined. These scenarios include past and present anti-terror and anti-drug-cartel missions, the Gulf war, the Yugoslavia conflict, as well as the Vietnam war. From those missions and threats, functions that the aircraft has to fulfill were derived and some first design choices were made

2.1. Key and Driving Requirement

In this section, only the driving requirements are discussed, which resulted from the RFP from the American Institute of Aeronautics and Astronautics, AIAA. These can be found in [Table 2.1](#), the requirements were used to set the boundaries of the design space.

Table 2.1: List of user requirements for the Light Attack Aircraft given by the AIAA

Requirement ID	Description
Payload	
LAA-PAY-WTH-1.1	The aircraft shall be able to carry 3 000 lbs of armament.
Performance	
LAA-PER-SER-1.1	The aircraft shall have a service ceiling of at least 30 000 ft.
LAA-PER-FEM-1.1	The aircraft shall have a ferry range of at least 900 nmi at a cruise altitude of at least 18 000 ft.
LAA-PER-DSM-1.1	The aircraft shall be able to take off over a 50 ft obstacle within a distance of maximum 4 000 ft at a density altitude of up to 6 000 ft on runways with CBR 5.
LAA-PER-DSM-2.1	The aircraft shall have a cruise altitude of at least 10 000 ft.
LAA-PER-DSM-2.2	The initial cruise of 100 nmi and following descent to 3 000 ft shall take no longer than 20 minutes.
LAA-PER-DSM-3.1	After the initial cruise phase, the aircraft shall be able to loiter for 4 hours at an altitude of 3 000 ft, without dropping stores.
LAA-PER-DSM-4.1	After a loiter period of 4 hours at an altitude of 3 000 ft without dropping stores, the aircraft shall be able to climb to cruise altitude with following cruise of 100 nmi.
LAA-PER-DSM-5.1	The aircraft shall be able to land over a 50 ft obstacle within a distance of maximum 4 000 ft at a density altitude of up to 6 000 ft on runways with CBR 5.
LAA-PER-DSM-5.2	After landing, the aircraft shall have enough reserves for a climb to 3 000 ft with following loiter period of 45 minutes.
Power and Propulsion	
LAA-PAP-DSM-1.1	Warm-up shall take no longer than 5 minutes.
LAA-PAP-DSM-1.2	Shutdown shall take no longer than 5 minutes.
Time	
LAA-TIM-SER-1.1	The aircraft shall enter service in 2025.
LAA-TIM-SER-1.2	The aircraft shall have a service life of at least 15 000 flight hours over 25 years.
Technology	
LAA-TEC-RDY-1.1	Critical technologies shall be above TRL 8 in 2020.
Structures	
LAA-STR-WPN-1.1	The aircraft shall feature a board canon to engage ground targets.

Table 2.1: List of user requirements for the Light Attack Aircraft given by the AIAA

Requirement ID	Description
LAA-STR-CRW-1.1	The aircraft shall be able to fit two crew members.
LAA-SUR-SAF-1.1	The aircraft shall be fitted with two zero-zero ejection seats.

2.2. Flight Profile

From the requirements, a flight profile diagram was made, which can be seen in [Figure 2.1](#). On the left, the flight profile starts. After the taxi and take off, a rejected takeoff, indicated in red, is taken into account. After a successful takeoff, the climb and cruise phase begin. Here, the ferry mission continues with an extended cruise phase, indicated in blue. However, the design mission continues with a descent for the loiter/combat phase. After the mission, the aircraft climbs back to cruise altitude. Following the cruise phase, the descent and landing will be done. Included is a possible aborted landing, including a loiter and landing. The flight profile ends at the taxi and shutdown phase.

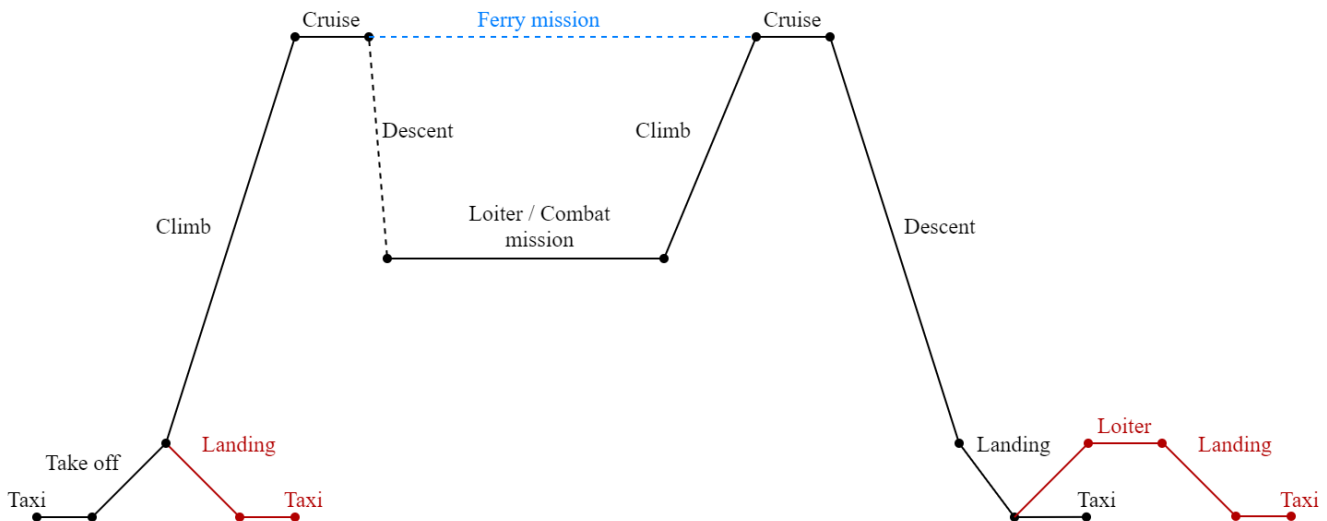


Figure 2.1: Flight Profile Diagram for the A-20 Chimera

2.3. Mission analysis

Military aircraft may be designed for multiple missions. The most common types of missions are described below.

1. **CAS against infantry:** One of the most important tasks of an attack aircraft is to provide CAS. The aircraft attacks hostile ground forces, providing support to allied forces close by. A high level of precision is required, because of the direct proximity of friendly troops. Often, integrated guns or precision guided missiles and bombs are used. Less common is the use of unguided ordnance, due to the lower accuracy and resulting increased risk of accidentally effecting friendly forces. Typical guided missiles that are used are the AGM-114 *Hellfire* or the AGM-65 *Maverick*. Guided bombs like the GBU-12 *Paveway* are generally more effective, at a cost of increased collateral damage. As mentioned

before, the use of an integrated gun is possible as well. This kind of attack commonly is titled 'strafing'. During a strafing run, the aircraft descends to a low level and engages the hostile troops for a short amount of time. Historically, machine guns and single barrel cannons were used. However, more modern aircraft use rotary cannons, as they provide a far higher rate of fire than conventional cannons. A prominent example is the GAU-8/A *Avenger*, that is installed in the A-10 *Thunderbolt II*¹.

2. **CAS against vehicles:** CAS against vehicles in many points is similar to the aforementioned combat against infantry, as the same means can be used. Typical targets are unarmored vehicles like cars, transporters and trucks, as well as armored vehicles like armored personnel carriers, infantry fighting vehicles and tanks. Commonly used weapons are the previously mentioned guided munitions. Depending on the caliber of the board cannon and the type of ammunition, it can be used against vehicles too.
3. **CAS against structures:** As with CAS against vehicles, similar weapon systems can be used against structures like walls, houses, shelters and infrastructure like bridges, while the latter is less common. Usually the board cannon is not used, as the caliber is too small and thus ineffective.
4. **Tactical bombing:** Tactical bombing describes an airstrike against targets with strategic importance like bridges, radar and surface-to-air missile, or SAM, sites, or enemy units. In contrast to CAS, these targets usually are not in close proximity to allied forces. They even can be far behind the enemy lines. As a result, strike accuracy is still valued, but not necessarily a critical requirement anymore, as no allied units can be harmed by nearby impacts. Furthermore, the flight profile of the aircraft changes significantly. To avoid being spotted and attacked, the aircraft has to either fly at high altitude or at very low altitude to avoid enemy radar. Frequently used weapon systems again are precision guided ammunition as well as unguided bombs. Cruise missiles like the German KEPD 350 *Taurus* or American AGM-158 *JASSM* are common as well. An advantage of cruise missiles is that the aircraft does not have to fly into enemy airspace, as the weapon can be deployed hundreds of kilometers away from the target. It can be deployed at a wide range of altitudes, from where it flies under its own power to the target, while different flight profiles can be selected. For example, a low, terrain following flight with pitch up shortly before the target can be selected. Modern cruise missiles like the Russian *Kalibr* and *Zircon* can reach supersonic and even hypersonic speeds.
5. **Reconnaissance:** During reconnaissance missions, the aircraft is used to gather intelligence on various items, ranging from enemy troop movements and numbers, over infrastructure to landscape features. This can be done by using radar or optical systems. Intercepting communication or identifying radar sites can be part of reconnaissance as well. Typically, reconnaissance flight profiles are chosen such that the chance of being spotted and/or attacked is minimized.
6. **Armed patrol:** During armed patrol missions, the aircraft patrols along critical paths and locations in a slow, low level flight. This can either be to deter the enemy from entering these areas, to show presence or to secure locations of strategic importance. Part of a patrol mission also is to identify and possibly engage enemy forces. Due to the flight profile, these missions usually are carried out by attack helicopters like the AH-64 *Apache*, because they can fly slower

¹<https://www.military.com/equipment/a-10-thunderbolt-ii>, Conducted on [25-11-2020]

than most fixed-wing aircraft².

7. **Air Combat Maneuvering/Intercept:** During these missions, the aircraft is used to intercept and/or engage enemy aircraft. These tasks require a high maneuverability and a high top speed. Combat between aircraft is carried out by using heat seeking, like the AIM-9 *Sidewinder*, or radar guided, e.g. AIM-120 *AMRAAM*, missiles or by using the integrated guns.

2.4. Threat Analysis

In the threat analysis different types of conflicts were examined with the corresponding threats for the aircraft. Per conflict the threats have been identified as well as the corresponding flight altitude this threat can occur.

In Table 2.2 the threats corresponding to *anti-terror* scenarios are given. As the enemy will be less-technologically advanced, the threats are less sophisticated. Commonly encountered threats are handheld weapons, like pistols and rifles. Even though they are very common, they only pose a minor threat to the aircraft, as the caliber is small, i.e. below .50cal/12.7mm. Thus, the potential damage is relatively small as well as the effective range. However, they can be a threat to the pilots of the aircraft, as small caliber projectiles still can penetrate the cockpit and injure or kill the crew. Other typical threats are mounted anti-aircraft, AA, guns. They pose a bigger threat, as the caliber is considerable bigger; it commonly is between 14.5 and 37mm. Due to that, the effective range is bigger as well. Lastly, shoulder launched missiles like older RPGs are encountered as well. If hit by an RPG, the damage can be extensive because of the high explosive mass. However, these are avoidable, as they are unguided and fly at a low speed with a very small effective range [1]. On the other hand, avoiding the missile is only possible, if the pilot sees the launch and/or projectile and the aircraft is maneuverable enough to fly a hard turn.

Table 2.2: Threat analysis per altitude for anti-terror mission.

Threats	Altitude		
	Low (<500 m)	Medium (500-5000 m)	High (>5000 m)
Handheld weapons (<.50 cal)	X		
AA guns/cannons	X	X	
Shoulder-launched missiles (unguided)	X		

Like anti-terror conflicts, *anti-narcotic operations*, e.g. operations against drug cartels, mainly fought in South-America, are a type of asymmetric warfare³. Hence, the threats listed in Table 2.3 are very comparable to the previously listed ones. However, compared to most terrorist groups, drug cartels are better funded⁴ and in the recent past, there were cases of individuals trying to acquire an FIM-92 *Stinger* missile⁵. Thus, it is not impossible that similar weapon systems could be used in conflicts and must be accounted for. Man-portable air-defense systems, MANPADS, like the *Stinger* are heat seeking fire-and forget missiles. They pose a significantly higher danger to aircraft than RPGs, because they actively target and home in on hot parts of the aircraft, like the engines and their exhaust. Furthermore, they are much faster and have a considerably higher range⁶.

²<https://www.defensie.nl/onderwerpen/materieel/vliegtuigen-en-helikopters/ah-64d-apache-gevechtshelikopter>, Conducted on [25-11-2020]

³<https://www.independent.co.uk/voices/latin-america-war-drugs-colombia-coca-honduras-donald-trump-a8744266.html>, Conducted on [24-11-2020]

⁴<https://www.nytimes.com/2012/06/17/magazine/how-a-mexican-drug-cartel-makes-its-billions.html>, Conducted on [24-11-2020]

⁵<https://www.dea.gov/press-releases/2011/05/02/guilty-pleas-two-mexican-nationals-conspiracy-acquire-stinger-missile-and>, Conducted on [25-11-2020]

⁶https://www.militaryfactory.com/smallarms/detail.asp?smallarms_id=30, Conducted on 25-11-2020

This makes evasion harder and requires active countermeasures like flares and evasive maneuvers⁷.

Table 2.3: Threat analysis per altitude for drug-cartel mission.

Threats	Altitude		
	Low (<500 m)	Medium (500-5000 m)	High (>5000 m)
Handheld weapons (<.50 cal)	X		
AA guns/cannons	X	X	
Shoulder-launched missiles (unguided)	X		
MANPADS (heat seeking, laser guided)	X	X	

Following the interview with former F-16 pilot Maj. ret. Richard *Hiker* Helldingen, the asymmetric warfare of the Vietnam War was analyzed, as it influenced warfare and society heavily. During the Vietnam War the asymmetry was not defined by the sorts of armament used, but more by the difference in tactics⁸. Aircraft encountered most of the already know threats. However, they were also confronted with radar guided anti aircraft guns and radar guided SAM⁹. Like heat-seeking missiles, they are more difficult to avoid, as they are actively guided and targeted using radar. Possible countermeasures can be anti-radiation missiles like the AGM-88 *HARM* or chaff⁷. Furthermore, enemy fighter jets were encountered as well, which majorly contributed to the loss of aircraft. Typically used weapon systems included radar guided and heat seeking air-to-air missiles as well as integrated guns. Possible countermeasures again are flares and chaff, as well as flying evasive maneuvers. The described threats are once more listed in Table 2.4. The threats in later military conflicts like the Yugoslav wars and Gulf

Table 2.4: Threat analysis per altitude for Vietnam like mission.

Threats	Altitude		
	Low (<500 m)	Medium (500-5000 m)	High (>5000 m)
Handheld weapons (<.50 cal)	X		
AA guns/cannons	X	X	
AA guns (Radar guided)		X	
Shoulder-launched missiles (unguided)	X		
SAM (Radar guided)	X	X	X
Enemy fighter AC	X	X	X

wars did not differ much in the type of previously listed threats. These conflicts only became more technologically advanced, making the evasion more difficult and the consequences of a failed evasion more serious.

Lastly, possible modern symmetric wars were considered. In symmetric warfare the enemy is defined to be of equal technological advancement. Thus, it is assumed that most modern threats are encountered on both sides. Examples again are MANPADS like *Stinger*, *Starstreak* or *Milan*, all types of guns, ranging from handheld weapons to mounted and guided cannons, as well as advanced SAM systems like *Patriot* or *THAAD*. Enemy aircraft with modern air-to-air missiles are encountered, as well as enemy airspace surveillance through aircraft like *AWACS* or ground based radars. These threats are listed in Table 2.5.

⁷<https://www.airforce-technology.com/features/feature49424/>, Conducted on [25-11-2020]

⁸<https://study.com/academy/lesson/asymmetric-warfare-definition-tactics-examples.html>, Conducted on [24-11-2020]

⁹<https://www.historynet.com/north-vietnams-light-anti-aircraft-artillery.htm>, Conducted on [25-11-2020]

Table 2.5: Threat analysis per altitude in symmetric warfare.

Threats	Altitude		
	Low (<500 m)	Medium (500-5000 m)	High (>5000 m)
Enemy Surveillance (Radar)		X	X
Handheld weapons (<.50 cal)	X		
AA guns/cannons	X	X	
AA guns (Radar guided)		X	
MANPADS (unguided, heat seeking, laser guided, manually controlled)	X	X	
SAM (Radar guided, heat seeking, laser guided)	X	X	X
Enemy fighter AC	X	X	X

2.5. Mission Environment and Encountered Threats

To limit the design space, it was decided to limit the aircraft's tasks and possible operational environments. The intercept of and combat against enemy aircraft, requires a design that can reach high speeds, is very manoeuvrable and can sustain high maneuver loads. Combined with the RFP requirement of designing a *best value* and *light attack* aircraft that has a payload capacity of 3 000 lbs, led to the decision to consider the air-to-air combat as out-of-scope. Combined with the threat of enemy airspace surveillance using radar and sophisticated SAM systems, this led to disregarding modern symmetric warfare in general. Following this logic, only asymmetric scenarios like anti-terror warfare and anti-narcotic operations are considered. However, this also reflects the general change in warfare that can be observed world wide and matches the RFP for "*a design of an aircraft that addresses this change in operational environment*" [2]. The final resulting threats can be found in [Table 2.6](#).

Lastly, based on the likelihood of encounter and the potential impact of a hit, requirements for the survivability of the aircraft were stated. To do so, the guidelines provided by the U.S. Department of Defense were followed to designate a "kill level" to the potential threats [3]. The levels differ based on the location of the hit. The assigned levels are meant as a *minimum*, a higher survivability always is desired. The level *MA* is defined as a mission abort. Hits from anti-aircraft guns are allowed to lead to *FL*, i.e. a forced landing under own power. Hits from MANPADS are allowed to lead to different levels, depending on the location of the hit. When the engines are hit, level *A* is allowed, i.e. loss of control after five minutes while still having sufficient control to reach allied units. When hit at the wing tips or control surfaces, the aircraft shall be controllable for 30 minutes, which corresponds to level *B*. A direct hit to structural elements like the fuselage, wing root, or tail is allowed to lead to a catastrophic failure, but the crew must still have enough time to make the decision to eject. This corresponds to level *K*. Lastly, a direct hit to the cockpit may lead to instant loss of the vehicle and crew, this is level *KK*.

2.6. Missions, Armament and Counter Measures

After the mission environment was defined, the available missions were revisited and the first design choices were made. It was decided to make CAS missions the main task of the A-20. As stated in [section 2.3](#), commonly used weapons for CAS missions are guided ammunitions like the AGM-114 *Hellfire*, AGM-65 *Maverick* and GBU-12 *Paveway*. To be able to carry those, and similar weapons, the A-20 was fitted with six external hardpoints with NATO interfaces for bombs and launch

Table 2.6: Final threat analysis with designated kill/survivability level

Threats	Altitude			Definition Survive
	Low (<500 m)	Medium (500-5000 m)	High (>5000 m)	
Handheld Weapons (<.50 cal)	X			MA
AA guns/cannons	X	X		FL
MANPADS (unguided, heat seeking, laser guided, manually controlled)	X	X		KK - direct hit to cockpit K fuselage, wing root, tail etc B - wing tips, control surfaces A - engine

rails. This also allows to satisfy requirement LAA-PAY-WTH-1.1¹⁰. External hardpoints were chosen over an internal bay, as an internal bay would increase the structural complexity and cost. Furthermore, external hardpoints are easier to fit with payloads. This comes at cost of increased drag, which will be further discussed in [chapter 12](#).

Furthermore, integrated board cannons were selected to satisfy requirement LAA-STR-WPN-1¹¹. Usually, modern aircraft features very fast firing large caliber rotary canons. However, it was decided to follow a different approach: two .50 cal GAU-19 rotary cannons were selected. The smaller caliber was chosen because of its lower weight and volume. For comparison, a 30 mm round of the GAU-8 weighs over 650 g¹², while a .50 cal round weighs about 115 g. The lower weight permitted to fit each GAU-19 with their maximum amount of ammunition, which is 1200 rounds. Together with the lower rate of fire of 1300 rounds per minute, this allows for almost a minute of sustained fire. Being able to fire longer is valued as it enables the aircraft to fly longer support mission, as it does not have to be rearmed as often. The smaller caliber also causes less collateral damage than larger rounds. This also was confirmed during the interview with Maj. ret. Richard *Hiker* Helsdingen, who appreciated both aspects. The firing time can be further increased, by using the cannons individually, leading to a firing time of two minutes. This also reduces the collateral damage further. A major drawback of the smaller caliber is that it cannot be used against vehicles as easily. Light vehicles like trucks can still be targeted. However, the cannons are ineffective against heavily armored vehicles like tanks. In these cases, the cannon of the A-10 *Thunderbolt II* is better suited. The A-20 can compensate by having access to a large arsenal of missiles and bombs, like the aforementioned AGM-114, which was developed for anti-armor use.

Tactical bombing may be executed by the A-20, but as the payload capacity is limited, other aircraft like the B-2 *Spirit*, B-1 *Lancer* or F-18 *Super Hornet* may be better suited. Even though the payload capacity is limited, the A-20 can still be used for long range precision strikes, as its hardpoints enable it to carry cruise missiles like the AGM-158 *JASSM*, AGM-158C *LRASM* and AGM-84E *SLAM*. They offer a range of up to 1 000 km¹³, while being stealthy. The large standoff distance also means, that the aircraft often can stay in friendly airspace, where it does not encounter enemy threats.

To make the A-20 a true multirole aircraft, it was decided to give it the capabilities of performing reconnaissance missions. To achieve that, it was fitted with a large suite of sensors including FLIR, optical camera systems and LiDAR. This is discussed

¹⁰LAA-PAY-WTH-1.1: The aircraft shall be able to carry 3 000 lbs of armament.

¹¹LAA-STR-WPN-1: The aircraft shall feature a board canon to engage ground targets.

¹²<https://www.gd-ots.com/wp-content/uploads/2017/11/30x173mm-Ammunition-Suite-MK44-Cannon-Version-3.pdf>, conducted on [19-01-2021]

¹³<https://www.lockheedmartin.com/content/dam/lockheed-martin/mfc/pc/jassm/mfc-jassm-er-pc.pdf>, conducted on [19-01-2021]

in more detail in [section 11.5](#).

Furthermore, it was decided to design the A-20 for armed patrol missions as well, to be able to take over a role that almost only helicopters can fulfill. To do so, the aircraft had to be designed for a low stall speed as well as good handling qualities and maneuverability, so it can fly slow enough, while being less susceptible to ground based threats.

To achieve the aforementioned kill levels, it was decided to armor the cockpit to protect the crew. This is further discussed in [section 6.2](#). To reduce the likelihood of being hit by MANPADS, flare launchers were included. Flare launchers eject burning pieces of Magnesium that are very hot compared to the engine exhausts. This makes heat seeking missiles lose their lock on the engines; they lock onto the flares instead, which results in a miss. The flare launchers were placed in the aft of the fuselage, flush with the skin.

To increase the effectiveness of the crew during all of these missions, it was decided to give them a good visibility by designing a large bubble-shaped canopy, which will be further discussed in [chapter 6](#).

3 Market Analysis

In this chapter a thorough market analysis will be given. Firstly, a list of involved stakeholders will be given and elaborated upon. Secondly, the market size for military fixed wing aircraft was analysed. Hereafter, a competition analysis, and lastly, a segment analysis will be discussed.

3.1. Stakeholder list

A stakeholder list is given below to summarize which stakeholders are involved in the design process. The stakeholders have an influence on the product and the cost for the product.

- **American Institute of Aeronautics and Astronautics:** The AIAA remains an important stakeholder for this project, due to the RFP. The user requirements given are the primary focus and direct the aircraft design.
- **Manufacturer:** For producing the aircraft, the manufacturer plays another important role. The manufacturer has to be able to produce the required components, which may be challenging. Additionally, the manufacturing process may be divided into multiple producers, meaning third-party manufacturers may be considered to acquire parts.
- **End-user:** The end-users of the product are mainly the pilots. A retired F-16 pilot was contacted to discuss his experience as an end-user, as well as a current F-35 pilot. From these conversations, one of the most important features mentioned was that the aircraft should be survivable against any kind of threat. The end-user must be able to operate the aircraft in the safest way possible. A mission and threat analysis was performed, as discussed in [section 2.3](#), in order to get an overview of the past and possible future war scenarios. Another important feature, is the ability to perform multiple roles during a mission or in combat. Next to the fighter pilots, other end-users include parties that communicate between pilots and troop's Joint Terminal Attack Controller.
- **Armed forces:** The countries' armed forces are still one of the key stakeholders that were considered. The purpose of the designed aircraft is to support ground troops. Hence, the countries military remains to be the primary customer.
- **Regulator:** Regulators such as the Department of Defense are another important stakeholder as they evaluate the airworthiness of the aircraft and give the certification requirements. These requirements have been followed from the start of the project and shall be referred back to in order to avoid termination of the project.

After looking at which stakeholders influence the design process, the market size was analyzed to observe the past, current and future market situation.

3.2. Market Size

The current market size for military fixed wing aircraft suggests that there is very little development of the market's spending per region from 2015 to 2025. Additionally, this analysis showed that North America, Pacific Asia and Europe are the major players contributing to the total spending. North America spends roughly 25-30 %, Asia Pacific spends roughly 30 % and Europe around 20 % of the total [4].

Next, the actual amount of spending per country was analyzed in order to identify the historical, current, and future market size. Only the data for the United States could be found. However, due to the fact that the US has a large dominance over military spending, it captures a good estimate that other countries also do not increase their military spending. The dominance over military spending comes from data that suggests that the US are number one with a spending of \$ 731.8 Billion on the list of military spending in 2019¹, The data containing the military spending suggest that from 2015 till 2021, there is a steep climb in the market, but afterwards, from 2011 till 2025, there is little fluctuation for total spending of military fixed-wing aircraft. It is expected that roughly 3 400 fighters will be produced in the coming 10 years²) [5].

Additionally, the trend for military fixed wing aircraft categories was investigated. This showed that it is expected that there is more demand for multi-role aircraft, and less for surveillance and reconnaissance aircraft [5]. Although this data is only provided for the US, it captures a good estimate of how other countries are motioned in the same way.

One could reason that, since there is expected to be lower spendings on fixed wing aircraft, there is a higher demand in affordable multi-role aircraft.

3.3. Competition

The data provided in this subsection originates from Defense Security Monitor². This showed that Lockheed Martin dominates the market with a market share of 58%.

Of the expected 3 400 fighters that will be manufactured, 46% will be F-35 produced by Lockheed Martin. This aircraft is in demand because of its multi-purpose functionality. However, as can be seen from [Table 3.1](#), the F-35 is very costly, which is why some nations in Europe and Asia rather choose the F-16. Aircraft like the JF-17 built by China in cooperation with Pakistan Aeronautical Complex are offered to Africa and Asia and are less expensive than the F-35.

In [Table 3.1](#), it shows that the Eurofighter is another expensive aircraft, but cheaper than the F-35. However, over longer terms and for high production quantities, it showed that it was less expensive. This led to the conclusion for Belgium's air force to choose the F-35 over the Eurofighter³.

[Table 3.1](#) is also used in the section hereafter, as well as for the weight estimations described in [chapter 5](#) and the cost analysis of [chapter 16](#).

¹<https://www.visualcapitalist.com/mapped-the-countries-with-the-most-military-spending/>, conducted on 17-12-2020

²<https://dsm.forecastinternational.com/wordpress/2019/06/19/fighter-aircraft-market-worth-260b-over-next-10-years/>, conducted on 17-12-2020

³<https://www.reuters.com/article/us-aerospace-belgium/belgium-picks-lockheeds-f-35-over-eurofighter-on-price>, conducted on 17-12-2020

Table 3.1: Reference aircraft for competitors list⁴

Aircraft	Unit Price in millions (USD)	OEW (kg)	Units sold	Role	Manufactured Region
A-10 Thunderbolt	\$40	10 710	716	Attack	North-America
Super Tucano	\$11	3 200	220	Attack	South-America
Eurofighter	\$58 - 70 ⁵	11 000	220	Multi	Europe
F-16	\$23	12 020	4600	Multi	North-America
A-4 Skyhawk	\$35	4 469	2960	Attack	North-America
F-4 Phantom II	\$26	13 757	5000	Attack	North-America
AV-8B Harrier II	\$25	6 336	337	Multi	Europe
Alpha Jet	\$18	3 515	480	Attack	Europe
Sepecat Jaguar	\$10	7 000	543	Attack	Europe
Super-Etendard	\$38	6 500	85	Attack	Europe
Panavia Tornado	\$60	14 100	990	Multi	Europe
Cessna A-37	\$0.16	2 817	577	Attack	North-America
F-35A/B/C	\$82/110/100 ⁶⁷	13 154	648	Multi	North-America
JF-17 Thunder	\$25	6 586	54	Multi	Asia
FA-50 Golden Eagle	\$34	6 470	72	Multi	Asia

3.4. Segment Analysis

A segment analysis was carried out to further understand the current market trend. The chosen segments are:

- By manufactured region: North America, Europe, Asia-Pacific, Middle East & Africa, Latin America
- By role: attack and multi role

For the segmentation, the same aircraft were considered as derived from [Table 3.1](#). Additionally, the segmentation looked at those which are still in on the market.

Firstly, the segmentation according to manufacturing region was looked at. [Figure 3.1](#) shows the segmentation of the aircraft that are produced, including ones out of service, this includes all aircraft from [Table 3.1](#). [Figure 3.2](#) shows the segmentation of what is currently on the market, this figure only includes aircraft that are still in service from [Table 3.1](#)⁸. This data shows that there are less aircraft manufactured in Europe that are currently in service.

The A-20 Chimera project is designed by members with a European citizenship. As Macron stated, a genuine European defence strategy is stronger, and he promotes European countries to invest in European offers⁹. This allows the A-20 to be offered to European countries looking for a multi role aircraft, which are now bought from American manufacturers.

⁴<https://www.wikipedia.org/>, conducted on 17-12-2020

⁵<https://www.aircraftcompare.com/aircraft/eurofighter-typhoon-t1/>, conducted on 17-12-2020

⁶<https://www.reuters.com/article/us-usa-lockheed-f35-idUSKBN1X8115>, conducted on 17-12-2020

⁷<https://www.f35.com/f35/about/fast-facts.html>, conducted on 17-12-2020

⁸<https://www.wikipedia.org/>, conducted on 17-12-2020

⁹<https://www.france24.com/en/20181026-france-belgium-aviation-macron-purchase-usa-f35-jets-eurofighter>, conducted on 18-12-2020

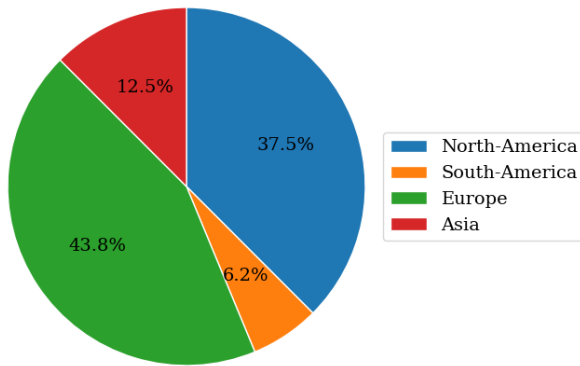


Figure 3.1: Geographical segmentation of reference aircraft that have been produced, including ones out of service

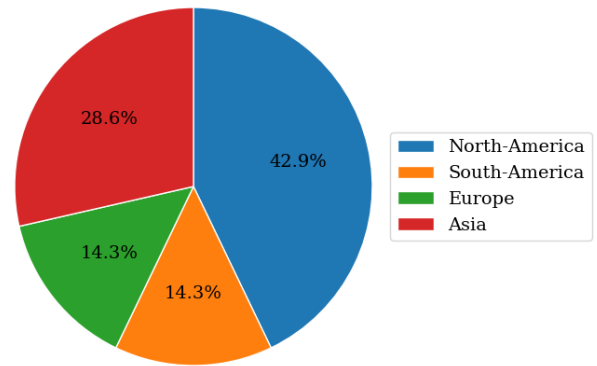


Figure 3.2: Geographical segmentation of reference aircraft that are currently in service

Secondly, the role of the aircraft were analyzed. As can be seen in [Table 3.1](#), the division of the roles of the aircraft consists of multi role and attack aircraft. When comparing the frequency of aircraft between produced and in-service, the multi role aircraft remains to be used. However, the attack aircraft are less in service, which could suggest that these are less in demand. It should also be noted that some aircraft listed in [Table 3.1](#) which are still in service, have been converted from attack role to multi-role, an example is the F-4 *Phantom II*. These aircraft have not been included in [Figure 3.3](#).

With the above observations, one could conclude that there is a higher demand in multi-role aircraft.

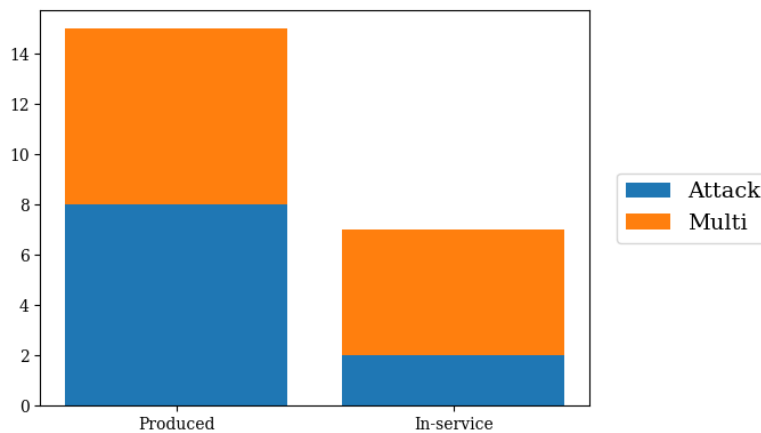


Figure 3.3: Histogram of aircraft roles, produced vs. in service

4 Design Approach and Concept Trade-off

In this chapter, the general design approach and concept trade-off are discussed. [Section 4.1](#) describes the design steps that were taken throughout the project and how the process was structured. Furthermore, initial concept designs are discussed. [Section 4.2](#) gives a summary of the trade-off on the previously discussed concepts.

4.1. Design Approach

To structure the design process of the aircraft, an N2 chart was made, which can be seen in [Figure 4.1](#). The blue boxes represent design steps of the the first class sizing. It was based on the requirements, which lead to a first order weight estimate. The weight estimate enabled the sizing of wings and propulsion unit. Following that, the weight and placement of major components was determined, which then was used to initially size the empennage. Lastly the landing gear was placed and sized. The entire Class I sizing was iterated until the weights and sizes converged. The Class II sizing is represented by yellow boxes. In this Class II design phase, more accurate estimations of the drag polar, and aircraft component weights were made. Furthermore, an airfoil for the wing and empennage were selected. From this, high lift devices and control surfaces were sized. Finally, all outputs of the design steps were an input for a stability & control analysis.

To start the design process, four initial concepts were created, which were all sized using Class I methods and were reiterated upon. A trade-off was performed on the four concepts. After the trade-off, all positive aspects were merged into a final, fifth concept. The trade-off is described in more detail in [section 4.2](#). The initial concepts are described below.

Concept 1: Survivability & Redundancy

The first concept was design with survivability & redundancy in mind. Due to the service ceiling requirement of at least 30 000 ft, reciprocating engines were not considered, as they under-perform heavily at high altitudes [6]. For increased fuel efficiency, slow flight and take off performance, turboprop engines were chosen. It was decided to use two engines to provide redundancy.

Following the redundancy and survivability thought, it was decided to use an H-tail, because it offers two separate vertical stabilizers as well as two separate rudders. This way, the aircraft can still be controllable after damage of a rudder or stabilizer. The tail is placed above the wing, to keep it out of the downwash of the wing.

As the aircraft is supposed to carry a considerable amount of armament, which is typically carried below the wings, the wings have to be stiff and strong. Thus, it was decided to increase the thickness of the wing. This comes at the cost of increased drag.

To make the armament more accessible, while not suffering from ground clearance issues, it was decided to use a mid-wing configuration. Combining the mid-wing design with high placed engines to prevent propeller ground clearance issues, it

was suggested to mount the engines on top of the wings. Using this configuration also keeps the engines accessible for maintenance, while also protecting them of threats from the ground, as they are shielded by the wings. This way, the heat signature of the engines is concealed as well. To further provide a smaller target for heat seeking missiles, the engine exhaust is directed towards the fuselage, where it will be carried away by the propeller slip-stream. A pusher configuration was considered as well, but was discarded due to conflicts with the flaps. Another possible benefit of wing mounted turboprops can be an increased take off performance due to the stream from the propellers over the wing.

To allow for hot-pit refueling and reloading, the turboprop engines are fitted with clutches, to decouple the propellers. This way, the engines can keep running to provide power, while not endangering the ground crew.

Concept 2: Canard

For the second concept a lifting canard lay-out was considered. The advantage of the canard over the conventional lay-out is the higher manoeuvrability which can be beneficial during combat missions. Another advantage is that a lifting canard provides additional lift to the aircraft, which is more efficient than a conventional tail.

For the propulsion unit two turbofan engines were chosen. The engines were blended-in on top of the wing to create enough clearance for the armament which will be placed under the wings. The twin-engine configuration was chosen to increase redundancy and survivability.

The wing has wingtips which extent up- and downward. The wingtips function as the vertical stabilizers and also include the rudder to control the yaw angle. A small dihedral angle was applied to the wing, to provide roll stability. Flaperons were placed on the outside of the wing.

The front wing was placed just behind the cockpit to limit the impact on the crew's angles of vision. The front wing includes the elevators to control the pitch angle of the aircraft. The cockpit provides the pilot with a lot of vision around the aircraft by placing it at the very front.

Concept 3: Affordability

The third design option was focused on the low cost design goal. The structural complexity and ease of manufacturing played an important role in each design decision.

The aircraft is powered by a single turboprop on the nose of the airplane. The advantage is that a single engine is the cheapest option, and a propeller is efficient at low speeds and altitudes. The main drawback is that it is not designed for redundancy.

A mid-wing configuration was selected. Aerodynamically, this configuration is most favoured compared to other configurations because it has a low interference drag. Secondly it has a neutral roll stability, which allows the aircraft to perform rapid roll movements. Finally, no structural reinforcements are necessary since the wing goes straight through the fuselage.

The cockpit of this aircraft was shifted backwards because of the single turboprop, located on the nose of the fuselage, which came at the cost of reduced visibility.

For the control surfaces, flaperons were selected. This allowed the use of larger flaps, which in turn reduces flap complexity, and thus cost.

A conventional tail was chosen. It has the advantages that it has a light weight structure and a low complexity. This results in a lower manufacturing and material cost. The horizontal tail planes were fitted with elevators and the vertical plane with a rudder.

The selected landing gear was a non-retractable tricycle configuration. This was chosen because it would be heavier and more expensive to retract the landing gear. The tricycle configuration is better for control, and visibility on the ground. Furthermore the aircraft can not tip over when the brakes are applied. The main disadvantage is the increased drag from the landing gear.

Concept 4: Hybrid

The fourth concept design is powered by a hybrid system, with a gas turbine to generate electricity, in order to power the electric motors which drive the propellers. This hybrid system provides freedom of the motor placement. Two of the propellers are located at the wing tip and equipped with the ability to fold in to improve aerodynamic efficiency when not used. Furthermore, the third propeller is located at the rear, behind the empennage, along the longitudinal axis of the body. Since the exhaust is at the rear, the thermal signature is diffused by this pusher prop. During high power demand scenario's, such as take-off, all three motors operate together in order to provide maximum thrust. However, during lower energy demand scenario's, such as loiter, only the rear motor is operative. This configuration allows the aircraft to consumes less energy, since the motors can operate closer to their design points.

As the gas turbine is operating at optimal efficiency, the remainder of the generated energy will be stored in a battery when less power is required. The stored energy can be used for climb, maneuvers and other subsystems when necessary. The air inlets are located on the top surface of the wing near the fuselage. When the aircraft has to take off from and/or land on rough runways, this reduces the probability of debris ingestion.

An H-tail configuration was chosen for the aircraft to help conceal the exhaust of the turbine. Furthermore, the H-tail configuration allows the vertical tail to be shorter which would be beneficial in terms of required hangar size.

Conceptual design sketches of all concepts can be found in [Figure 4.2](#), [Figure 4.3](#), [Figure 4.4](#) and [Figure 4.5](#). [Figure 4.6](#), [Figure 4.7](#), [Figure 4.8](#) and [Figure 4.9](#) show the concepts after the Class I design steps.

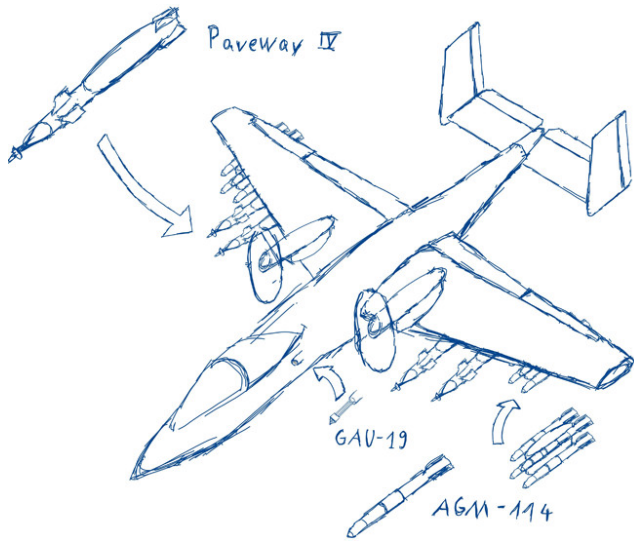


Figure 4.2: Concept drawing of concept 1

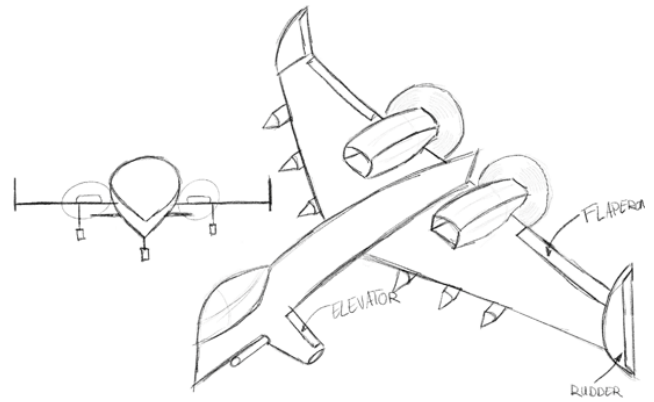


Figure 4.3: Concept drawing of concept 2

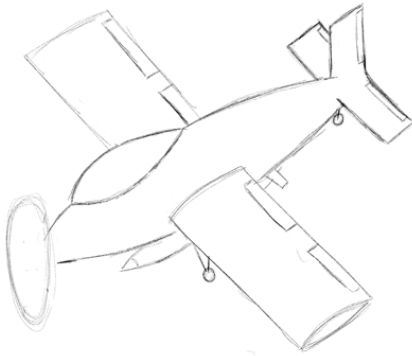


Figure 4.4: Concept drawing of concept 3

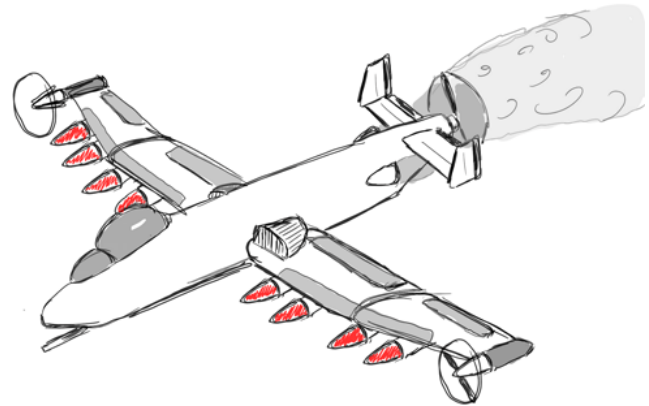


Figure 4.5: Concept drawing of concept 4

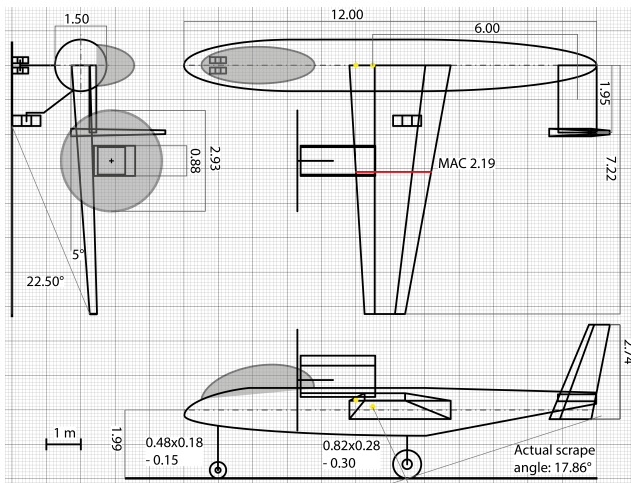


Figure 4.6: Three-view drawing of concept 1

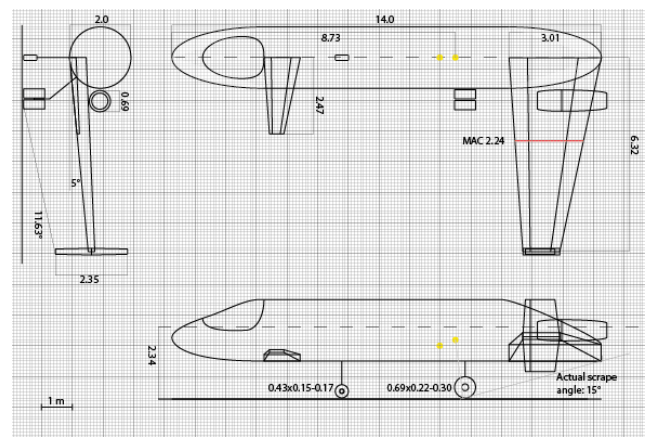


Figure 4.7: Three-view drawing of concept 2

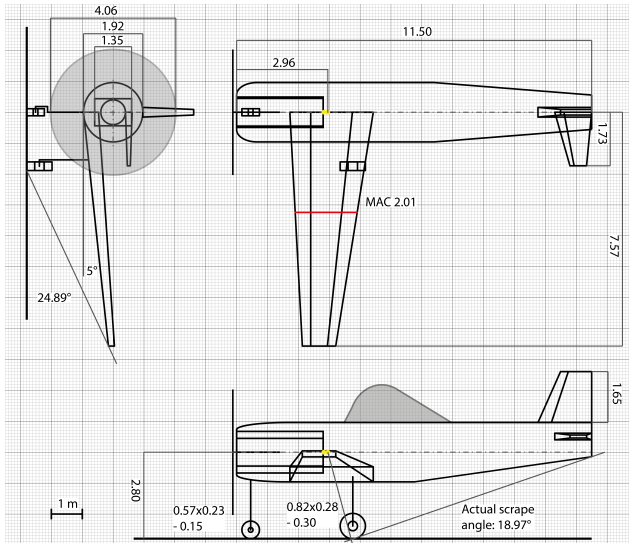


Figure 4.8: Three-view drawing of concept 3

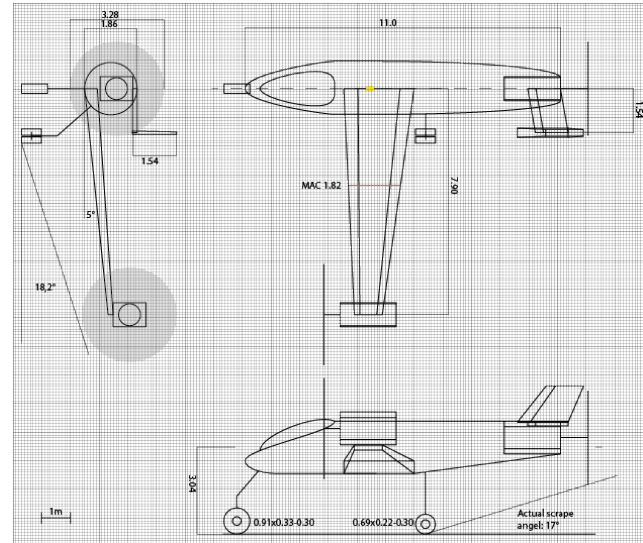


Figure 4.9: Three-view drawing of concept 4

4.2. Trade-Off

As said before, the four concepts were sized using the Class I methods. Based on that, a trade-off was performed on the overall layout and configuration of the aircraft. Below the different criterion are discussed.

Survivability was rated the highest, since the aircraft will operate in war zones. The pilots must be able to safely operate the aircraft and be able to return home safely. The survivability is split into susceptibility and vulnerability. The susceptibility is scored on the ability to avoid threats, while vulnerability is the ability to sustain damage and survive when the aircraft is hit.

Another important criterion was the cost. The maintenance costs were given a higher weight than its production costs. This is due to the long service life and the maintenance capabilities on austere airfields.

The flexibility takes into account the ability of the aircraft to adapt to different mission profiles. The feasible amount of hardpoints, as well as operations and logistics of the aircraft determined this result.

Sustainability of the aircraft is with regards to the environmental and operational considerations. The fuel was considered, due to being expensive in remote locations. Therefore a lower specific fuel consumption was seen as better. The operational empty weight was also considered for each aircraft, based on the logic that the weight is related to the material usage.

Lastly, the performance was evaluated on its turn radius, climb rate at sea level and maximum cruise speed.

Table 4.1 shows the trade-off weight with respect to its criteria. Every concept was given a score between zero and one, based on the feasibility and relative result between the concept designs. For non-quantifiable trade-off criteria, the scores from Table 4.2 were used.

Table 4.1: Trade-off table with assigned scores

Criteria	Weight	Concept 1	Concept 2	Concept 3	Concept 4
Survivability	30.0%				
- Susceptibility	15.0%	0.75	1	0.25	0.5
- Vulnerability	15.0%	1	0.75	0.25	0.75
Subtotal Survivability		26.3%	26.3%	7.5%	18.8%
Costs	25.0%				
- Maintenance costs	15.0%	0.5	0.5	1	0.25
- Production costs	10.0%	0.75	0.5	1	0.25
Subtotal Costs		15.0%	12.5%	25.0%	6.3%
Flexibility	20.0%				
- Feasible amount of hardpoints	8.00%	0.75	1	1	1
- Operations	6.0%	0.75	0.75	0.5	0.5
- Logistics	6.0%	0.75	0.25	0.75	0.5
Subtotal Flexibility		15.0%	14.0%	15.5%	14.0%
Sustainability	15.0%				
- Fuel Consumption	10.5%	0.82	0.74	1	0.72
- OEW	4.5%	0.85	0.80	1	0.78
Subtotal Sustainability		12.4%	11.4%	15.0%	11.1%
Performance	10.0%				
- Turn Radius	3.5%	0.92	0.77	1	0.77
- Climb Rate at sea level	3.5%	0.93	0.56	1	0.44
- Max Cruise Speed	3.0%	0.89	1	0.89	0.90
Subtotal Performance		9.2%	17.7%	9.7%	6.9%
Total	100.0%	77.9%	71.8%	72.7%	57.0%

Table 4.2: Non-quantifiable trade-off scores

	Excellent	Good	Feasible	Bad	Not Feasible
Score	1	0.75	0.5	0.25	0

According to the trade-off table, concept one scored overall best through all criterion, making this the winner. A sensitivity analysis of the trade-off was performed to see the impact of changing the weights and removing categories of the trade-off criteria, which can be seen in Table 4.3. Different scenarios were considered; equal score weights, reduced survivability and cost weight, increased performance and sustainability weight, a performance weight of zero, and finally, a higher weight for sustainability. Nonetheless, concept one remained the winner in most scenarios of the sensitivity analysis.

Table 4.3: Sensitivity analysis on the trade-off input parameters

Scenario	Concept 1	Concept 2	Concept 3	Concept 4
Tradeoff	78%	72%	73%	57%
Equal	80%	72%	80%	60%
Survivability -	76%	68%	86%	56%
Cost -	81%	75%	71%	64%
Performance +	81%	73%	78%	61%
Performance 0	76%	71%	71%	56%
Sustainability +	79%	73%	78%	60%

4.3. Trade-Off Result

Finally, a fifth concept, the *Chimera*, was created, which was mostly based on concept one. It included all the strengths of concept one, which were survivability and redundancy. However, it also addressed the downsides of concept one, which were the engine placement and propeller diameter. To avoid catastrophic damage to the wing structure due to turbine disk failure, the engines had to be placed far ahead of the leading edge. This exposed the engines, negating the benefit of placing them on top of the wings. Furthermore, the propellers were very large to create the high thrust required during the cruise phase. Not only did the propellers add a lot of cost and weight, they also had caused problems during ground operations. They also had an impact on the placement of hardpoints, as missiles and rockets had interfered with the props. To solve those problems, it was decided to fit the aircraft with 2 turbofan engines, that are placed high on the fuselage between wing and empennage. This helps concealing the heat signature of the engines, as they are partially covered by both wing and horizontal tail plane, when seen from the ground. This is shown in [Figure 4.10](#).

In [Table 4.4](#) another trade-off was performed, which showed that concept five indeed scored better.



Figure 4.10: A-20 tail plane covering engine exhausts

A technical drawing of the A-20 *Chimera* after Class I and Class II design steps can be seen in [Figure 4.11](#).

Table 4.4: Trade summary table

Criterion	Survivability [30%]	Costs [25%]	Flexibility [20%]	Sustainability [15%]	Performance [10%]	Total score
Concept 1	0.88	0.60	0.75	0.83	0.92	77.9%
Concept 2	0.88	0.50	0.70	0.76	0.77	71.8%
Concept 3	0.25	1	0.78	1	0.97	72.7%
Concept 4	0.63	0.25	0.70	0.74	0.69	57.0%
Concept 5	1	0.6	0.85	0.85	0.83	83.0%

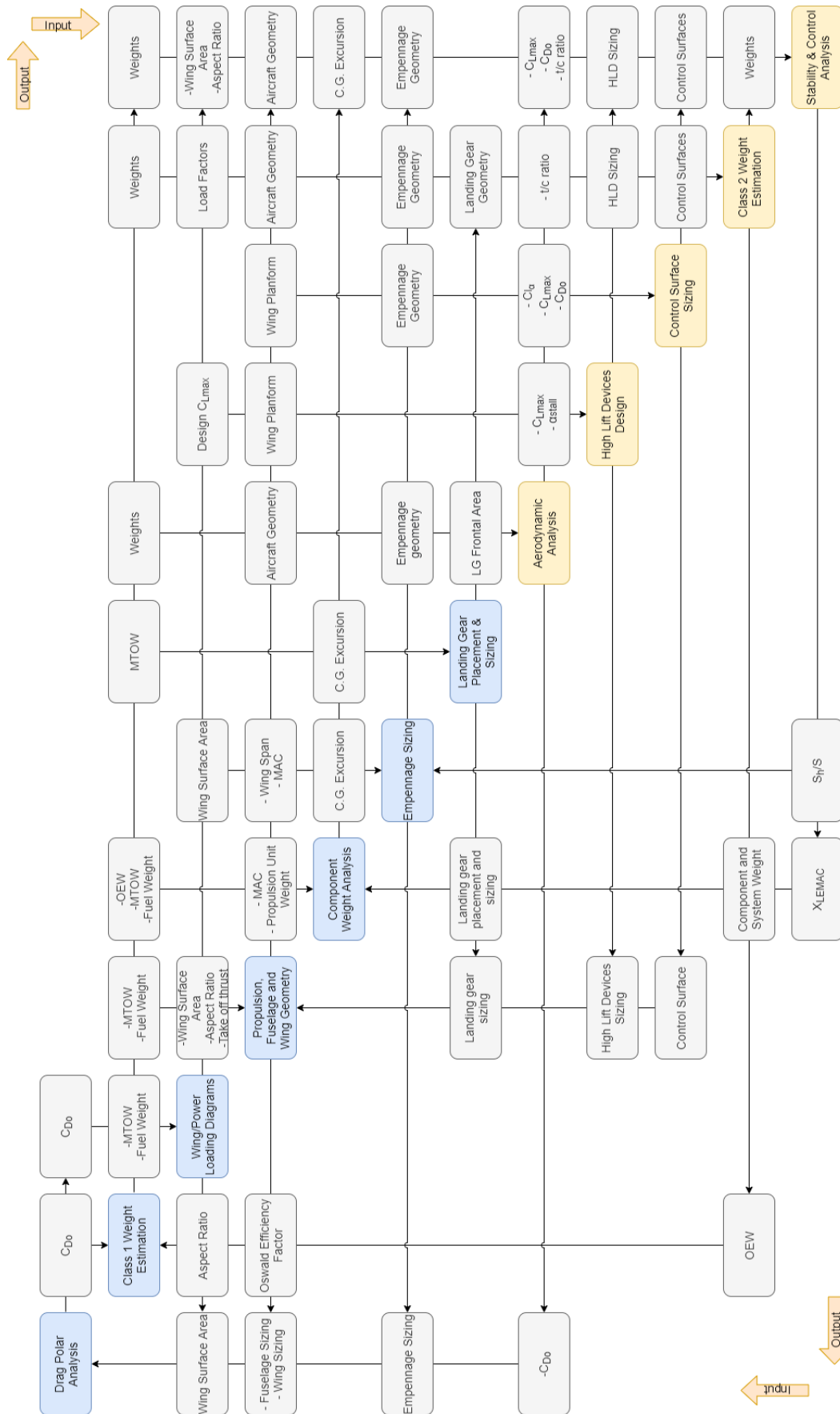


Figure 4.1: N2 chart of the aircraft design process.

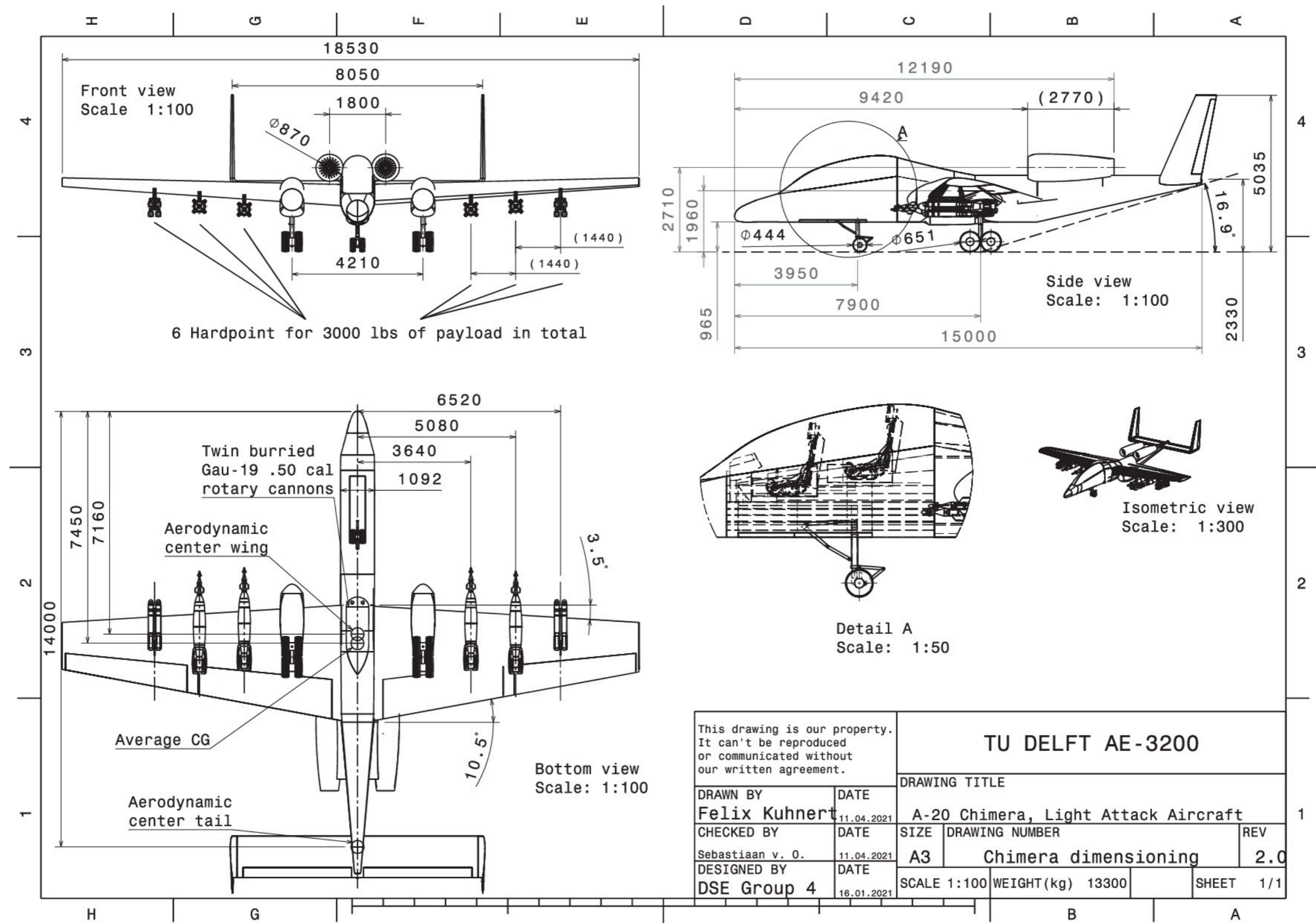


Figure 4.11: Three-view drawing of A-20

5 Weight Estimations

In this chapter, an approximation of the aircraft weight is presented. First, a rough weight estimation, the Class I weight estimation, is discussed. This is followed by a more detailed weight estimation in the Class II sizing, which is based on components weights of comparable aircraft.

5.1. Class I Weight Estimation

The Class I weight estimation finds an initial approximation of the take off weight, W_{TO} , operational empty weight, W_{OE} , and fuel weight, W_F . W_{OE} includes the empty weight, W_E , of the aircraft, the weight of the trapped fuel and oil, the weight of the crew and the armor weight. Typical values for the trapped fuel, $0.005W_{TO}$, and total crew weight, 180 kg, were taken from Roskam part I, chapter 2 [7]. The empty weight of the aircraft was taken from reference aircraft, from which a linear relation between W_{TO} and W_E was found, shown in Figure 5.1. The armor weight was determined to be 626 kg, which is elaborated on in chapter 6.

W_F was determined by applying the fuel fraction method of Roskam chapter 2 [7], with the use of the mission profile diagram. The mission profile diagram is given in Figure 2.1, as explained in chapter 2. The fuel fractions of the cruise and loiter phases were calculated using Breguet's equations for range and endurance for jet aircraft. For the return cruise of the combat mission the optimum L/D ratio was used with lower speed, as this part was not specified in the RFP [2]. A specific fuel consumption of 0.391 lbs/hr/lbf was chosen for these calculations, based on a reference engine, more on this in chapter 9. The L/D ratios were based on the drag polar from chapter 12. This resulted in the use of the fuel fractions in Table 5.1, which gave a W_F of $0.3W_{TO}$. The payload weight was set by requirement LAA-PAY-WTH-1.1¹ as 3 000 lbs.

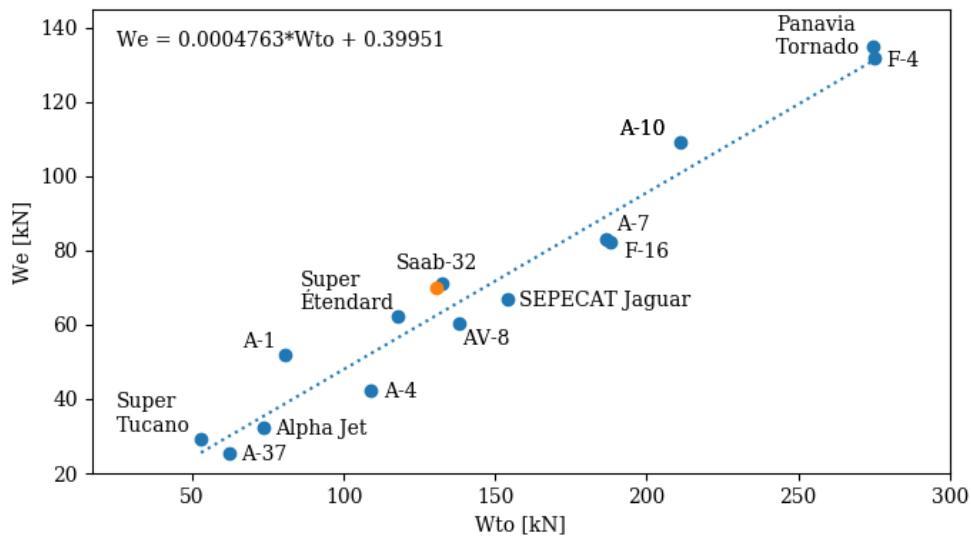
Table 5.1: Used fuel fractions for W_F calculations.

Flight phase	Fuel fraction	Flight phase	Fuel fraction
Engine start/ warm-up	0.99	Climb	0.96
Taxi	0.99	Cruise (2)	0.98
Take-off	0.99	Descent	0.99
Climb	0.96	Climb	0.96
Cruise (1)	0.98	Loiter (45 min)	0.98
Descent	0.99	Descent	0.99
Loiter (4h)	0.88	Landing, Taxi, Shut-down	0.99

5.2. Class II Weight Estimation

To provide a more accurate prediction of the empty weight, the Statistical Group Weight Method found in Raymer, chapter 15.3, was used [8]. This method estimates the weight of different components, based on historical data. The equations from the Fighter/Attack Weight were used in order to estimate the different component group weights. The resulting empty weight

¹LAA-PAY-WTH-1.1: The aircraft shall be able to carry 3 000 lbs of armament.

Figure 5.1: Linear correlation between W_{TO} and W_E .

was then used to update the OEW in the Class I estimation, and iterated upon until the the values for all weights converged to less than 1% difference compared to the previous iteration. The resulting component weights are listed in [Table 5.2](#).

Table 5.2: Component weights from the Class II weight estimation with the Statistical Group Weight Method, as per Raymer [8], converted to kilograms

Component Group	Weight [kg]	Component Group	Weight [kg]
Wing	1508	Vertical Tailplane	136
Fuselage	938	Air Conditioning and Anti-Ice	105
Engine	815	On-board Gun	96
Armor	626	Instruments	93
Avionics	491	Hydraulics	67
Main Landing Gear	485	Engine Mount	23
Electrical Systems	384	Engine Controls	23
Flight Controls	324	Engine Section	13
Fuel Tank	319	Pneumatic starter	12
Horizontal Tailplane	238	Handling Gear	4
Nose Landing Gear	202	Firewall	3
Furnishing	197		
Empty Weight			7075

The increase in weight in the iterative process had a large influence on the wing, engine, empennage, and landing gear sizing. The breakdown of the MTOW, and corresponding OEW is presented in [Figure 5.2](#).

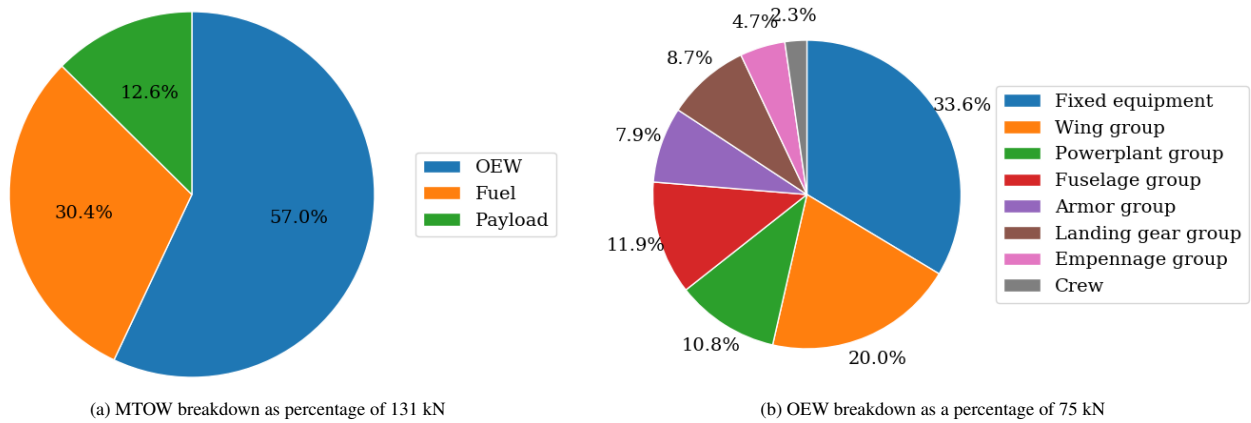


Figure 5.2: Weight breakdown of the A-20 Chimera

5.3. Mass Moment of Inertia

From the Class II weight estimation the mass moment of inertia (MMOI) could be calculated. The MMOI's are eventually needed for the stability and control calculations, which can be found in [section 13.4](#). For the MMOI calculations the component group weights from [Table 5.2](#) were used and the approximated location with respect to the most aft center of gravity location axis. In order to make the calculations more accurate, the component weights were split up into a left and right side variant. The calculated values can be found in [Table 5.3](#). These values were verified and validated with a first order MMOI estimation from Roskam V, chapter 3 [9]. The results in [Table 5.3](#) fell within 5% of the first order estimation.

Table 5.3: Results moment of inertia around the most aft center of gravity

Mass Moment of Inertia	[kg/m ²]
I_{xx}	$61.1 \cdot 10^3$
I_{yy}	$49.2 \cdot 10^3$
I_{zz}	$104.3 \cdot 10^3$

5.4. Verification and Validation

The verification and validation of the 1st order weight estimation was done in two steps. First, all values were computed manually and then compared to the output of the tool. This was done to see if the under laying equations were implemented correctly. The second step was to plot the resulting weight on trend line of reference aircraft, shown in [Figure 5.1](#). This was done as a sanity check, to see if the outputs are realistic.

The input and output values of the first step can be found in [Table 5.4](#) were used. Both, the manually calculated values and tool outputs are listed. As can be seen from the results, one can assume that this was the case, as the error is so small, that it can be neglected during first order design steps. It is very likely due to rounding errors.

Also, as can be seen in [Figure 5.1](#), the designed concept lies close to the trend line, which indicates that the design is within reasonable limits.

Table 5.4: Results of verification process Class I weight estimation.

Initial Values			Jet				Propeller		
			Results:	Hand	Tool	Error	Hand	Tool	Error
c_j	$1.7 \cdot 10^{-7}$	[kg/Ns]	$\frac{W_5}{W_4}$	0.9882	0.9882	-	0.9799	0.9799	-
$\frac{L}{D}_{cruise}$	7	[-]	$\frac{W_7}{W_6}$	0.9355	0.9356	10^{-3}	0.9556	0.9556	-
$\frac{L}{D}_{loiter}$	9	[-]	M_{used}	0.2429	0.2428	10^{-3}	0.2395	0.2395	-
V_{cruise}	200	[m/s]	W_{TO}	56145	56071	10^{-3}	55401	55405	10^{-5}
e	0.7	[-]							
Cruise range	100,000	[m]							
Endurance time	3600	[s]							
c_p	$1.014 \cdot 10^{-7}$	[kg/J]							
η_p	0.7	[-]							
V_{loiter}	80	[m/s]							

For the verification of the Class II weight estimation a similar approach was taken as for the Class I weight estimation. Equations from Raymer were manually computed and compared to the tool output. It was found that all results were within 10^{-3} % of each other. Based on that, it can be assumed that the equations were implemented correctly.

The validation of the Class II weight estimation was done by using component weight data which was given in Roskam part V, appendix A [9]. Different aircraft from the appendix were used as input for the tool. The resulting group weights were compared to those found in Roskam. It was found that the difference between these results were within 5% of each other. This difference can be explained due to assumptions made for some input values, such as the length of the landing gear, as well as the wing mounted control surface areas.

6 Fuselage Design

The main task of the fuselage is to accommodate the crew and their cockpit, the majority of the electric and hydraulic subsystems, as well as the cannons and their ammunition. Furthermore, it has to mechanically connect the wing and the empennage, while transferring their loads and being as aerodynamic as possible. This chapter describes the steps taken for the fuselage design. First, an overview of the fuselage is given, followed by a discussion of the design methods, starting with the cockpit. After that, the rest of the fuselage design is discussed, including the design of the structure.

6.1. Design Overview

Figure 6.1 shows the fuselage of the aircraft. It is 15 m long and has an oval shape with flattened sides. It is 1.1 m wide and 1.5 m high, excluding the cockpit. The tail cone is 5.3 m long and is angled upwards. The fuselage houses the cockpit including armor, the cannons including ammunition, as well as the majority of all electric and hydraulic subsystems as well as the nose landing gear. The rotating cannons are placed below the wing box. They are placed such that the firing barrel sticks out of fuselage. To reduce drag, they are hidden behind an aerodynamic fairing, with small cutouts for the muzzles. The cockpit features thick Steel-Steel Composite Metal Foam, CMF, plates to armor the crew against rounds of handheld weapons, heavy machine guns and AA cannons with a caliber of at least 14.5 mm. The cockpit also features a big bubble shaped canopy, to provide the crew with good visibility.

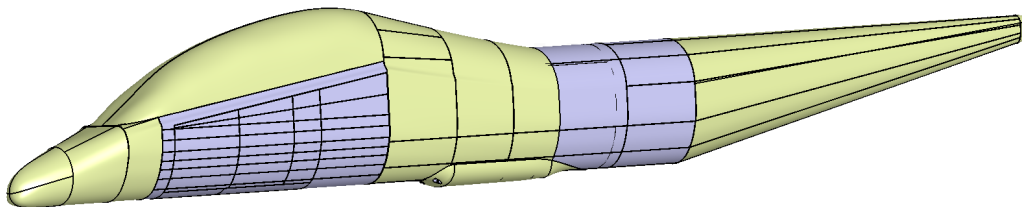


Figure 6.1: 3D model of the fuselage

6.2. Cockpit

The cockpit design is based on the crew that has to be accommodated as well as their vision angles and general ergonomics. The starting point of design of the cockpit were the two zero-zero ejection seats, as per requirement LAA-SUR-SAF-1.1¹. Three dimensional models of these seats² were imported into CATIA. After that, two average American male mannequins from the CATIA Ergonomics & Design workbench were placed in the seats. The tool bench allows full manipulation of the

¹LAA-SUR-SAF-1.1: The aircraft shall be fitted with two zero-zero ejection seats.

²<https://grabcad.com/library/ejection-seat-2>, conducted on [17-01-2021]

mannequins to check, whether modeled control elements are reachable or not. Based on this, basic control elements like side stick, rudder pedals, thrust lever and screens were placed as well. A head-up display, or HUD, was not implemented, as the crew will be equipped with modern helmets, featuring integrated displays, which will be discussed in [section 11.5](#). However, the cockpit is still equipped with big digital screens, in order to reduce clutter inside the cockpit.

It was decided to place the crew members behind each other and to have one pilot, and one weapons systems officer. It was decided to have only one pilot, because the work load of piloting a modern attack aircraft is small enough that a second pilot does not add any benefits. This was also confirmed during the interviews with Maj. Pascal *Smiley* Smaal and Maj. ret. Richard *Hiker* Helsdingen.

The pilots were placed behind each other, in order to make the fuselage as thin as possible. Next, the seats, including crew and controls, were placed on the longitudinal axis of the aircraft and spaced such that there is a sufficient amount of leg room for the crew, i.e. they can stretch their legs past the rudder pedals/feet rests without colliding with the front wall. According to Roskam, the rear crew member needs a downward viewing angle of at least 5°. Thus, the rear seat was raised, to achieve the downward angle. After that, a dummy fuselage cross section was placed around the seats, to determine the required seat height, so that the pilot has a sideways downwards viewing angle of 45 ° and a forward viewing angle of 15 ° downwards [10]. Next, the cross section was trimmed to size, while keeping enough free space for the nose landing gear wheel-well and armor plating. As the cockpit is designed for 2 crew members, requirement LAA-STR-CRW-1.1³ is met.

As armor, 54.3 mm thick Steel-Steel CMF was chosen. Steel-Steel CMF consists of hollow steel spheres embedded in a steel matrix. It has shown to be able to absorb a large amount of impact energy and to stop 14.5 mm armor piercing incendiary rounds as used in anti tank rifles and anti aircraft guns. It is likely to stop even larger calibers, however, this was not tested yet. Even though the CMF is made of steel, it is only slightly heavier than aluminum, 3.0 g/cm³ versus 2.8 g/cm³ of bulk aluminum [11]. The armor was placed below, in front and to the sides of the cockpit, protecting the crew of ground based projectiles. The armor adds a weight of 625.7 kg, which is a significant weight. However, compared to the armor of an A-10, this is relatively light; the titanium armor of the A-10 weighs 540 kg [12], while only protecting a single pilot. Furthermore, as steel has significantly lower material and production costs, the armor will be cheaper too.

Next, a big bubble shaped canopy was placed on top of the cockpit, to maximize the crew's visibility. It was shaped by trying to avoid big slopes, while giving the pilots enough room overhead. Lastly, the cockpit fuselage was closed off with a nosecone. Focus has been put on rounding all interfaces between segments.

To increase the vision angles of the crew, it was decided to augment the viewing angles by using fuselage mounted cameras and screens in the cockpit and helmets. This is further discussed in [section 11.5](#).

³LAA-STR-CRW-1.1: The aircraft shall be able to fit two crew members.

6.3. Fuselage

A factor that influences the shape of the fuselage is the flight speed. However, this only becomes visible when flying in trans- and supersonic flight regimes. When reaching those speeds, the fuselage has to be designed with the Whitcomb area rule in mind, where the cross sectional area of the entire aircraft has to stay as constant as possible, to reduce the formation of shocks⁴. Since the A-20 does not reach transsonic speeds, the shape of the fuselage was based on the shape of the cockpit. The fuselage was originally designed to be 12 m long to fit in a 40 ft shipping container. However, during the empennage sizing, as further discussed in [chapter 8](#), the decision was made to increase the fuselage to 15 meters. This decision was made to increase the tail arm, which would result in a smaller empennage. The fuselage will still fit in a shipping container, as specified in [chapter 15](#). However, the container size had to be increased to 53 ft. The task of the remaining fuselage is to connect cockpit, wing and empennage while also housing the electric and hydraulic subsystems and cannons.

To be able to remove the wing for transport, the wingbox is not continuous, but split along the center line. This way, the wing can be transported in halves. To connect the halves to the fuselage, a 'socket' of the shape of the wingbox is fixed to large ribs, which connect to the fuselage. The halves can be slid in the socket and fixed by using bolts. The two GAU-19 rotary cannons and their ammunition were placed below the wingbox. They were placed such that the firing barrel sticks out of the cross section of the fuselage. To reduce drag, a fairing with cutout was placed over the cannons. To increase the tail strike angle and to lift the empennage out of the wake of the wing, the tail cone was sloped upwards.

Even though this method of sizing the fuselage might seem arbitrary, the determined fuselage diameter, length and tail cone shape fit very well into the range of reference values provided by Roskam [10].

6.3.1. Fuselage Structural Overview

The skin of the fuselage is made of quasi-isotropic carbon fiber epoxy composite. A carbon fiber composite was chosen over aluminium due to its very high specific strength, which allows to save weight. The skin is reinforced with longitudinally running aluminium stringers to carry bending moments as well as compression. Aluminium was chosen because it allows to extrude the stringer profiles, which simplifies production. Furthermore, aluminium has a high specific strength. The fuselage is further reinforced with aluminium ribs. The ribs support the skin so the fuselage cross section keeps its shape. Furthermore, they allow introducing the weight of individual components into the fuselage structure.

Since the radar is housed in the nosecone, the nosecone has to be radio transparent. Because of that, carbon fiber composites cannot be used, as they are electrically conductive. Thus, glass fiber reinforced polymers were chosen. A cross section of the fuselage can be seen in [Figure 6.2](#).

⁴<https://history.nasa.gov/SP-4219/Chapter5.html>, conducted on [18-01-2021]

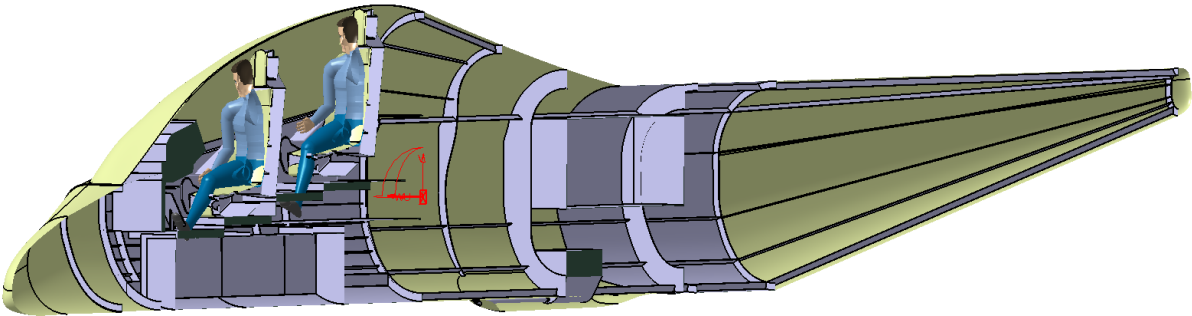


Figure 6.2: Section view of the fuselage

7 Wing Design

In this chapter the design of the wing is discussed. First, the resulted design is shown and discussed. After which the approach of the design is explained. The required area is calculated using the wing loading diagram. After this the airfoil selection, aileron sizing and flap sizing are discussed. Finally the structure of the wing is discussed.

7.1. Design Overview

The overall shape and structure of the wing is shown in [Figure 7.1](#). The wing spans 18.5 m, and has a surface area of 49 m². For the high lift devices, double-slotted Fowler flaps were selected. They span 4.3 m, at 35% of the chord starting from the fuselage. The ailerons span 3.9 m, at 35% of the wing chord, and are located as close as possible to the wing tips.

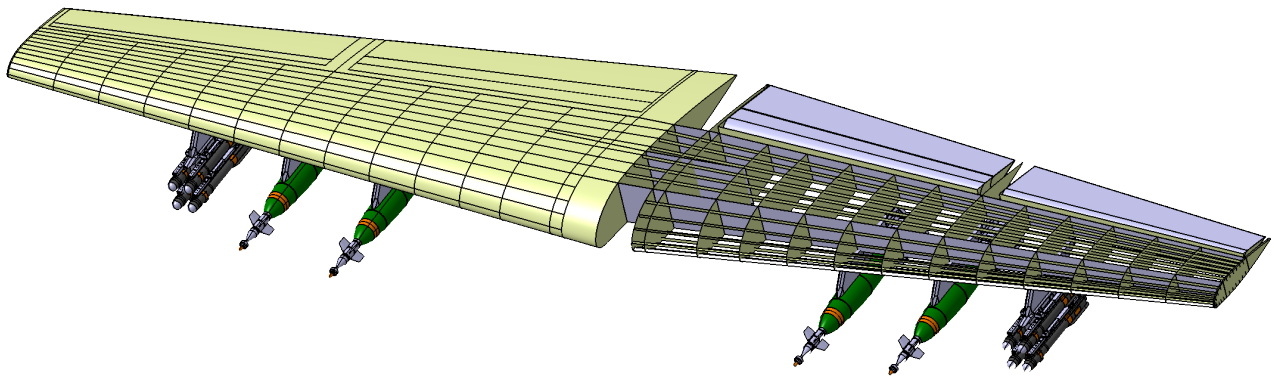


Figure 7.1: Geometry of the A-20 wing

7.2. Design Approach

During the design of the wing several steps were taken to determine the final geometry of the wing. The methods used to decide on this are explained in this section.

7.2.1. Wing/Thrust loading

To determine the wing dimensions required, a thrust and wing loading diagram, T/W-W/S diagram, was constructed. From this graph, the critical wing and thrust loading for stall speed, take off, landing, maximum cruise speed, and climb were determined. The loading diagram was constructed using the methods shown in Roskam [7], and is shown in [Figure 7.2](#). In the graph, the vertical, yellow line represents the maximum wing loading at stall conditions. In this particular case, the stall speed is chosen to be the stall speed in landing configuration at a density altitude of 6 000 ft, as it was the most critical condition.

The red line represents the relationship between the thrust and wing loading at cruise speed of 200 m/s and altitude of 10

000 ft, with a selected AR of 7. The design point should be on, or above this line. The cruise altitude was chosen to satisfy requirement LAA-PER-DSM-2.1¹.

The green line relates the thrust and wing loading in take off conditions, considering the required runway length at 6 000 ft altitude. The design point should be on, or above this line. The thrust loading will be further discussed in Chapter 9.

Looking at the the thrust and wing loading diagram, the take off requirements, and stall speed determine the design point for the thrust and wing loading. From this design point a wing loading of 2662 N/m² was found.

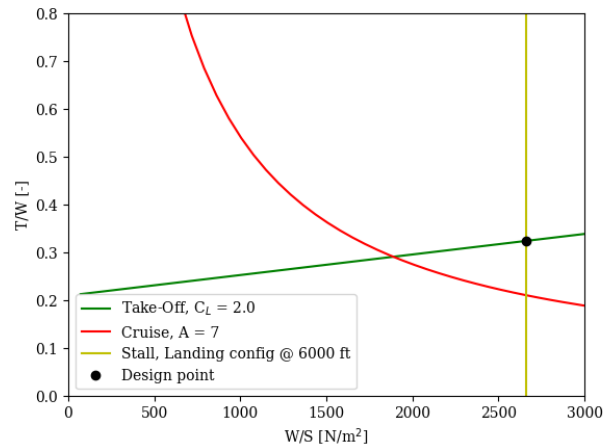


Figure 7.2: T/W-W/S diagram of the A-20

7.2.2. Wing sizing

The required wing area of 49 m² was calculated by dividing the the W_{TO} determined in chapter 5 by the W/S from the design point in Figure 7.2.

With the determined wing area, and chosen AR, the wing geometry was designed. A mid-wing configuration was chosen, as this would give the best aerodynamic performance and result in a decent wing height for maintenance. The sweep angle of the quarter-chord line $\Lambda_{c/4}$ was determined to be 0°, since the aircraft cruises at Mach 0.61, which means that it does not reach trans-sonic speeds and no sweep is required.

The taper ratio, λ , of the wing was determined as per Raymer [8]. Raymer chapter 4 states that NACA wind tunnel tests determined the taper for quarter chord sweep to achieve the elliptical lift distribution, which resulted in a 0.4 taper. This resulted in a root chord c_r and tip chord c_t of the wing. The thickness to chord ratio t/c was determined to have a maximum value of 0.18. As this leads to a better wing weight, volume and maximum lift. However, the higher t/c ratio also leads to a higher wing drag. Hence, it is advised to do a more thorough optimisation for the t/c ratio in future design stages.

According to Raymer a dihedral angle Γ of 3° should be used for an unswept mid-wing configuration [8]. The wing geometry is summarized in Table 7.1.

¹LAA-PER-DSM-2.1: The aircraft shall have a cruise altitude of at least 10 000 ft.

Table 7.1: Dimensions of the main wing

parameter	value	unit	parameter	value	unit
S	49.0	[m ²]	c_r	3.78	[m]
b	18.5	[m]	c_t	1.51	[m]
MAC	2.81	[m]	λ	0.4	[-]
Γ	3	[°]	$\Lambda_{c/4}$	0	[°]

7.2.3. Airfoil selection

In order to size the aileron and flaps, the airfoil of the wing was chosen. From the airfoil selection different parameters, such as the wing lift curve slope, wing zero lift drag and design lift coefficient, were needed in the sizing of the control surfaces.

The airfoil selection started at identifying the design lift coefficient, which was chosen as the lift coefficient used in the loiter part of the mission, as this is the most fuel intensive part of the mission. A design lift coefficient of 0.68 was chosen, as this resulted in an optimal L/D ratio. The thickness of the airfoil was also calculated in the Class I sizing. The thickness ratio was determined to be 0.18. Using a NACA 5 digit airfoil generator from *Airfoil Tools*², an airfoil was generated. As a result the NACA 44018 airfoil was selected.

7.2.4. Aileron Sizing

For the aileron sizing, the method presented in Aircraft Design, A Systems Engineering Approach by Sadraey was used [13]. To derive the required aileron size, the roll damping of the wings, the aileron effectiveness, aileron deflection, and flight speed were considered, this was done by using Equation 7.1.

$$p = -\frac{C_{l_{\delta\alpha}}}{C_{l_p}} \cdot \delta\alpha \cdot \frac{2 \cdot V}{b} \quad (7.1)$$

$C_{l_{\delta\alpha}}$ was calculated using Equation 7.2, while C_{l_p} was found by using Equation 7.3.

The limits of the integral in Equation 7.2 were used to size the aileron to achieve the required roll rate of 90° in 1.3 seconds, as per military specifications. This roll rate has to be reached during all stages of flight. To size the ailerons for the most critical flight condition, the airspeed is assumed to be the flapped stall speed at sea level of approximately 40.9 m/s, or 80 kts.

As the required roll rate is quite high, the ailerons are placed outboard for maximum effect. They have an offset of 10 cm from the wingtip, to provide some space for hinge mechanisms. The lower limit was chosen such that $C_{l_{\delta\alpha}}$ is big enough to yield the desired roll rate. For the ailerons, a relative chord length of 0.35 was chosen, again to maximize the effect. This left 5% of the chord length between the rear spar and the aileron, to accommodate the hinge mechanism, a τ_a of 0.56 was used.

²<http://airfoiltools.com/airfoil/naca5digit>, conducted on [17-12-2020]

$$C_{l_{\delta\alpha}} = \frac{2 \cdot C_{l_{\alpha}} \cdot \tau_a}{S \cdot b} \cdot \int_{b_1}^{b_2} c(y) \cdot y dy \quad (7.2)$$

$$C_{l_p} = -\frac{4 \cdot C_{l_{\alpha}} + C_{d_0}}{S \cdot b^2} \cdot \int_0^{b/2} c(y) \cdot y^2 dy \quad (7.3)$$

Using the equations stated above, it was found that the required aileron span was 3.9 m, while having a symmetric deflection of ± 30 degrees. This led to a single aileron area of 2.4 m². The results have presented in [Table 7.2](#) on the left hand side.

There are multiple ways of augmenting the roll of the aircraft. One option is the addition of spoilers to use them as spoilerons. Spoilerons have the advantage, that they can negate the adverse yaw effect of ailerons. This makes the aircraft easier to fly, as it leads to a partial decoupling of roll and yaw. It also makes the integrated guns easier to target, as small roll corrections do not lead to a yawing moment and thus do not bring the guns off target. Furthermore, the ailerons could be made smaller, while achieving the same roll rate. However, the addition of spoilers would add more moving parts, which leads to an increase in weight, complexity and cost, while impacting the reliability negatively. This also increases the required maintenance time and cost.

Another way of augmenting the roll, is using the tail control surfaces as tailerons. However, this requires a mixing of control surfaces, which in turn requires a more complex control and flight augmentation system. It would also reduce the elevator authority if roll and pitch are used at the same time, which then requires bigger elevators.

The flaps could be used as well, making them flaperons. However, as calculations in [subsection 7.2.5](#) show, the aircraft requires more complex flap systems, that typically are less suitable for the use as flaperons due to their slow deployment speed.

Lastly, it has to be considered if it even is necessary to augment the roll to reduce aileron size. The ailerons are very large, but when visually comparing them to ailerons of similar aircraft, such as the A-10 and Super Tucano, one finds that they are very comparable in proportion. On the other hand, a reduction in aileron size would increase the available area for flaps, allowing the use of simpler flap systems. However, as discussed in [subsection 7.2.5](#) it would not significantly reduce the flap complexity. Thus, a roll augmentation was not further considered.

7.2.5. Flap Sizing

Based on the required $\Delta C_{L_{\max}}$, the method described in Torenbeek, appendix G, was used in order to determine the required wetted flap area [14]. The results are given in [Table 7.2](#) on the right hand side.

One has to keep in mind that not the entire wing span is available for flaps, as a part is covered by ailerons and another part lies within the fuselage. In order to meet the required $\Delta C_{L_{\max}}$, double slotted Fowler flaps were chosen. This choice comes at cost of increased complexity compared to simpler flap systems. However, the use of simpler flap systems only is possible when used in combination with leading edge high lift devices and/or when reducing the aileron size, which increases the complexity again. However, it was discussed earlier to be not implemented.

The trailing flaps take up 35 % of the chord, leaving a space of 5% of the chord between flap and rear spar to accommodate the hinge mechanism. Together with the required area, the span of a single flap was found to be 4.3 m in span, measured from

the fuselage.

Table 7.2: Results from the aileron and flap sizing

parameter	value	unit	parameter	value	unit
p	1.21	[rad/s]	$\Delta C_{L_{\max}}$	1	[-]
c_a/c	0.35	[-]	c_f/c	0.35	[-]
δ_a	± 30	[°]	δ_f	40	[°]
$b_{a,1}$	5.3	[m]	$b_{f,1}$	0.6	[m]
$b_{a,2}$	9.2	[m]	$b_{f,2}$	4.9	[m]
$S_{\text{aileron, total}}$	4.8	[m ²]	$S_{\text{flap, total}}$	9.4	[m ²]

7.2.6. Structure

The main structural components of the wing are spars, ribs, skin, and stringers. The ribs help to maintain the aerodynamic profile. Furthermore, they introduce the loads from the skin into the spars. The spars take up the load exerted on the wing and resist bending and torsion. Furthermore, longitudinal stringers are used to reinforce the skin against buckling. Ribs, spars and stringers are made of aluminium

The wing has a multi-spar construction. There are 2 spars running along the entire wing span. To support the main landing gear, there is a third spar, which extends from the wing root to the main landing gear. The aircraft has 14 ribs per wing. There is a rib at every location where a load is introduced, such as the hard points, landing gear, and control surfaces. The skin and control surfaces are made carbon fiber epoxy composite. Again, carbon fiber composites were chosen due their very high specific strength. The structure of the wing can be seen in [Figure 7.3](#).

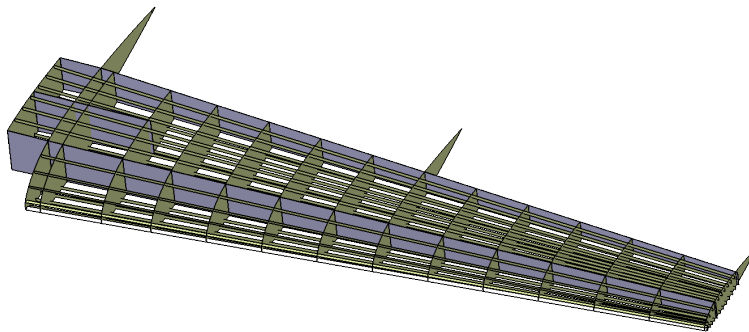


Figure 7.3: Catia render of the wing structure

8 Empennage Design

In this chapter the empennage design is discussed. The empennage is sized with regard to the center of gravity, c.g., which is dependent on the wing position. For the controllability and stability requirements to be met, the c.g. range of the aircraft, given a certain wing position, should lie between the X-plot lines, which will be further discussed in [section 8.2](#). Furthermore, the structure of the empennage is explained. A sensitivity analysis for assumed values in the empennage design is given, of which a justification of the assumed values are given in the verification and validation. Finally, the integration between the Class I, Class II, c.g. analysis and X-plot is briefly explained.

8.1. Design Overview

In [Figure 8.1](#) the overall shape of the empennage is presented. The entire empennage uses a symmetric NACA-0010 airfoil. The horizontal stabilizer has a span of 7.7 m and an AR of 5.8. The horizontal tail has a constant chord of 1.3 m over the entire span. The vertical tails have an individual span of 2.7 m and an AR of 2.7. The vertical tails have a root chord equal to the chord of the horizontal tail and has a taper ratio of 0.5.

The horizontal tail is fitted with two elevators which both span 3.5 m over 25% of the chord. The vertical tails are likewise fitted with rudders spanning 2.4 m over 25% of the chord.



Figure 8.1: Catia render of the empennage

8.2. Design Approach

The empennage design was sized using a combination of a loading diagram and an X-plot. The loading diagram shows the c.g. of several loading configurations of the aircraft with regards to the wing position, while the X-plot analyzes the static stability and control of the aircraft. The combination of the two plots gives a position of the wing and the horizontal tail surface area.

8.2.1. Loading Diagram

The loading diagram analyzes several loading scenario's with regards to payload. Possible combinations of attached stores, ammunition and fuel were considered. Item 1 from the list below portrays the standard mission profile, while items 2 and 3 sketch special cases of the loading diagram.

1. 2400 round of ammunition, the payload weight attached to the hardpoints and fuel required for the mission flight profile, as seen in [Figure 2.1](#), i.e. 477 kg ammo, 1361 kg on the hardpoints, and 4199 kg fuel.
2. Only the ammo for the integrated gun is considered and fuel required for the mission flight profile, i.e. 477 kg of ammo, and 4199 kg fuel.
3. The maximum weight of the payload is attached under the hardpoints and fuel required for the mission flight profile, i.e. 1361 kg of armament on the hardpoints, and 4199 kg fuel.

A combination of loading procedures was used to plot a loading diagram. It was assumed that there is no specific loading procedure for the military aircraft. Hence, a different plot was observed, unlike the ones seen for commercial aircraft, that implements the "window-aisle" procedure [14]. Also including the fuel stored inside the wings, this results in 4 scenario's that are plotted.

The payload on the hardpoints is assumed to be located on the same longitudinal position. These are typically located from the leading edge spar till the trailing edge spar. The armament attached to those hardpoints have to protrude out from the wing planform for sufficient clearance. Therefore, the c.g. location of the payload attached to the hardpoints are assumed to be located at the front spar of the Mean Aerodynamic Chord, i.e. 20% of the MAC. Therefore, the linear variance due to the sweep at the leading edge is neglected.

[Equation 8.1](#) gives an equation of the c.g. shift per weight component. The OEW was used as starting value. Afterwards several combination of the items, i.e. the ammo, the fuel and the payload attached on the hardpoints, are used as item. For each new contribution, the weight and the location of the previous calculation was used as input for the subscript "old".

$$x_{c_{g_{new}}} = \frac{x_{c_{g_{old}}} \cdot m_{old} + x_{c_{g_{item}}} \cdot m_{item}}{m_{old} + m_{item}} \quad (8.1)$$

For the fuel location, Torenbeek was used to obtain the lateral fuel c.g. location with respect to the fuselage symmetric line. It is considered that the fuel is stored between the spars, located at 20% and 60% of the local wing chord, whereby the longitudinal c.g. position of the fuel stored in the wing is located in the middle of the spars, at 40% of the local wing chord [14].

An additional margin of 2% was added after all scenario's was plotted for the outer values, in order to account for c.g. variations due to landing gear retracting, and other movable items. This yielded the maximum and minimum locations of the c.g. locations.

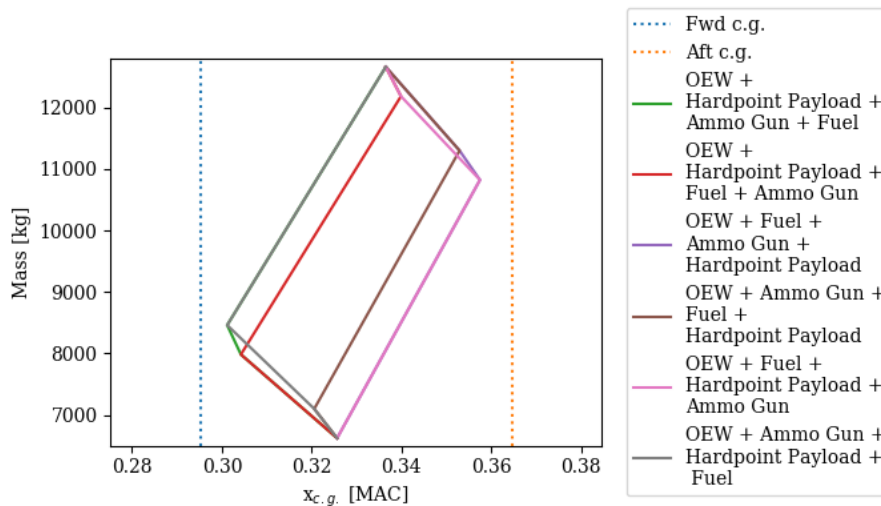


Figure 8.2: Loading diagram of the six possible load paths.

Finally, a graph was made using the maximum and minimum location as mentioned above and was plotted according to variable wing positions, by changing the longitudinal position of the leading edge MAC, x_{LEMAC} , for several positions, a c.g. range diagram was created. In Figure 8.3, they are plotted as the dashed and dotted lines. The dashed lines represent the most forward c.g., while the dotted lines represent the most aft c.g.

8.2.2. X-plot

The X-plot in figure Figure 8.3, which is represented by the solid line, presents the controllability line and the stability lines of the aircraft. There are two stability lines, one without stick-fixed static margin, S.M., and one including an S.M. The S.M. is usually applied to account for stick-free stability and stick forces. However, in this aircraft a fly-by-wire system is applied, so the stick forces are not considered. Therefore, a S.M. of 5% was chosen to account for the stick-free stability. The controllability line and the stability lines were created using the methods provided by Torenbeek [14]. The input variables and intermediate values for the values are given by Table 8.1. It should be noted that for stability, the values for some parameters are different because they were analyzed for landing.

Table 8.1: Input/Intermediate values for constructing the X-plot

Control		Stability	
Parameter	Value	Parameter	Value
$C_{L_{A-h}}$	2.6	$C_{L_{\alpha_{A-h}}}$	5.60
C_{L_h}	-0.629	$C_{L_{\alpha_h}}$	5.57
$C_{m_{ac}}$	-0.508	S.M.	0.05
\bar{x}_{ac}	0.206	\bar{x}_{ac}	0.213
l_h	6.82	l_h	6.82
\bar{c}	2.81	\bar{c}	2.81
$\left(\frac{V_h}{V}\right)^2$	0.85	$\left(\frac{V_h}{V}\right)^2$	0.85

The c.g. of the aircraft should be on the right of the controllability line for the aircraft to be controllable and on the left of the stability line including S.M. to be stable. To see where the c.g. fits between the X-plot, the c.g. range diagram is merged on top of the X-plot. Then the c.g. range diagram is shifted up or down to fit the most forward and most aft c.g. on the X-plot lines, this results in the minimal required tail size, S_h , and a x_{LEMAC} appropriate to that size. After finding these values, a new iteration on the Class I and Class II estimations were done. After which the same process with the c.g. plot and the X-plot was carried out. After the first iteration, it was concluded that it would be beneficial to increase the fuselage length to 15 meters to reduce the tail size. The final iteration then led to a x_{LEMAC} at 6.55 m as measured from the nose and a horizontal tail to wing surface ratio of 0.22. The X-plot and the corresponding c.g. range diagram can be seen in figure 8.3.

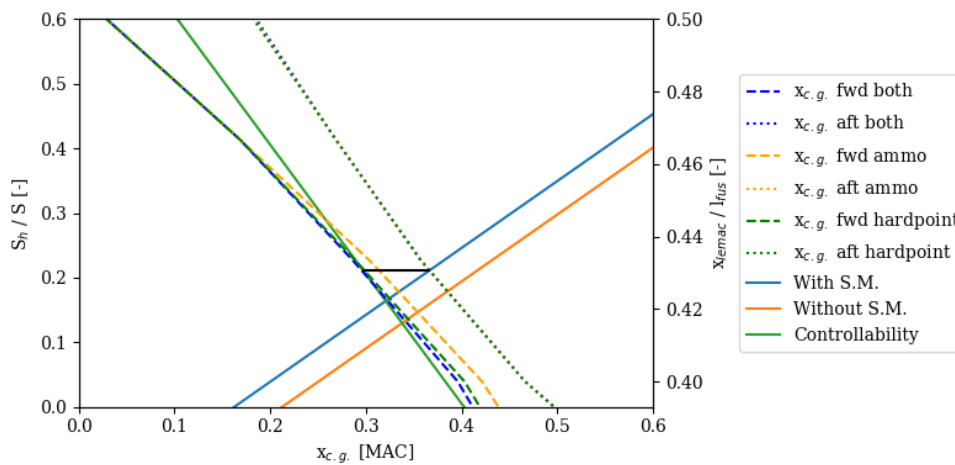


Figure 8.3: X-plot including c.g. range diagram.

8.2.3. Structural overview

The empennage structure is very similar to the structure of the wing. Ribs help maintain the aerodynamic shape of the surfaces and introduce the loads from the skin into the spars. The spars run along the span of the horizontal and vertical stabilizer and transfer the load into the fuselage structure. The skin is reinforced by stringers. The empennage structure is shown in Figure 8.4

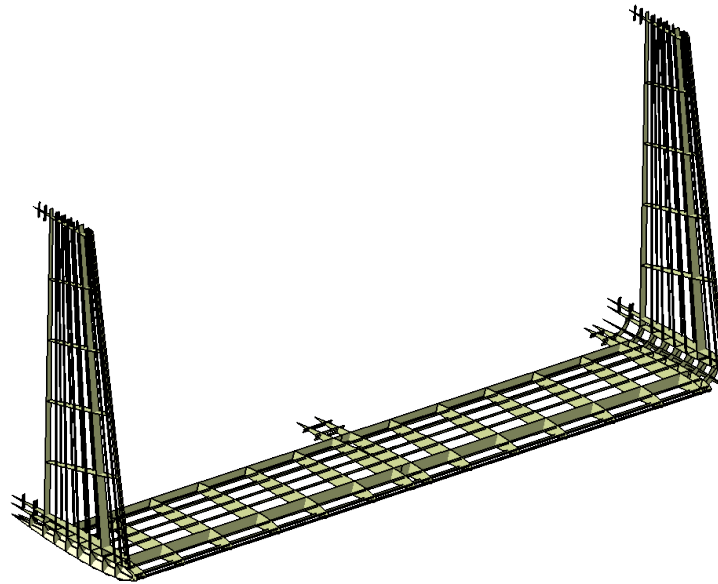


Figure 8.4: Catia render of the empennage structure

Again, stringers, ribs and spars are made of aluminium. The skin is made of carbon fiber composite, again. However, the inboard side is fitted with Titanium sheet metal, to prevent local hot spots, due to impinging engine exhausts.

8.3. Sensitivity Analysis

In [section 8.2](#), multiple parameters were assumed. In the sensitivity analysis these input variables are given a slight change, in order to see how the corresponding output values change.

For the loading diagram, the c.g. location of the the hardpoint positions, the ammo position and the fuel location were varied along the longitudinal axis, as these numbers were assumed. The [Table 8.2](#) shows the sensitivity analysis given the changes.

The locations that were used as sensitivity analysis for the c.g. range, showed that the forward and aft c.g. increase or decrease accordingly with the change that was made for the input variables. For the top row, the initial values were used with a 2% margin. The values given in the other rows are shown without the 2% margin. The 2% margin was not given here, in order to see whether they fall within the given margin.

8.4. Verification and Validation

In this section, the verification and validation of the tools, used to determine the empennage sizing in [section 8.2](#), is carried out. It also gives the integration of Class I, Class II, c.g. analysis and X-plot, as a consequence of the empennage sizing.

8.4.1. Verification and Validation of c.g. analysis

As verification for the weight components, all possible loading procedures were added. These were then checked whether, after adding all components, the c.g. location converge to the same point. An example of this convergence can be seen from [Figure 8.2](#).

Table 8.2: Sensitivity analysis of c.g. range

Initial values with 2 % margin					
$x_{cg_{payload,hardpoint}}$	$x_{cg_{ammo}}$	$x_{cg_{fuel}}$	Forward c.g. [%MAC]		Aft [%MAC]
7.121	7.976	7.713	0.293		0.370
changes in $x_{cg_{payload,hardpoint}}$ (on TE spar, TEMAC, LEMAC respectively) without 2% margin					
$x_{cg_{payload,hardpoint}}$	$x_{cg_{ammo}}$	$x_{cg_{fuel}}$	Forward c.g. [%MAC]		Aft [%MAC]
8.262	7.976	7.713	0.318		0.387
6.551	7.976	7.713	0.265		0.363
9.402	7.796	7.713	0.318		0.438
changes in $x_{cg_{ammo}}$ (on LE spar, TE spar, respectively) without 2% margin					
$x_{cg_{payload,hardpoint}}$	$x_{cg_{ammo}}$	$x_{cg_{fuel}}$	Forward c.g. [%MAC]		Aft [%MAC]
7.121	7.713	7.713	0.270		0.352
7.121	9.402	7.713	0.299		0.399
changes in $x_{cg_{fuel}}$ (on 30%, 50%, 35%, 45% of the local chord respectively) without 2% margin					
$x_{cg_{payload,hardpoint}}$	$x_{cg_{ammo}}$	$x_{cg_{fuel}}$	Forward c.g. [%MAC]		Aft [%MAC]
7.121	7.976	7.413	0.298		0.338
7.121	7.976	8.013	0.299		0.401
7.121	7.976	7.563	0.298		0.344
7.121	7.976	7.863	0.299		0.382

Similarly, the contribution of the c.g. location were checked and whether they impact the loading diagram as expected. When increasing the weight of a component ahead of the $x_{cg_{oeiw}}$, the c.g. location of the combined load must shift forwards to the LEMAC. When the weight of a component behind the $x_{cg_{oeiw}}$ was increased, it was observed that the c.g. location of the combined load was shifted aft.

Additionally, when moving the c.g. location of a component towards the LEMAC, the combined c.g. location shifted forwards. While moving the c.g. location of a component towards the trailing edge of the mean aerodynamic chord, the combined c.g. location shifted backwards.

These results showed that the weight components were adopted correctly into the calculations and shift the c.g. location accordingly with component c.g. location and weights.

Another aspect that was checked, was regarding the loading order, as observed in the loading diagram. For commercial airlines, a typical loading procedure is adopted, such as the window-seating rule. However, for military aircraft there is no significant procedure to be taken into account. The hot-pit refueling also further emphasizes on having no strict loading order, as the aircraft has to re-arm and re-fuel simultaneously. This was taken into account for the loading diagram, by taking all loading procedures, the variety of loading procedures are observed in [Figure 8.2](#). This resulted in a wider array of c.g. margins.

Regarding the sensitivity analysis that was carried out, some values represented fall outside the c.g. range with 2% margin. However, these values are justified to be never the case of the aircraft and do not pose any threats to the balance of the aircraft.

First regarding the c.g. ranges outside for shifting the payload on the hardpoints. For the changes in $x_{cg_{payload,hardpoint}}$ it is highly unlikely that the c.g. locations are located in front of the LE spar or behind/at the TE spar. Moreover, as the payload on the hardpoints must protrude the wing planform for a small section due to clearances, the initial assumption of the c.g. location

to be placed on the front spar is taken as reasonable.

For the changes in $x_{cg_{\text{ammo}}}$ the ammo for the integrated gun is also unknown. However, given the fact that the guns themselves are placed behind the LEMAC, the ammo must be stored close to this location. Additionally, the ammo location is considered a design choice. Hence, it should be placed, such that it falls within the initially set c.g. range.

Despite this being a design choice, certain factors had not been considered for the integration of the entire design. For example, when adding the ammo at the pre-determined location, the fuel tanks inside the fuselage, the landing gear and the available cross-sectional area of the fuselage at this location should also be considered.

As future recommendation, these should be taken into account by making a sketch and confirm the available space.

Lastly, it was assumed that the c.g. location of the fuel is placed 40% of the local chord, which was calculated using Torenbeek [14]. Given the upwards dihedral, the fuel is depleted from the tip to the root, which means the c.g. location of the fuel moves backwards. According to [Table 8.2](#), a c.g. location shift forwards would still fall within the margin that was given, which is the opposite direction of what would be the case. However, considering that there is little sweep and the fuel tanks themselves are rectangular, the c.g. would not shift drastically, and thus not fall beyond the 45% of the local chord.

8.4.2. Integration of Class I, Class II, c.g. analysis and X-plot

As a final check, all procedures have been followed from the Class I estimation, the Class II estimation, the c.g. curve and finally, the X-plot. The methods used for first class estimation and second class estimation have already been checked in previous steps of this project and are assumed to be verified and validated. Adding the contribution of the current step, all steps were followed and seen if the components converge to a same point. This was indeed observed after several iterations.

9 Propulsion Unit Design

The propulsion system shall provide the required thrust/power in all flight phases. It should be reliable, and as economical as possible. As the aircraft enters service in 2025, this gives little time for engine manufacturers to build a new engine. Therefore, the chosen engine is based on an existing engine with modifications. This chapter explains the engine sizing method.

9.1. Design Overview

The two most realistic design options for the propulsion system were a turboprop and a turbofan. The turbofan was selected because of its smaller size. The turboprop engines required very large diameter propellers, which heavily impacts the placement of the engines and the aircraft ground performance. Furthermore, large propellers are an easy target. Having more freedom when it comes to the engine placement, allows for better protection from enemy fire. Furthermore, turbofan engines are capable of reaching a higher cruise speeds. As the required cruise speed of Mach 0.6 is on the high side for turboprop engines, the turbofan was chosen. The propulsion system was designed with survivability in mind. The aircraft has two engines, so it is still able to fly in case one engine is hit, or fails. The engines are mounted between wing and empennage, and placed high on the fuselage to avoid ingestion of dirt/debris on the austere field. The engine inlets are covered by the wing when looking at the airplane from the ground at an angle. This makes them harder to target than wing-mounted engines. Furthermore, the hot exhaust is partially covered by the horizontal tail plane, which reduces the susceptibility to heat-seeking missiles from the ground. To reduce the heat signature even more, a mixer was added, which mixes the hot gases from the engine core with the colder gases from the bypass flow. An added benefit of the mixer is a reduction in noise emission and an increase in efficiency, at the cost of extra weight.

9.2. Design Approach

To determine the required thrust, one has to go back to the wing and thrust loading diagram discussed in [chapter 7](#), shown in [Figure 7.2](#). To construct the green line of the graph, the take off requirements had to be considered. LAA-PER-DSM-1.1¹ states that the aircraft shall be able to take off over an obstacle within a distance of 4 000 ft. This is mostly impacted by the thrust and wing loading. The allowable wing loading already was determined in [chapter 7](#), leaving only the thrust loading.

The methods of Roskam were used to relate the take off distance to the allowable ground run [10]. The allowable ground run is shorter than the takeoff distance, since the takeoff distance also includes and air born phase up to the obstacle. The ground friction coefficient of 0.17 for this method was determined from the required CBR 5 air field, which corresponds to a very soft grass field [15]. The cruise performance was also analyzed, but since is was not the limiting factor for the design, it will not

¹LAA-PER-DSM-1.1: The aircraft shall be able to take off over a 50 ft obstacle within a distance of maximum 4 000 ft at a density altitude of up to 6 000 ft on runways with CBR 5.

be elaborated further upon.

The required thrust of 42 kN was determined from the design point on the wing/thrust loading diagram, discussed in [subsection 7.2.1](#). As the aircraft features two engines, the required thrust per engine is 21 kN. The engines were sized, based on a reference engine with similar thrust, the P&W305B by Pratt & Whitney. An initial "rubber sizing" was done by directly scaling the size and weight from the reference engine, by the reference engine thrust compared to the required thrust. The engine nacelle was sized according to the methods of Torenbeek [14]. The total length of the engine is 2.8 m, and the diameter is 0.87 m, including nacelle. The bypass ratio of 4.3 is the same as the reference engine.

10 Landing Gear Design

In this chapter, a brief description of the landing gear design is given, after which the design approach is discussed. Finally, the sensitivity analysis and verification and validation are discussed.

10.1. Design Overview

To size the landing gear, there are three major components to be considered; location, strut length and tire dimension. The nose landing gear was placed 3.5 m in front of the most aft c.g.. The the main landing gear was placed 0.45 m behind this c.g.. Furthermore, the track of the main landing gear was determined to be 4.2 m. Moreover, the strut length for nose and main landing gear was set so the fuselage is 0.97 m above the ground. Lastly, the tire dimensions were determined by the contact loads and runway surface. The nose landing gear is fitted with two 6.00-6 tires. The main landing gears are both in double-bogie configuration, with four 8.50-10 tires per strut.

10.2. Design Approach

First, the configuration of the landing gear was determined. It was decided to use a conventional tricycle configuration with a steerable nose landing gear. This allows to steer on the ground, while giving a high ground clearance and an advantageous load distribution. It was decided to make the landing gear retractable, which drastically reduces drag in flight. The nose landing gear is stored in the fuselage under the cockpit, while the main landing gear is stored in fairings under the wing. All gear legs fold forward, so that in case of a hydraulics failure, they can be released so gravity and the air stream lock the landing gear in place.

Afterwards, the longitudinal position of the main landing gear was determined. For that, Roskam's method for positioning the landing gear was followed [7]. If the landing gear is too far aft, it becomes difficult to rotate around the pitch axis during take off. If it is too far to the front, the aircraft can tip over onto its tail. Additionally, the tail strike angle has to be considered as well, so that the tail does not strike the ground when landing at a high angle of attack or when performing a cross wind landing with a bank angle. Just before the landing, the aircraft flies at an angle of attack of 13° . Furthermore, a bank angle of 8° was accounted for, as it brings the horizontal tail closer to the ground. These angles together lead to a required tail strike angle of 17° . Considering all aforementioned points, a ground clearance of 0.97 m, with respect to the bottom of the fuselage, and a distance of 0.45 m between main landing gear and aft c.g. were chosen. After that, the wheel base was determined. This was done to make sure, that the aircraft does not tip over laterally when maneuvering on the ground. The wheel base was determined to be 4.2 m wide.

Once the position of the main landing gear was determined, the load per gear strut was calculated. The distance of the nose

landing gear with respect to the aft c.g. has to be chosen such that the nose landing gear carries at least 8% of the aircraft weight, to assure controllability. Considering this, a distance of 3.5 m was chosen.

Next, requirements LAA-PER-DSM-1.1¹ and LAA-PER-DSM-5.1² were analyzed with regards to the CBR of 5. The CBR of 5 yielded a maximum allowable tire pressure of 3.5 kg/cm². The tire pressure should be equal or smaller than this value for the aircraft to not sink into the soil.

Using the maximum tire pressure and the load per gear leg, the amount of tires and the tire dimensions could be determined. The choice of the amount of wheels was done by performing a trade-off; more wheels meant a more complex and bulkier landing gear assembly, less wheels resulted in larger individual tires. As a result of using Torenbeek's method for tire selection, two 6.00-6 tires have been chose for the nose landing gear. Four 8.50-10 tires in double-bogie configuration have been chosen for each main landing gear leg [14].

10.3. Sensitivity Analysis

To see the impact for a different amount of wheels, a sensitivity analysis was made. The results can be found in Table 10.1. At first, the amount of nose wheels was reduced to one, while keeping the amount of main wheels constant. After that, the amount of nose wheels was set to its original number of two and the amount of main wheels was halved to four. The tire size changes due to varying amounts of wheels then were compared to the initial sizes. It showed that the size of the tires increased by about 25-50% when the amount of tires was halved. Since the tires already were very big and the landing gear assemblies were very bulky, the amount of wheels was left unchanged.

Table 10.1: Sensitivity analysis of landing gear tire size. For better size comparison, the tire sizes dimensions were converted to meters.

Initial tire size			
#Nose wheels	Tire size nose wheels: outer tire diameter [m] X tire width [m]	#Main wheels	Tire size main wheels: outer tire diameter [m] X tire width [m]
2	0.45 X 0.15	8	0.65 X 0.25
Reducing number of nose wheels			
#Nose wheels	Tire size nose wheels	#Main wheels	Tire size main wheels
1	0.65 X 0.25	8	0.65 X 0.25
Reducing number of main wheels			
#Nose wheels	Tire size nose wheels	#Main wheels	Tire size main wheels
2	0.45 X 0.15	4	0.82 X 0.31

¹LAA-PER-DSM-1.1: The aircraft shall be able to take off over a 50 ft obstacle within a distance of maximum 4 000 ft at a density altitude of up to 6 000 ft on runways with CBR 5

²LAA-PER-DSM-5.1: The aircraft shall be able to land over a 50 ft obstacle within a distance of maximum 4 000 ft at a density altitude of up to 6 000 ft on runways with CBR 5.

11 Additional Subsystems

Now that the aircraft has been scaled and all geometric values are known, the subsystems can be designed. Although most of these subsystems are generally not visible when looking at an aircraft, they should still be included and thought off. In this chapter the fuel system, hydraulic system, electrical system, environmental control system, and avionics and sensors are discussed.

11.1. Fuel System

The fuel system configuration was mainly determined by the location of the fuel and the location of the engines. The fuel was considered to be located in self-sealing tanks between the main spars, while the engines are located above the wings and are mounted on the fuselage, as could be seen in the three-view drawing in [Figure 4.11](#).

It was chosen to have a fuel pump system in order to ensure a constant fuel flow to the engines and APU. In [Figure 11.1](#) a schematic of the fuel system is given, do note that this is a simplified schematic to give a general overview of the system.

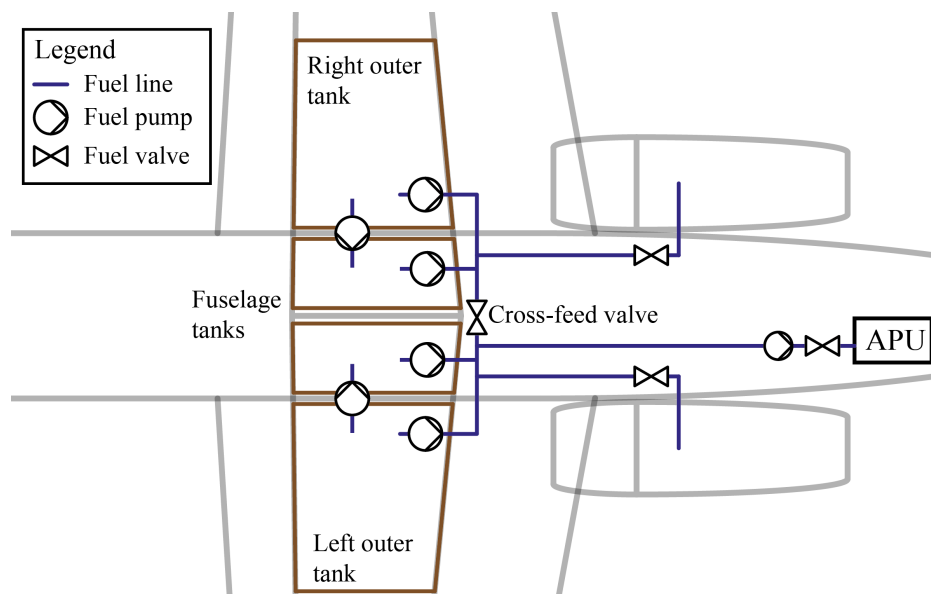


Figure 11.1: Simplified schematic of the fuel system

There are two options for fuel systems, a gravity-feed system and a fuel-pump system¹. As the engines are placed above the fuel tanks, the fuel-pump system was chosen. Next to this, as the aircraft is an attack aircraft, which can experience high maneuver loads, the fuel pump is needed in order to ensure to constant feed of fuel to the engines. There are two types of pumps chosen; the transfer pump and the boost pump. The transfer pump was used for transfer of fuel between different tanks,

¹<https://www.flightliteracy.com/aircraft-fuel-systems-part-one/>, conducted on [06-01-2021]

the boost pump would provide the engines with fuel [16].

As the fuel tanks were sized in order to fit the required fuel for the loiter mission, requirement LAA-PER-DSM-3.1² and LAA-PER-DSM-5.2³ can be checked off.

11.2. Hydraulic System

The hydraulic system is used to actuate several aircraft components. For this aircraft, the hydraulic system is designed to actuate control surfaces, landing gears, braking and steering. An Electric-Hydrostatic Actuation, EHA, system was chosen as the hydraulics system, which consist of multiple, self-contained hydraulic systems at the actuation points and is controlled by an EHA-processor, the EHA-CPU. In [Figure 11.2](#) an overview of the electric-hydraulic system can be found, the electric system will be further elaborated in the next section.

Looking at the similar aircraft and current trends, it was decided to use Electro-Hydrostatic Actuation system. The system is self-contained and only needs electrical power in order to operate. In addition, the system aids to reduce the aircraft weight, thanks to the scaled size for each point of actuation, which can results in a saved weight of up to 5 kg per actuator⁴.

As mentioned, the EHA system requires electrical power to operate. As there are two systems that can provide power to the system, this will add redundancy. It was chosen to have redundant actuators at the ailerons, flaps and main landing gear in order to still be used when one actuation point fails. Next to this redundancy, the total hydraulic system will be more reliable, as each actuation point has its own hydraulic system.

11.3. Electrical System

As the hydraulic system is dependent on the electrical system, redundancy is key. To ensure redundancy, two separate system have been implemented into the aircraft. Each system consists of a power delivery system, PD, a battery and the flight control computer, FCC, connected to this is the EHA-CPU for the hydraulic actuation. The cockpit power is distributed in the cockpit-distributor, CD. For power generation two starter-generators, S/G, are implemented on the engines. For auxiliary power, an auxiliary power unit, APU, is fitted at the rear of the aircraft. The starter-generators are connected to each PD, the FCCs can be powered by both PDs. An overview of the electric-hydraulic system can be found in [Figure 11.2](#), the redundant electrical lines are indicated as dotted lines. As discussed earlier, the power for the aircraft is generated by two starter-generators and an APU. The starter-generator is used in order to start the engines with the help of the APU and batteries. When the engines reach a self-sustaining speed, the starter-generator is used for generation of power. This start-up sequence can be done within 5 minutes, checking off requirements LAA-PAP-DSM-1.1⁵ and LAA-PAP-DSM-1.2⁶.

The APU is a second power source for the aircraft electrical system. As the hydraulic system is powered by the Flight Control Computer, it is necessary to ensure there is enough power to be used in all flight stages. As discussed before, the APU is also used in order to start the engines.

²LAA-PER-DSM-3.1: After the initial cruise phase, the aircraft shall be able to loiter for 4 hours at an altitude of 3 000 ft, without dropping stores.

³LAA-PER-DSM-5.2: After landing, the aircraft shall have enough reserves for a climb to 3 000 ft with following loiter period of 45 minutes.

⁴<https://www.mobilehydraulictips.com/electrohydraulic-actuation-technology-improving-global-aviation-industry/>, conducted on [08-01-2021]

⁵LAA-PER-DSM-1.1: Warm-up shall take no longer than 5 minutes.

⁶LAA-PER-DSM-1.2: Shutdown shall take no longer than 5 minutes.

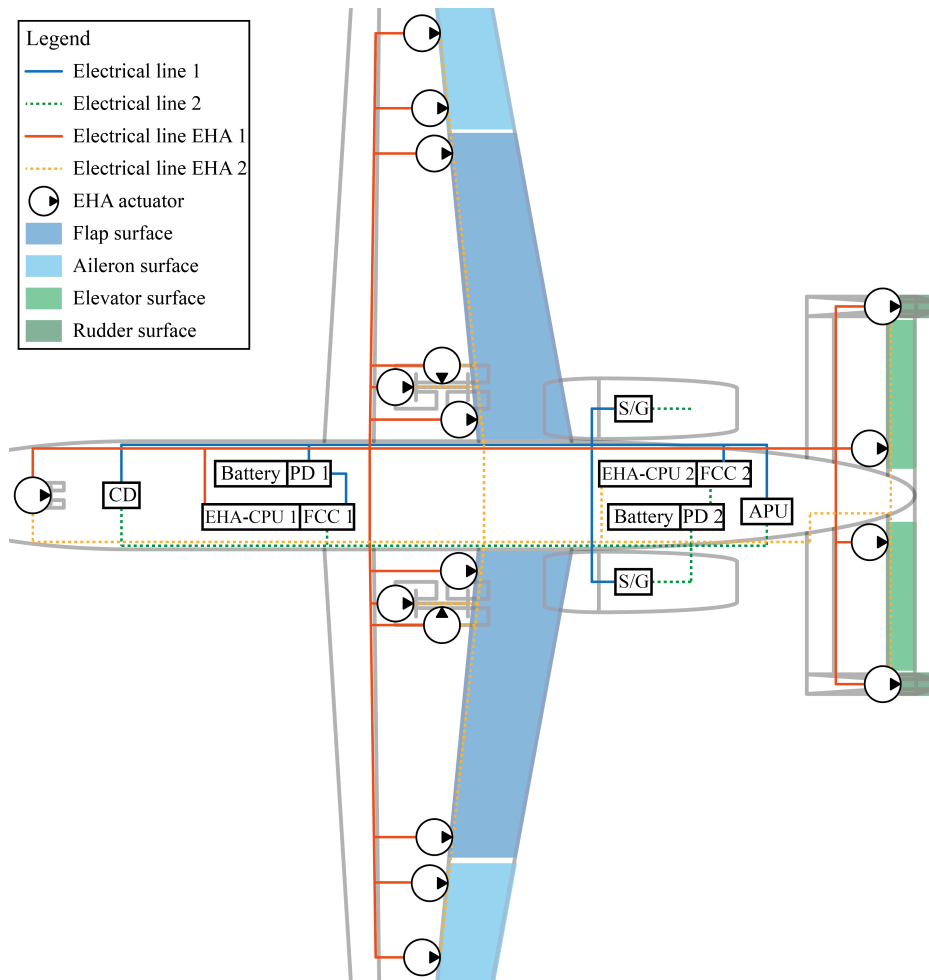


Figure 11.2: Schematic of the electric-hydraulic system

11.4. Environmental Control System

The overall function of the environmental control system, ECS, is to provide pressurization and thermal control of the cabin for the crew. Even though the cabin is pressurized, the crew will still be equipped with an oxygen mask. The reason for this is that it can supply pressured air during high load maneuvers, giving a higher g tolerance [17]. Furthermore, it can supply the crew with oxygen in case of emergency, like a pressure drop in the cockpit, an internal fire, or when operating in hazardous environments.

For the thermal control system it was found that it is desired to keep the cockpit temperature below 28° C [18]. The ECS system works collaboratively with a pneumatic system known as Engine Based Air System. In addition to that, the cabin is also equipped with pressure valves to regulate the interior pressure by entering high pressure bleed air [19].

The pressurization of the cabin is chosen to increase linearly with increasing height. This is for having a lower stress on the airframe. It was decided that the pressure of the cabin will follow the trend of an average fighter aircraft which is as follows: the cabin is under-pressurized for altitudes up to 8 000 ft, for altitudes higher than this, the pressurization system will keep the

cabin pressure at the pressure of 8 000 ft which is at 10.92 psi, or 565 mmHg.⁷

It was recommended to take a closer look at the design of the thermal control system in future design stages.

11.5. Avionics and Sensors

The data handling and avionics system consists of sensors, data processors, actuators and distributors. The chosen system architecture for this aircraft is a federated architecture. In this type of system, the hardware of the control system is distributed over the locations of application, while the software is centralized. Even though the software is centralized, there are multiple computers. These computers work in parallel for the sake of redundancy. A federated structure is not the lightest architecture, but it is still lighter than a system in which both hardware and software are centralized. In comparison to other configurations, this control system is also known to be cheaper and easier to maintain because it is easier to reach the localized hardware [20]. It was decided to fit the A-20 with a fly-by-wire system. This was done to allow for an augmentation of the flight behaviors. This comes in handy in case control surfaces are hit, because the system can compensate by using the other control surfaces. This increases redundancy and reduces pilot work load in case of a damage. Furthermore, it allows to use control surfaces without trim tab, as the control surfaces can be adjusted accordingly, without that the pilot has to handle the load. Lastly, it allows for the use of PID controllers, as discussed in [section 13.5](#). To allow the A-20 and its crew to perform all chosen missions, the aircraft has to be fitted with a variety of sensors. They are listed below.

- **Radar:** Radar utilizes radio frequency to measure the distance, angle and velocity of objects. It is mainly used to detect things such as other aircraft, weather and terrain. A typical radar system consists of a transmitter, receiver and processor. As the A-20 is not designed for air-to-air combat, the radar does not have to provide tracking/locking capabilities, which simplifies the radar system. The final radar system chosen/designed shall be in line with the MIL-STD-469B [21], which gives a thorough description of the requirements on military radar systems.
- **GPS:** The Global Positioning System (GPS), is a location technology that utilizes the run time of signals and trigonometry to identify the user's location at any time. Depending on the amount of connected satellites and the feasible amount of post processing, the position can be measured in the millimeter range. A GPS systems has to be included to effortlessly determine the position of the aircraft and to navigate to the mission area and/or target. Furthermore, the aircraft needs an interface to send GPS locations to the payload, as bombs like the JDAM or cruise missiles like the JASSM need a GPS coordinate of their target.
- **MAW:** Missile Approach Warning (MAW) systems can notify the crew of launched and approaching missiles. To do that, they either can use a Doppler radar system, or detect infrared or ultraviolet, emitted from the missiles. The radar systems can precisely determine the direction and speed of incoming missiles. However, they require complex and heavy on board systems. Infrared systems can detect the heat of the missile motor, even after it burned out. Depending on the speed of the missile, they can also detect the friction heat of the missile it self. The downside is, that they can easily be irritated by the sun or other hot objects on the ground. Ultraviolet MAW systems can not be irritated by the sun

⁷<https://www.highskyflying.com/are-fighter-jets-pressurized/>, conducted on [11-01-2021]

or ground objects, as they are 'sun-blind', i.e. they ignore the spectrum stemming from the sun. They use the UV light that comes from the hot exhaust of the missile motor. The downside is, that they cannot detect a missile after the motor has burned out. Considering that the A-20 will fly the majority of its missions close to the ground and that MANPADs are the only threat when it comes to missiles, long range missiles with long coast phases can be neglected. Thus, it can be assumed that the motor of the missile is burning for the majority of the, mostly, very short flight, which alleviates the major drawback of UV MAW systems. Thus, a sun-blind UV MAW system will be fitted to the A-20.

- **Camera:** Cameras on the aircraft can be used for multiple reasons. One reason is to reach the set requirement of the pilots' visibility, 30 degree down and forward looking, 70 degrees down and sideways looking, which could not be reached with the cockpit design. Hence, multiple fixed cameras will be included to increase the pilots field of view, giving them the ability to 'see through the aircraft'. Cameras can also be used for reconnaissance missions. They can provide intelligence on enemy forces and the terrain, which allows for a mapping of entire regions. As the A-20 also shall perform reconnaissance missions, it was fitted with a gimballed camera system with high power optics. It can also be used for acquiring targets. The system is placed in the nose of the aircraft, under the cockpit. It sits in a fuselage cutout, covered by glass, similar to the camera system of the F-35. This way it has an unobstructed view, while being protected and creating less drag.
- **FLIR:** Forward-looking infrared (FLIR), is a technique which uses infrared radiation, to create either images or video. This allows the user to find heat signatures in their surroundings⁸. This type of imagery can be used when operating under low visibility conditions or when trying to identify targets. From the interview with Pascal Smaal, a former F-35 pilot, it became apparent that many of the aircraft's missions will typically be executed during night time. Hence, a FLIR system is a necessity, as it is vital to perform missions. Again, the system also can be used for reconnaissance missions, allowing for the mapping of terrain at night, or the identification of enemy units. The FLIR system is housed in the same gimbal mechanism as the optical camera.
- **LiDAR:** Light Detection And Ranging (LiDAR) is a comparable technology to radar, however instead of radio waves it uses laser pulses to measure the distance of objects. LiDAR is mainly used for 3D imaging of surfaces, which is useful during a reconnaissance mission. Thus, a LiDAR system is included as well.
- **User interface:** The data gathered of course has to be visualized for the pilot. Modern day advancements allow for a glass cockpit⁹. However, digital instruments in the cockpit are not the only way of giving the pilot the data that is needed. The aircraft could feature a HUD, giving the pilot all the important information needed while flying the aircraft. Lockheed Martin and others took it a step further and placed it in the visor of the helmet. They also included some other functionalities, like 'looking through the aircraft' and seeing the surroundings. Although the helmet is much more expensive than a normal HUD, from the interview with Pascal Smaal it became apparent that for CAS missions, the helmet is worth it, considering the enhanced situational awareness. Hence, it was chosen to feature a modern helmet instead of an HUD.

⁸<https://www.sciencedirect.com/topics/engineering/forward-looking-infrared>, conducted on 04-01-2021

⁹<https://www.nasa.gov/centers/langley/news/factsheets/Glasscockpit.html>, conducted on 04-01-2021

12 Drag Analysis

In this chapter the drag analysis performed for the final conceptual design is discussed. Firstly, it is discussed how the first order drag analysis was performed, of which the results were used in the iterative sizing process. Secondly, the approach for the second order drag analysis is explained, after which the methods used is explained in more detail. Finally, the chapter will conclude with the results obtained from the second order drag analysis, followed by a verification of the method used.

12.1. First Order Drag Analysis

For the Class I sizing, Equation 12.1 was used to calculate the drag of the aircraft. This drag then was used in the determination of the L/D of the aircraft in both cruise and loiter. From Equation 12.1 it becomes apparent that the drag coefficient exist from two components, i.e. zero lift drag, C_{D_0} , and lift induced drag.

C_{D_0} was determined using Equation 12.2. Where the wetted area was estimated using the method provided by Torenbeek and an assumed skin friction coefficient, C_{fe} , of 0.004 as per Raymer, chapter 12.5 [8, 14]

$$C_D = C_{D_0} + \frac{C_L^2}{\pi A e} \quad (12.1)$$

$$C_{D_0} = C_{fe} \frac{S_{wet}}{S} \quad (12.2)$$

12.2. Second Order Drag Analysis

Roskam suggest that for a second order drag analysis, the drag coefficient of the aircraft can be split up in separate components of the aircraft, see Equation 12.3 [22].

$$C_D = C_{D_{wing}} + C_{D_{fus}} + C_{D_{emp}} + C_{D_{np}} + C_{D_{flap}} + C_{D_{gear}} + C_{D_c} + C_{D_{store}} + C_{D_{trim}} + C_{D_{int}} + C_{D_{misc}} \quad (12.3)$$

As drag is depending on a lot of factors such as speed, altitude, aircraft configuration etc., it has been predicted for four different aircraft configurations, which allowed for an analysis on the sensitivity of different objects creating drag.

- **Clean:** Where the aircraft is flying clean without stores, at cruise conditions.
- **Stores:** Where the aircraft is flying with stores, at cruise conditions.
- **Landing gear:** Where the aircraft is flying with stores and landing gear out, at maximum approach speed.
- **Flapped:** Where the aircraft is flying with stores, landing gear out and flaps deflected.

The clean configuration was chosen as it would be the optimal case for lowest drag the aircraft would encounter, since it would be flying without stores and flap deflection. For the same reasoning the flapped configuration was chosen, as this would yield the maximum drag force during a mission. Stores and landing gear configurations were chosen to see the effect of the individual components. Below the assumptions for the drag analysis is given.

1. It was assumed that the aircraft is designed following the area rule, described by Roskam VI chapter 4.3.4 [22]. Due to this assumption the interference drag coefficient can be neglected for all flight stages.
2. It was assumed that there are no extra items mounted on the outside aircraft, i.e. no targeting pods, camera's, etc. This assumption makes that the miscellaneous drag coefficient can be neglected.
3. Because the shape of the canopy is integrated in the shape of the fuselage, it was assumed that the canopy does not create any extra drag. Hence the canopy drag coefficient can be neglected.
4. From the trim calculations it became apparent no elevator deflection was needed to fly in trimmed conditions, hence it was assumed that trim drag could be neglected.
5. For all configurations a constant weight was assumed, which was set equal to the weight of the aircraft at the beginning of the respective flight stage. For the clean and stores configuration the cruise weight was assumed, for landing gear and flapped the maximum landing weight of 130 kN was assumed as this would be the most extreme case.
6. The air viscosity, μ , used in the calculations for the Reynolds number, was assumed to be constant.
7. For all calculations it was assumed that the aircraft is only flying at subsonic speeds, as the cruise speed was set to be roughly 0.6 M. This assumption was later validated, using the dog-house plots discussed in [chapter 14](#).
8. It was assumed that the wing, fuselage and horizontal tail are the only components creating lift. Hence, the lift induced drag component for all the other components are neglected.
9. It was assumed that the stores mounted on the wings are MK-82 bombs, as this is a rather common bomb used in the weight class specified by the RFP [2].
10. During landing it was assumed that the flaps would only be extended, after the C_L required to fly exceeded the $C_{L_{max, clean}}$. The flap deflection required for the extra C_L , was assumed to be linear with the extra C_L created.
11. It was assumed the landing gear would only be deployed after a speed of 250 kts, as this was found to be a reasonable speed¹.

12.3. Results

Using the method as explained before and the input variables stated in [Appendix 19](#), four different drag polars were plotted, shown in [Figure 12.1a](#) and [Figure 12.1b](#). From the drag polars and [Table 12.1](#) the effect of the added objects to the different configurations becomes clear. For the landing gear configuration it was observed that the starting point is shifted to the right, this is due to the maximum speed assumed for landing gears out. Which is lower than the maximum speed used for the other

¹<https://contentzone.eurocontrol.int/aircraftperformance/details.aspx?ICAO=A10>, conducted on 16-01-2021

configurations, resulting in a higher required C_L . For the flapped configuration the y-axis is given another range, this is due to the assumption that the flaps are extended, only after the $C_{L_{\max_{\text{clean}}}}$ is reached.

The trend lines in [Figure 12.1a](#) and [Figure 12.1b](#) are plotted such that the values C_{D_0} and e could be determined from it. In [Table 12.1](#) the values found for the different configurations are listed.

Table 12.1: Values found from trend lines of the drag polars.

Configuration	C_{D_0}	e
Clean	0.017	0.76
Stores	0.028	0.76
Landing gear	0.043	0.78
Flapped	$0.061\Delta C_L + 0.038$	0.57

Where the formula for the flapped configuration is due to the dependency of the profile drag on the flap deflection angle. Which, as stated before, was assumed to vary linearly with the ΔC_L required.

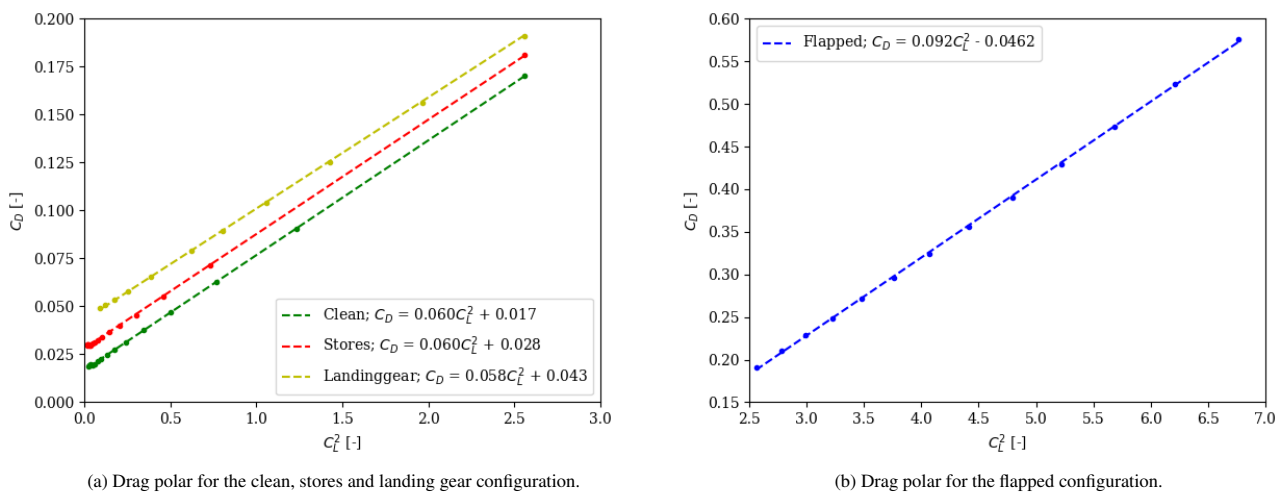


Figure 12.1: Drag polars as result of the drag analysis.

12.4. Verification and Validation

In [subsection 7.2.3](#) it is explained how the airfoil was selected. Here it was stated that the airfoil should have a design lift coefficient of 0.68, as this would yield an optimal L/D during the loiter phase. Hence, from the second order drag estimation the drag polar and the corresponding L/D curve were plotted, see [Figure 12.2a](#). On this curve the airfoil design point at a lift coefficient of 0.68 and the calculated L/D was plotted. It was observed that the design point indeed coincides with the L/D curve, and hence verifies the airfoil selection.

The first step that was taken to verify the results from the drag estimation method used, was inspecting the resulting values. This was done by comparing the C_{D_0} used in the first order drag estimation with the value obtained from the second order weight estimation. If the difference would be too large, the equations used in the program would be checked for syntax errors.

The second step was to pick a configuration and check if the calculated value in the program were equal to hand calculated values. This step also aimed to reduce the amount of syntax errors.

The final step to verify the program was to plot both the first order estimated drag polar and the second order estimated drag polar for the stores configuration. Of which the result is shown in Figure 12.2b. It can be observed that the Oswald efficiency factor was overestimated and the C_{D0} underestimated in the first order estimation. Which explained the offset at the beginning and the growth in difference.

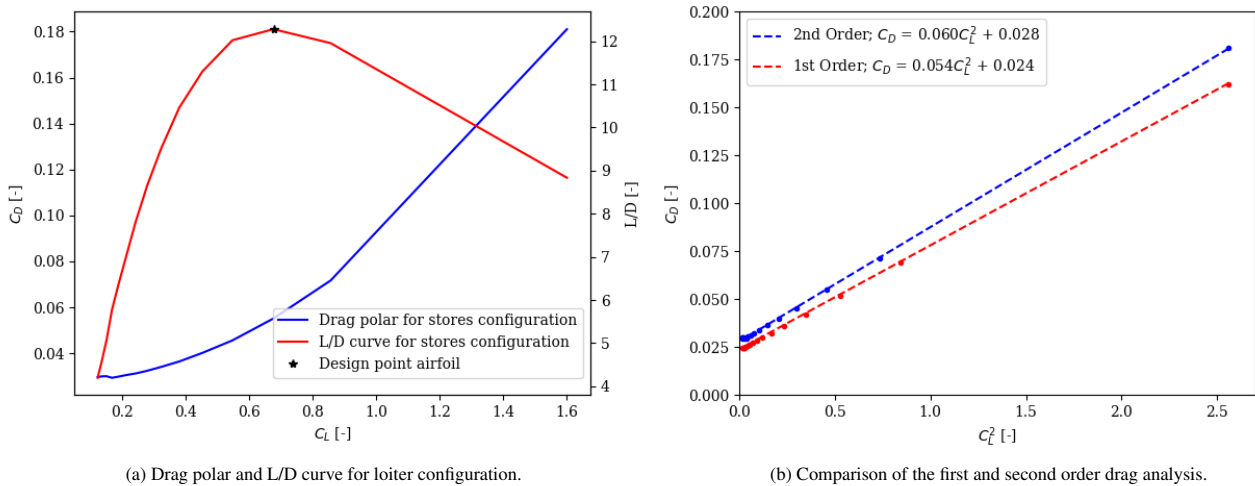


Figure 12.2: Drag polars as result of the drag analysis.

Due to the amount of assumptions made in this method, it is recommended that a more thorough analysis would be performed in future design steps. A computational fluid dynamics, or CFD, analysis of the 3D model might be performed to investigate more exactly what the effect of certain features might be. This eventually could be verified by a wind-tunnel experiment, confirming the actual drag created in different configurations.

13 Stability and Control Analysis

In order to operate an aircraft safely, the aircraft has to be stable and controllable. This chapter analyzes the control and stability characteristics of the aircraft. First, the static stability was evaluated in longitudinal and lateral direction, respectively. Secondly, the dynamic stability and controllability were analyzed with attention to handling qualities. In this chapter, the methods from Roskam and Torenbeek were applied [14, 22]. The used conventions of positive angles and axes can be found in [Figure 13.1a](#) and [Figure 13.1b](#). In many cases, the sign of the static stability derivatives indicates if an aircraft is stable or not. In the tables, the 'required' sign is given in curly brackets next to each derivative, if applicable.

The stability and control analysis was done for three different flight phases, do note that these differ from the ones introduced in [chapter 12](#).

- **Loiter:** As the loiter period is the longest phase in the flight profile, it deserves special attention. The aircraft loiters at an altitude of 3 000 ft, with a speed of 86 m/s. At the beginning of the flight stage, the aircraft weighs 12.2 tons. Furthermore, it was assumed that the aircraft flies in non-flapped configuration.
- **Cruise:** For the cruise phase, an altitude of 10 000 ft, the MTOW of 13.1 tons and the cruise velocity of 201.3 m/s were used. Just as for the loiter phase, it was assumed that the aircraft flies in a non-flapped configuration.
- **Landing:** The landing was analyzed at a density altitude of 6 000 ft, an aircraft mass of 13.1 tons and a speed of 53 m/s. The mass is high, because an emergency landing immediately after takeoff was considered.

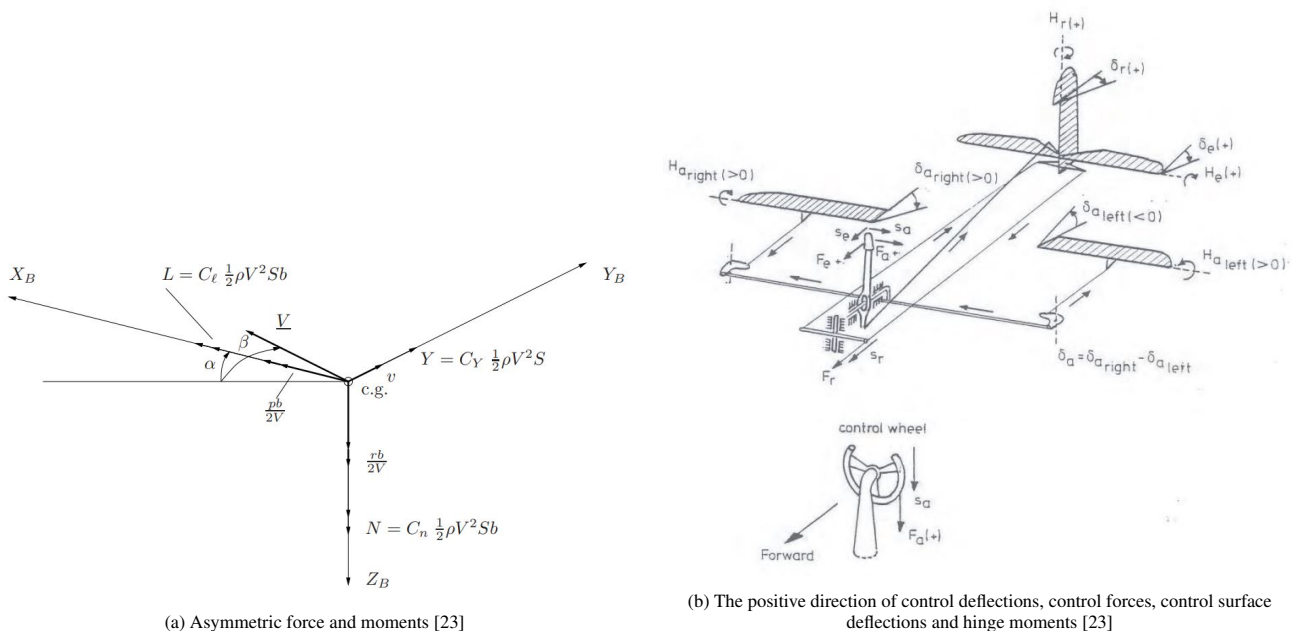


Figure 13.1: Conventions for positive angles and axes used in the stability and control analysis

13.1. Longitudinal Static Stability

In this section, the longitudinal static stability characteristics of the aircraft were analyzed. Flapped and non-flapped configuration were considered at Mach 0.14 and 0.61, respectively. The neutral point for static pitch stability was calculated using the method from Torenbeek [14]. The lift curve slope C_{L_α} was calculated using the methods from Torenbeek [14]. It was calculated for the three aforementioned flight conditions: loiter, cruise, and landing. The values can be found in [Table 13.1](#).

Table 13.1: Results C_{L_α} per configuration

Configuration	C_{L_α} {-} [rad^{-1}]
Loiter	5.4
Cruise	6.1
Landing	5.8

For the flapped configuration, a correction was added to include the contributing effects of the flaps. They increase the lift curve slope, the maximum achievable lift and the angle of attack at zero-lift. These calculations were provided by Torenbeek [14].

It was assumed that the aerodynamic center of the wing and the horizontal tail is located at 25% of the MAC of each surface.

All configurations were evaluated at the most aft c.g., as this is the most critical case. The c.g. location was derived using Torenbeek's method for empennage sizing [14]. When the c.g. is ahead of the neutral point, the aircraft is statically stable. This reflects in the moment coefficient derivative C_{m_α} , which becomes negative. The values for C_{m_α} are provided in [Table 13.2](#).

Table 13.2: Results C_{m_α} per configuration

Configuration	C_{m_α} {-} [rad^{-1}]
Loiter	-0.86
Cruise	-0.90
Landing	-0.70

13.2. Lateral Static Stability

In this section, the lateral static stability derivatives due to sideslip, yaw-rate and roll-rate were analyzed. All derivatives were calculated following the method described in Roskam part VI [22].

The resulting values are given in [Table 13.3](#). The derivatives indicate that the aircraft is laterally stable. It was noted that during the cruise and loiter phase, the yawing moment stays neutral. This is due to the fact that there is no flap deflection in this clean configuration.

Table 13.3: Results lateral stability derivatives with respect to sideslip angle, roll rate, and yaw rate

Configuration	C_{y_β} {-} [rad ⁻¹]	C_{l_β} {-} [rad ⁻¹]	C_{n_β} {+} [rad ⁻¹]
Loiter	-0.44	-0.086	0.12
Cruise	-0.44	-0.083	0.12
Landing	-0.43	-0.072	0.13
	C_{y_p} {-} [rad ⁻¹]	C_{l_p} {-} [rad ⁻¹]	C_{n_p} {-} [rad ⁻¹]
Loiter	-0.092	-0.49	0.00
Cruise	-0.092	-0.50	0.00
Landing	-0.017	-0.51	-0.34
	C_{y_r} {+} [rad ⁻¹]	C_{l_r} {+} [rad ⁻¹]	C_{n_r} {-} [rad ⁻¹]
Loiter	0.27	0.74	-0.18
Cruise	0.27	0.22	-0.17
Landing	0.28	1.7	-0.22

13.3. Longitudinal Dynamic Stability

In this section the longitudinal dynamic stability of the aircraft is described. For the longitudinal direction two motions are described: the short period motion and the phugoid. To approximate the respective derivatives, Roskam book part VI was used [22]. The symmetric equations of motion in longitudinal direction are described in [Equation 13.1](#).

$$\begin{bmatrix} C_{X_u} - 2\mu_c D_c & C_{X_\alpha} & C_{Z_0} & 0 \\ C_{Z_u} & C_{Z_\alpha} + (C_{Z_{\dot{\alpha}}} - 2\mu_c) D_c & -C_{X_0} & C_{Z_q} + 2\mu_c \\ 0 & 0 & -D_c & 1 \\ C_{m_u} & C_{m_\alpha} + C_{m_{\dot{\alpha}}} D_c & 0 & C_{m_q} - 2\mu_c K_Y^2 D_c \end{bmatrix} \begin{bmatrix} \hat{u} \\ \alpha \\ \theta \\ \frac{q\bar{c}}{V} \end{bmatrix} = \underline{0} \quad (13.1)$$

Short Period Motion

The short period motion is characterized by its heavily damped oscillation, which occurs no longer than a few seconds. In the following calculations the airspeed was assumed to be constant. Thus, the symmetric equations of motion reduce to [Equation 13.2](#). The values of the stability derivatives can be found in [Table 2](#).

$$\begin{bmatrix} C_{Z_\alpha} + (C_{Z_{\dot{\alpha}}} - 2\mu_c) \lambda_c & C_{Z_q} + 2\mu_c \\ C_{m_\alpha} + C_{m_{\dot{\alpha}}} \lambda_c & C_{m_q} - 2\mu_c K_Y^2 \lambda_c \end{bmatrix} \begin{bmatrix} \alpha \\ \frac{q\bar{c}}{V} \end{bmatrix} = \underline{0} \quad (13.2)$$

In order to determine the handling qualities during the short period motion, the damping ratios were compared to the boundaries set in MIL-F-8785-C [24]. The damping ratios of the short period motion were evaluated for the mission loiter phase, corresponding to category A, cruise phase, corresponding to category B, and landing phase, corresponding to category C. According to said specification, level 1 handling qualities are defined as "Flying qualities clearly adequate for the mission flight phase". Level 2 was described as "Flying qualities adequate to accomplish the mission flight phase, but some increase in pilot workload or degradation in mission effectiveness, or both, exists". Finally, level 3 was described as "Flying qualities

such that the airplane may be operated safely but the pilot workload is excessive or mission effectiveness is inadequate, or both. Category A flight phases can be terminated safely, and category B and C flight phases can be completed".

Furthermore, MIL-F-8785C describes different airplane categories, where the A-20 *Chimera* matched category IV. Thus, all handling qualities were checked for this category. The achieved damping ratios as well as the ratios corresponding to the different levels of handling quality can be found in [Table 13.4](#).

Table 13.4: Short period motion handling qualities and damping ratios

Flight Phase	Level 1	Level 2	Level 3
Category A & C	$0.35 \leq \zeta \leq 1.3$	$0.25 \leq \zeta \leq 2.0$	$0.15 \leq \zeta$
Loiter	$\zeta = 0.89$		
Landing	$\zeta = 0.90$		
Category B	$0.30 \leq \zeta \leq 2.0$	$0.20 \leq \zeta \leq 2.0$	$0.15 \leq \zeta$
Cruise	$\zeta = 0.71$		

Phugoid Motion

The phugoid motion of an airplane is a long period motion described by a large variation in air-speed, pitch angle and altitude. During this motion, the rate of the angle of attack was considered to be constant as well as the change of the pitch rate. This led to the following simplification of [Equation 13.1](#).

$$\begin{bmatrix} C_{X_u} - 2\mu_c D_c & C_{X_\alpha} & C_{Z_0} & 0 \\ C_{Z_u} & C_{Z_\alpha} & 0 & 2\mu_c \\ 0 & 0 & -D_c & 1 \\ C_{m_u} & C_{m_\alpha} & 0 & C_{m_q} \end{bmatrix} \begin{bmatrix} \hat{u} \\ \alpha \\ \theta \\ \frac{q\bar{c}}{V} \end{bmatrix} = \underline{0} \quad (13.3)$$

The numerical values for the coefficients can be found in [Table 2](#). To evaluate the handling qualities, the damping ratios were computed. These are presented in [Table 13.5](#) together with the MIL-F-8785C specified requirements for comparison [24]. Do note that Level 1 and 2 have a damping ratio, while level 3 has a time to double, T_2 , requirement.

Table 13.5: Phugoid motion handling qualities

Flight Phase	Level 1	Level 2	Level 3
All categories	$\zeta \geq 0.04$	$\zeta \geq 0.0$	$T_2 \geq 55$ [s]
Loiter	$\zeta = 0.92$		
Cruise	$\zeta = 0.16$		
Landing	$\zeta = 1.0$		

13.3.1. Longitudinal Eigenvalue Locations

In [Figure 13.2](#), it can be seen that for the short period, represented by the color blue, the imaginary components of the eigenvalues are situated around the ± 0.06 line. Furthermore, it can be seen that the imaginary part is largely related to the lift curve slope, C_{L_α} , leading to the landing phase having the smallest imaginary part. This can also be seen in [Table 13.4](#), where the

damping ratio for the landing is the largest closely followed by the loiter.

Secondly, for the phugoid, it can be seen that the eigenvalues are located close to the origin. The real value for all three configurations is located at the negative side of the axis, meaning the phugoid will be damped, as shown in Table 13.5. Finally, it must be noted that during landing the imaginary part of the eigenvalue is equal to zero, leading to a damping coefficient of 1.

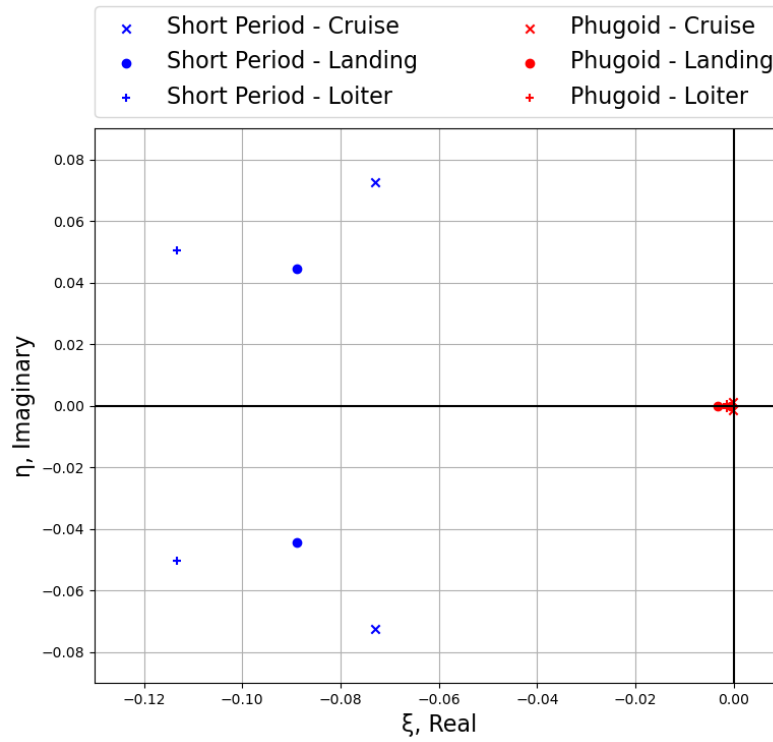


Figure 13.2: Representation of the eigenvalues of the motions in longitudinal direction

13.4. Lateral Dynamic Stability

In this section the lateral dynamic stability is described. Three motions are described in the lateral direction: the aperiodic roll, the Dutch roll, and the aperiodic spiral.

The characteristic equation for the asymmetric motions are found in Equation 13.4. For computing the characteristic parameters, there are no changes with respect to the longitudinal motions. However the mean aerodynamic chord is replaced by the wing span. The eigenvalues for the lateral motions are indicated as λ_b . In order to give a first approximation, some assumptions were made. Firstly, C_{Y_p} was set to zero since it is a relatively small derivative. Secondly, C_{Y_r} is very small compared to $4\mu_b$ and hence neglected. Lastly, the non-dimensional product of inertia K_{XZ} is relatively small compared to K_X^2 and K_Y^2 and thus omitted.

The first two assumptions are acceptable since the aircraft has a straight wing with a small dihedral [23].

$$\begin{bmatrix} C_{Y_\beta} + (C_{Y_\beta} - 2\mu_b) D_b & C_L & C_{Y_p} & C_{Y_r} - 4\mu_b \\ 0 & -\frac{1}{2} D_b & 1 & 0 \\ C_{l_\beta} & 0 & C_{l_p} - 4\mu_b K_X^2 D_b & C_{l_r} + 4\mu_b K_X Z D_b \\ C_{n_\beta} + C_{n_\beta} D_b & 0 & C_{n_p} + 4\mu_b K_X Z D_b & C_{n_r} - 4\mu_b K_Z^2 D_b \end{bmatrix} \begin{bmatrix} \beta \\ \varphi \\ \frac{pb}{2V} \\ \frac{rb}{2V} \end{bmatrix} = 0 \quad (13.4)$$

13.4.1. Aperiodic Rolling Motion

For the aperiodic roll motion, a few assumptions were made in order to compute the eigenvalue. The first assumption was that the aircraft only rolls about the longitudinal axis. Thus the columns corresponding to the angle of sideslip, β , and non-dimensional yaw rate, $\frac{rb}{2V}$, disappeared from the equation. Secondly, from the first assumption it was concluded that the roll angle φ does not occur anymore in the remaining equation, which resulted in the approximate solution Equation 13.5 [23].

In order to check which level of handling quality the aircraft achieves, the time constant had to be determined. Table 13.6 shows the maximum values for the roll-mode time constant per category and level.

$$\lambda_b = \frac{C_{l_p}}{4\mu_b K_X^2} \quad (13.5)$$

In Table 13.6, the resulting handling qualities for the aperiodic roll are presented. As can be seen, the aircraft complies with the level 1 flying quality for all three flight phases.

Table 13.6: Aperiodic roll motion handling qualities [24]

Flight Phase	Level 1	Level 2	Level 3
Category A	$\tau \leq 1.0$	$\tau \leq 1.4$	
Loiter	$\tau = 0.34$		
Category B	$\tau \leq 1.4$	$\tau \leq 3.0$	$\tau \leq 10.0$
Cruise	$\tau = 0.18$		
Category C	$\tau \leq 1.0$	$\tau \leq 1.4$	
Landing	$\tau = 0.58$		

13.4.2. Dutch Roll Motion

For the Dutch roll motion, a few assumptions were made to obtain an approximation for the eigenvalues. Firstly, the rolling component was neglected. Consequently, φ and $\frac{pb}{2V}$ were set to zero and thus, the corresponding columns in Equation 13.4 disappear. Since the rolling moment remains in balance, the rolling moment equation was omitted. Furthermore, the C_{n_β} and C_{Y_β} derivatives were neglected, which then resulted in Equation 13.6.

$$\begin{bmatrix} C_{Y_\beta} - 2\mu_b D_b & -4\mu_b \\ C_{n_\beta} & C_{n_r} - 4\mu_b K_Z^2 D_b \end{bmatrix} \begin{bmatrix} \beta \\ \frac{rb}{2V} \end{bmatrix} = \underline{0} \quad (13.6)$$

In addition to the damping ratio ζ , the aircraft also needs to meet the requirement for the eigenfrequency ω_n . The values for these handling qualities, given in [Table 13.7](#), are minimum values. For all three phases the aircraft complies with the level 1 handling qualities. However, it should be noted that the level 1 handling quality in category A, specifically for a ground attack phase, has a higher requirement when it comes to the damping ratio [24].

Table 13.7: Dutch roll motion handling qualities [24]

Flight Phase	Level 1	Level 2	Level 3
Category A	$\zeta \geq 0.19, \omega_n \geq 1.0[\text{rad/s}]$	$\zeta \geq 0.02, \omega_n \geq 0.4[\text{rad/s}]$	$\zeta \geq 0.0, \omega_n \geq 0.4[\text{rad/s}]$
Loiter	$\zeta = 0.19, \omega_n = 2.0$		
Category B	$\zeta \geq 0.08, \omega_n \geq 0.4[\text{rad/s}]$	$\zeta \geq 0.02, \omega_n \geq 0.4[\text{rad/s}]$	$\zeta \geq 0.0, \omega_n \geq 0.4[\text{rad/s}]$
Cruise	$\zeta = 0.16, \omega_n = 4.2$		
Category C	$\zeta \geq 0.08, \omega_n \geq 1.0[\text{rad/s}]$	$\zeta \geq 0.02, \omega_n \geq 0.4[\text{rad/s}]$	$\zeta \geq 0.0, \omega_n \geq 0.4[\text{rad/s}]$
Landing	$\zeta = 0.20, \omega_n = 1.2$		

13.4.3. Aperiodic Spiral Motion

Since the aperiodic spiral motion is usually very slow, it was assumed that all linear and angular accelerations were negligible.

This implied that $D_b\beta = D_b \frac{pb}{2V} = D_b \frac{rb}{2V} = 0$. This resulted in the simplified matrix given in [Equation 13.7](#).

$$\begin{bmatrix} C_{Y\beta} & C_L & 0 & -4\mu_b \\ 0 & -\frac{1}{2}D_b & 1 & 0 \\ C_{l\beta} & 0 & C_{l_p} & C_{l_r} \\ C_{n\beta} & 0 & C_{n_p} & C_{n_r} \end{bmatrix} \begin{bmatrix} \beta \\ \varphi \\ \frac{pb}{2V} \\ \frac{rb}{2V} \end{bmatrix} = \underline{0} \quad (13.7)$$

This characteristic equation reduced to a first order equation due to the many zeros. The solution of the eigenvalue is given by [Equation 13.8](#).

$$\lambda_{b4} = \frac{2C_L (C_{l\beta} C_{n_r} - C_{n\beta} C_{l_r})}{C_{l_p} (C_{Y\beta} C_{n_r} + 4\mu_b C_{n\beta}) - C_{n_p} (C_{Y\beta} C_{l_r} + 4\mu_b C_{l\beta})} \quad (13.8)$$

In order to state the level of handling quality of the aircraft for the spiral, the time to double amplitude was calculated. [Table 13.8](#) shows the handling quality levels for the three phases. Only during cruise the aircraft reaches level 1. For the loiter and landing phase, level 3 and no level were reached, respectively. This is not desirable, hence a Proportional-Integral-Derivative, or PID, controller was designed, as described in [section 13.5](#), in order to make sure the aircraft can safely operate during those phases.

Table 13.8: Aperiodic spiral motion handling qualities [24]

Flight Phase	Level 1	Level 2	Level 3	> Level 3
Category A & C	$T_2 \geq 12[\text{s}]$	$T_2 \geq 8[\text{s}]$	$T_2 \geq 4[\text{s}]$	
Loiter			$T_2 = 5.0[\text{s}]$	
Landing				$T_2 = 1.8[\text{s}]$
Category B	$T_2 \geq 20[\text{s}]$	$T_2 \geq 8[\text{s}]$	$T_2 \geq 4[\text{s}]$	
Cruise	$T_2 = 70.0[\text{s}]$			

13.4.4. Lateral Eigenvalue Locations

This subsection investigates the eigenvalues of the motions in lateral direction, which are presented in [Figure 13.2](#).

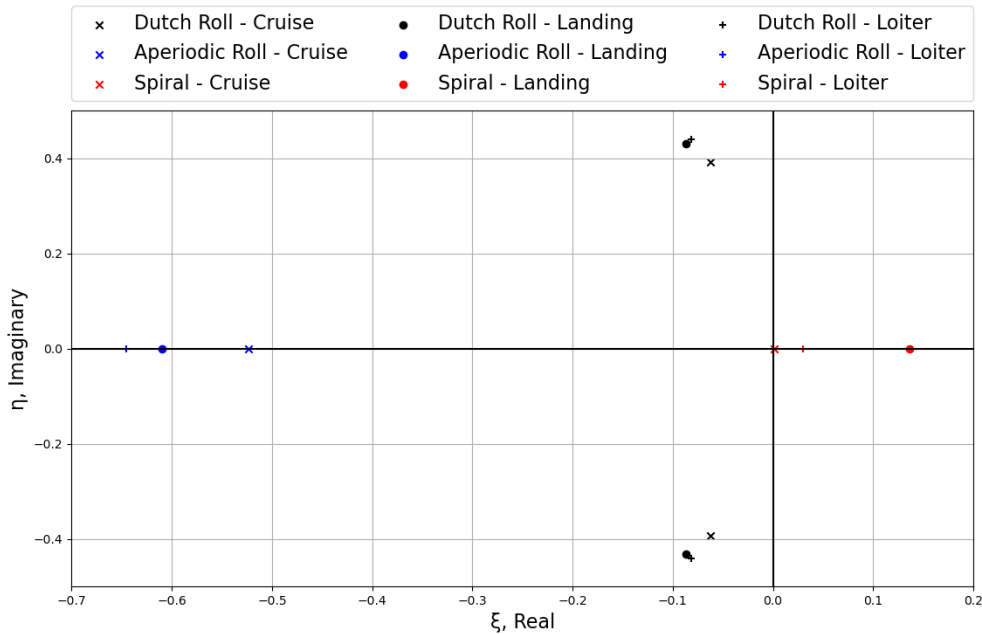


Figure 13.3: Representation of the eigenvalues of the motions in lateral direction

For the Dutch roll mode, represented in black, it becomes clear that the larger the absolute value of the imaginary part is, the sooner the motion will damp out. This can also be concluded from [Table 13.7](#), in which it can be seen that the Dutch roll damping coefficient is lowest during cruise. Secondly, for the aperiodic roll, represented in blue, the real eigenvalue is located relatively far from the origin. This leads to a higher time constant as can be seen in [Table 13.6](#). The fact that the time constant is highest for the landing phase, is related to the lower airspeed. Finally, for the aperiodic spiral, represented in red, it was observed that the eigenvalues are situated on the positive side of the real axis, leading to an unstable motion. A more positive eigenvalue, as can be seen for the landing phase, leads to a more unstable spiral. When the spiral is unstable, it is important that the double amplitude time is sufficiently large, as shown for the boundary values in [Table 13.8](#).

13.5. PID Controller for Aperiodic Spiral

In order to support the pilots when entering an aperiodic spiral during flight, a PID controller was designed. Since a spiral is caused by a change in bank angle of the aircraft due to a disturbance, the PID controller supports the ailerons to counteract the roll rate and bank angle, and thus the spiral motion.

In [Figure 13.4](#) the block scheme of the PID controller is shown as a double closed loop system. For simplicity, a first order system was made for the aileron actuator, where the transfer function was determined by the time constant τ . This value was assumed to be between 0 and 0.5, where a larger time constant represents a slower response [25]. The value for τ was then

put in Equation 13.9.

$$\frac{\delta_a(s)}{\delta_{ac}(s)} = \frac{1}{\tau s + 1} \quad (13.9)$$

In the same manner the transfer function for the aircraft dynamics block was found by using the time constant τ which was calculated for stall conditions with the eigenvalue from the aperiodic roll λ_b . With the aileron deflection from the aileron actuator block as input and the value for τ in Equation 13.9, the bank angle, ϕ , and roll rate, p , were computed. Lastly, it was assumed that these sensors have a transfer function equal to 1, meaning that the measurement of the bank angle or roll rate by the PID controller is perfect.

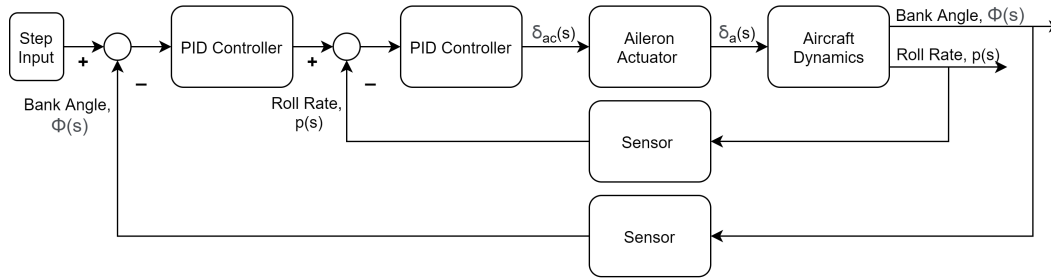


Figure 13.4: Block scheme of the PD controller for the bank angle and roll rate.

After the transfer functions were determined, the gains of the PID controllers were tuned. Iterations were performed while using different terms of the PID controllers. It was found that with two PD controllers, the step responses converged fastest without overshooting too much. Adding the integral term, resulted in a slightly lower overshoot, but also a slower step response. In Figure 13.5, the step responses with different time constants for the aileron actuator are plotted. It can be seen that for a higher actuator time constant, the controller represents a slower response.

It can be concluded that this PD controller will be able to make sure to counteract a roll moment within a short amount of time, resulting in a reduced workload for the pilot. However, the PD controller is not finished as of yet. It is a simplified controller that has to be tested in the future. Additionally it was assumed that the sensor gives a perfect measurement of the roll rate and bank angle. In practice, this is not the case and probably a rate-integrating gyroscope will be used. This will result in a slower response of the system.

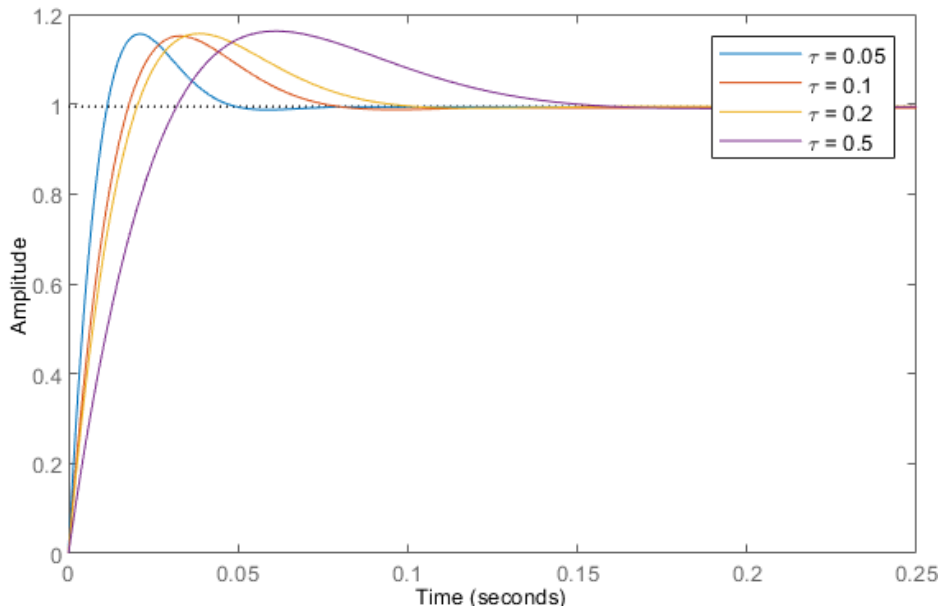


Figure 13.5: Step response PD controller for different actuator time constants

13.6. Control Derivatives due to Elevator, Aileron and Rudder

To complete the stability and control analysis, the control derivatives of the control surfaces had to be determined. These derivatives were calculated using the equations as provided by Roskam [22]. Only elevators, ailerons, and rudders had to be evaluated, since no other control surfaces were implemented on the aircraft. All control derivatives were analyzed for cruise and landing configuration.

In Table 13.9 the results of these control derivatives are presented. The control derivatives with respect to the aileron deflection were analyzed for cruise and landing conditions. The side force due to aileron deflection, $C_{Y_{\delta_a}}$, was neglected since the ailerons are not in close proximity of the vertical tail. $C_{l_{\delta_a}}$ and $C_{n_{\delta_a}}$ have signs as expected, which means the aircraft reacts to an aileron deflection as conventional.

The control derivative due to a positive rudder deflection was also analyzed for the same convention as shown in Figure 13.1a and Figure 13.1b. The resulting values were positive/negative according to the description given. Therefore, the aircraft reacts as expected to a rudder deflection and is stable for a δ_r contribution.

Table 13.9: Control derivatives due to elevator deflection

Configuration	$C_{D_{\delta_e}}$ [rad ⁻¹]	$C_{L_{\delta_e}}$ [rad ⁻¹]	$C_{m_{\delta_e}}$ [rad ⁻¹]
Cruise	0.52	1.1	-1.3
Landing	0.52	0.96	-1.3
	$C_{Y_{\delta_a}}$ [rad ⁻¹]	$C_{l_{\delta_a}}$ [rad ⁻¹]	$C_{n_{\delta_a}}$ [rad ⁻¹]
Cruise	0	-0.40	0.009
Landing	0	-0.40	0.10
	$C_{Y_{\delta_r}}$ [rad ⁻¹]	$C_{l_{\delta_r}}$ [rad ⁻¹]	$C_{n_{\delta_r}}$ [rad ⁻¹]
Cruise	1.6	0.20	-0.58
Landing	1.3	0.022	-0.50

13.7. Sensitivity Analysis

This section describes the sensitivity analysis of the dynamic motions in cruise phase. Each of the changed parameters were performed using the one factor at a time approach.

Table 13.10: Sensitivity analysis stability and control in cruise phase

Parameter	Short period	Phugoid	Aper. roll	Dutch roll	Spiral
No changes	$\zeta = 0.71$	$\zeta = 0.16$	$\tau = 0.18$	$\zeta = 0.16, \omega_n = 4.2$	$T_2 = 70[s]$
Increase Γ by 3°	$\zeta = 0.71$	$\zeta = 0.16$	$\tau = 0.18$	$\zeta = 0.16, \omega_n = 4.2$	$T_2 = 190 [s]$
Decrease S_v by 50%	$\zeta = 0.73$	$\zeta = 0.16$	$\tau = 0.18$	$\zeta = 0.16, \omega_n = 2.3$	$T_2 = 135 [s]$
Weight without stores	$\zeta = 0.72$	$\zeta = 0.18$	$\tau = 0.18$	$\zeta = 0.16, \omega_n = 4.2$	$T_2 = 97 [s]$
AR wing increase by 1	$\zeta = 0.72$	$\zeta = 0.16$	$\tau = 0.17$	$\zeta = 0.16, \omega_n = 4.2$	$T_2 = 74 [s]$
$\Lambda_{c/4}$ increase to 20°	$\zeta = 0.89$	$\zeta = 0.17$	$\tau = 0.18$	$\zeta = 0.15, \omega_n = 4.7$	$T_2 = 67 [s]$

When looking at the results of the sensitivity analysis in [Table 13.10](#), no big changes occurred for the short period motion. Only when increasing the quarter chord sweep, the damping ratio increases. For all cases this motion stayed in flying quality level 1. The same applies for the phugoid and aperiodic roll, no big changes were found for all cases. For the Dutch roll, in two cases there was a relatively large change. Firstly, when the dihedral angle was increased, the eigenfrequency lowered, which is not beneficial for the flying quality. However, it was still well above the requirement for level 1. Secondly, when the quarter chord sweep was increased, the eigenfrequency increased, which was beneficial for the flying quality.

In general, the sensitivity analysis showed that the aircraft was well designed for these four motions. However, the sensitivity analysis showed some interesting cases for the aperiodic spiral. For almost every case, the time to double amplitude increased, except for the case where sweep was increased. Since the spiral was not in the desired level of flying quality for the loiter and landing phase, these changes were not implemented into the design as of yet for some require a new iteration process. This must be looked into in the future.

13.8. Verification and Validation

A first step of verifying the results for the derivatives obtained, was by inspection. Chapter 11 of Roskam part VI provides examples of stability derivatives [22]. An example similar to the design of the A-20 *Chimera* was used to make a first comparison. Both the sign of the derivative and the order of magnitude were inspected to gain a first insight whether the result could be trusted. Secondly, the python program that is used to calculate the eigenvalues of the lateral and longitudinal motions, was verified by filling in the example values provided in the Flight dynamics reader provided by the lecture AE3212-I at the Delft University of Delft [23]. The eigenvalue, and the damping ratio of both the short period motion as the phugoid, were compared to the results provided in the reader. The resulting values provided equal and proven to be verified.

14 Aircraft Performance Analysis

When designing an attack aircraft, performance is a key feature. Hence, a thorough analysis was executed to find the payload range and payload combat radius diagram, and the flight envelope by using several performance diagrams. Firstly, the payload range and payload combat radius diagram are discussed. Secondly, the gust and manoeuvre load diagram is given, after which the specific excess power plots for several flight configurations are given, next to this, the turn rate diagrams will be discussed. Finally the verification of the methods will be given.

14.1. Range Diagrams

This section includes the approach and the results for both payload range and payload combat radius diagrams.

14.1.1. Payload Range Diagram

The range of an aircraft is heavily influenced by the payload and fuel on board. Therefore, to represent the relationship between these variables, a payload-range diagram was constructed, which is given in [Figure 14.1a](#), the numerical results are given in [Table 14.1](#). Point A is at maximum payload without fuel and point B is at MTOW. In order to increase the range further, the payload has to be reduced while maintaining maximum fuel weight.

Point C shows the range at 60% payload capacity, which is required for the ferry mission, as per requirement LAA-PER-FEM-1.1¹. In the graph it can be seen that point C is around 6300 km, or 3400 nmi, which means the requirement for the ferry mission is met.

14.1.2. Payload Combat Radius Diagram

Similar to the payload range diagram mentioned before, the combat radius is heavily influence by the payload and fuel on board. The payload combat radius diagram represents the relationship between these variables, which is shown in [Figure 14.1b](#). However, unlike the payload range diagram, the payload combat radius diagram has excluded the 4 hours and 45 minutes loiter range credit. This is because the aircraft remains in the same region during the loiter phase. Furthermore, the combat radius is a more accurate representation of range during a mission, as the aircraft has travel to and from the battlefield. Therefore, the combat radius was determined by dividing the range by 2.

Similar to payload range diagram, point B illustrates the combat radius when the aircraft is at MTOW. In addition, point C shows the maximum combat radius without payload. Lastly, the vertical line represents the design mission cruise range as set by requirement LAA-PER-DSM-2.2², which is met. As the radius is determined by dividing the range by 2, requirement LAA-PER-DSM-4.1³

¹LAA-PER-FEM-1.1: The aircraft shall have a ferry range of at least 900 nmi at a cruise altitude of at least 18 000ft.

²LAA-PER-DSM-2.2: The initial cruise of 100 nmi and following descent to 3 000 ft shall take no longer than 20 minutes.

³LAA-PER-DSM-4.1: After a loiter period of 4 hours at an altitude of 3000 ft without dropping stores, the aircraft shall be able to climb to cruise altitude

Table 14.1: Results

	Payload Weight [kg]	Range [km]
Payload Range A	1400	0
Payload Range B	1400	5900
Payload Range C	820	6300
Payload Combat Radius A	1400	0
Payload Combat Radius B	1400	190
Payload Combat Radius C	0	640

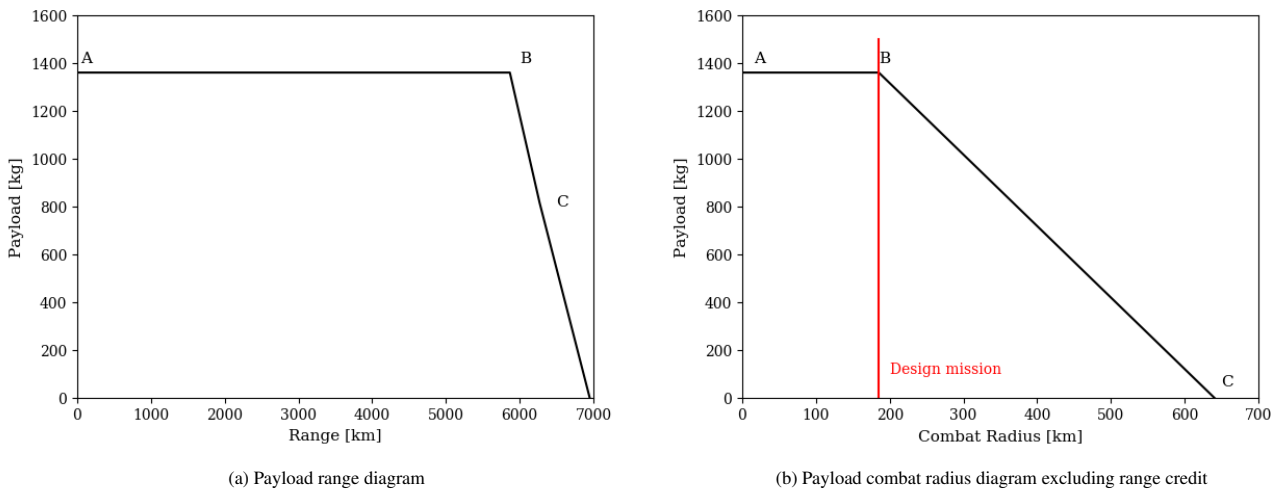


Figure 14.1: Range diagrams for the A-20 Chimera

14.2. Gust and Manoeuvr Load Diagram

The gust and manoeuvr load diagram, or V-n diagram, is a graph which provides information about the combination of speeds and load factors, which the aircraft should be able to sustain. The diagram is built up from two sources of load factors. The first load factors are due to maneuvering, which is explained in the first subsection. The second source of a load factors are gust loads, which are discussed in the second subsection. Finally, the V-n diagram is presented in [Figure 14.2](#).

14.2.1. Maneuverability

As an aircraft maneuvers it encounters a certain amount of load on its structures, of which the highest load the aircraft has to withstand is the limit load. For an attack aircraft the MIL-A-8861B specifies that the design limit load of an attack aircraft should be 7.5g. Hence, this number was used in the construction of the maneuvering diagram. [26]

To construct the line from 0 to A the minimum stall speed in clean configuration was calculated for the different load factors. However, due to structural limits the load factor cannot be allowed to keep increasing, hence a n_{max} has to be chosen. As mentioned before a limit load of 7.5 from the MIL-A-8861B standard was chosen [26].

The line from 0 to H was determined using the same method. However, a smaller negative limit load was used as can be seen with following cruise of 100 nmi.

in [Figure 14.2](#). From MIL-A-8861B it was determined to be -3 [26]. Crossing the curves 0 to A or 0 to H would result in stall, hence the vertical line around 50 m/s in the graph. This vertical line represents the stall speed at $1g$.

Point C on the V-n diagram represents the cruise speed, this speed was determined during the Class I sizing to be 201.3 m/s. When converted to EAS the cruise speed becomes 173.0 m/s. Point D is the design diving speed, which was calculated using MIL-A-8860 and Anderson [27, 28]. In the MIL-A-8860 document it is stated that the dive speed needs to be 120% of the maximum achievable speed. The maximum speed was calculated by equating the thrust available to the thrust required. This led to a maximum cruise speed, at the cruise altitude, of 230 m/s or an EAS of 200 m/s, which then resulted in a dive speed of 240 m/s. For point F in the diagram, the cruise speed is used, from which a straight line is drawn to point E. Which was determined by the limiting gust loads, which will be discussed in the following subsection.

The small red lines in [Figure 14.2](#) represent the V-n diagram for the aircraft when flaps are extended. The lines were made using the same method as explained above. However, for a flap extended flight the aircraft has a lower limit load. Which is specified by MIL-8861B to be 2. The limit speed for flap extended flight was specified to be $1.75V_s$, using the same document [26].

14.2.2. Gust Loads

When flying through turbulent air, symmetrical vertical gusts subject the aircraft. This will change the load factor and generate a gust load. The gust load might exceed the maneuver load and thus alter the V-n diagram. The gust load factors were computed using standard equation . Since gust velocity profiles are not sharp-edged but more uniformly shaped, the gust alleviation factor accounts for this. It is based on the mass ratio for subsonic speeds given in MIL-STD-8861B [26, 29].

According to MIL-A-8861B, the aircraft must be able to withstand particular positive and negative gust velocities [26]. As is shown in [Figure 14.2](#), three different positive and negative gust velocities, indicated by the gray dotted lines, were considered. Gust velocities at the design cruising speed were assumed to be ± 15 m/s equivalent speed at altitudes between sea level and 20 000 ft. From 20 000 ft to 50 000 ft, these gust velocities were reduced linearly to 7.5 m/s. For the design driving speed, positive and negative gusts of 7.5 m/s were also considered at altitudes between sea level and 20 000 ft. Lastly, a gust velocity of ± 20 m/s was considered for rough air gusts at altitudes between sea level and 20 000 ft. This maximum gust velocity determines the design speed for maximum gust velocity V_B , which is the speed that causes the aircraft to stall at the assumed maximum gust velocity. [29]

When looking at [Figure 14.2](#), one can see that the gust loads limit the flight envelope only for the negative gust velocity of 7.5 m/s, i.e. point E.

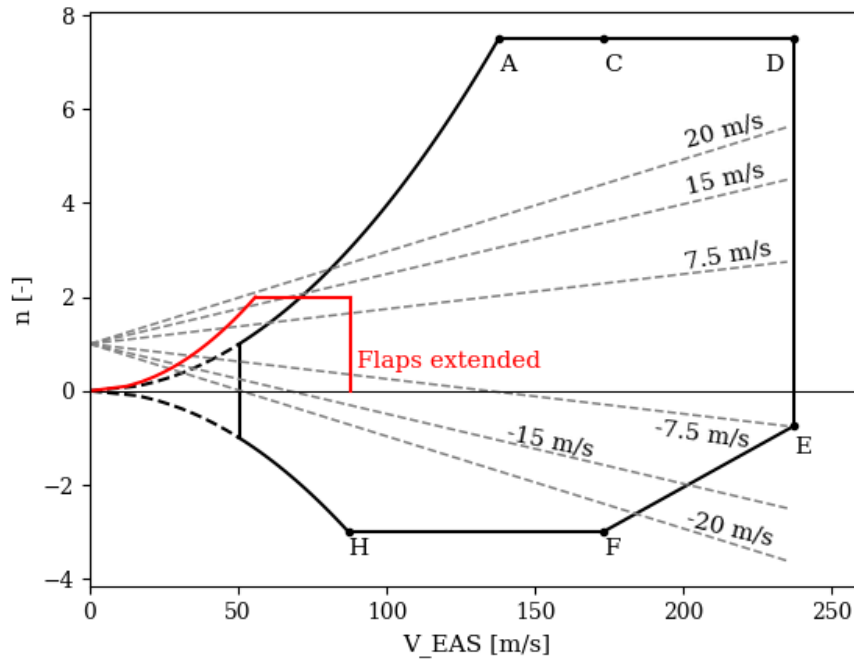


Figure 14.2: V-n diagram for the designed aircraft.

14.3. Specific Excess Power Diagrams

In order to evaluate the performance of the aircraft, a specific excess power diagram was made. In this plot the specific excess power, P_s , is given as a contour plot. P_s can be used for acceleration, to climb or for sustained turns, all for a specified weight, thrust and configuration. The configuration determines the maximum lift coefficient and zero-lift drag coefficient.

14.3.1. Approach

For the specific excess power the thrust and drag are to be calculated, both depend on the altitude. The thrust available was calculated using the method described in Ruijgrok, chapter 6 [29].

In order to determine the drag, the drag coefficient, as calculated in chapter 12, and required lift coefficient, which was calculated for the speed, air density and specified weight, were used.

Additionally, the stall speed was calculated for each altitude and the $C_{L_{max}}$ as per the specified configuration.

For the different flight stages, the configuration data is given in Table 14.2.

Table 14.2: Configuration for different flight stages

	W [kN]	$C_{L_{max}}$ [-]	C_{D_0} [drag counts]	V [m/s]	h [m]
Take off	128	2.0	760	61	1 800
Cruise, stores	122	1.6	280	200	3 000
Loiter, stores	118	1.6	280	86	910
Landing	96	2.6	1200	50	1 800

14.3.2. Results

From the configurations given in the previous section, the specific excess power diagrams could be made. In [Figure 14.4a](#) the specific excess power diagram of the take off configuration is given. The stall speed, or lift limit line, for the specific configuration is indicated with a blue line. Values with negative specific excess power and the area left of the lift limit line are both grayed out, as there is no sustained level flight possible in these areas. The red dot in the excess power plots represent the speed and altitude for each configuration, as given in [Table 14.2](#).

In [Table 14.3](#) the results for each flight stage are given. In the table the specific excess power at the design point is given, the maximum P_s and the speed of this maximum P_s is given as well. Next to this the stall speed is given. Furthermore, the maximum altitude of $P_s = 0$ and maximum speed at the configuration altitude given in [Table 14.2](#). The P_s diagrams of the take off, cruise, loiter and landing configurations are given in [Figure 14.4a](#), [Figure 14.4b](#), [Figure 14.4c](#), and [Figure 14.4d](#), respectively.

From the results it can be seen that the requirement on the service ceiling, LAA-PER-SER-1.1⁴, can be checked off as the maximum altitude is calculated to be 14.6 km, or approximately 48 000 ft.

Table 14.3: Results from the specific excess diagrams for the different flight stages

	P_s [W/N]	$P_{s,max}$ [W/N]	$V_{P_s \max}$ [m/s]	V_{stall} [m/s]	h_{max} [km]	V_{max} [m/s]
Take off	9.3	12	86	51	11	140
Cruise, stores	13	23	139	59	14	230
Loiter, stores	22	28	134	52	15	230
Landing	11	13	68	38	11	110

14.4. Turn Rate Diagrams

From the performance graphs as explained above, the specific excess power for a given altitude and speed combination can be determined. From this the optimal climb rate of the aircraft can be found. However, excess power can also be used for turning. To investigate what the turn performance of the A-20 Chimera is, two excess power plots were made as shown in [Figure 14.3](#).

The black lines in [Figure 14.3](#) are the specific excess power lines, ranging from -40 [m/s] at the top, to 25/20 [m/s] at the bottom, cruise with stores and loiter with stores respectively. The green lines represent constant load factor lines, where the x-axis represents the 1-g line. The red lines represent the turn radius for the given combination of speed and turn rate. The left blue line represents the stall speed at different turn rates, the right blue line is determined by the maximum speed of the aircraft.

The constant load factor lines were calculated keeping the load factor constant while the speed varied. Using the ultimate load factor found in [subsection 14.2.1](#), the corner velocities were found to be 160 m/s for cruise configuration, as seen in [Figure 14.3a](#), and 142 m/s for the loiter configuration, as seen in [Figure 14.3b](#).

⁴LAA-PER-SER-1.1: The aircraft shall have a service ceiling of at least 30 000 ft.

For the specific excess power lines first the turn rate was found for a given combination of load factor and speed. For the same values of load factor and speed the specific excess power was calculated. Where the drag was multiplied with the load factor. This resulted in the obtained contour lines, shown in Figure 14.3.

It was chosen to plot both loiter and cruise in stored condition, as these are the main flight stages in which the maneuverability is most important.

14.5. Verification and Validation

For both the V-n diagram analysis and the performance diagram analysis tools were created to calculate and plot the needed values. Hence a verification of these tools was carried out, to make sure the obtained values and information was correct.

For both tools the first steps taken to verify, were aimed to find syntax errors in the plugged in equations. First step taken to find these errors was to have a sanity check of the output values. Second step was to take a point for which the values were hand calculated and checked if these values compared to the output values for the same point. These steps were assumed to be enough to verify the plugged in equations.

To validate the obtained plots, aircraft data would be needed, combined with their performance diagram. However, the combination of both data and plots were hard to find. Therefore the plots have not been validated with a real life case. A future recommendation would be to obtain this data and complete a thorough validation of the tools and methods used.

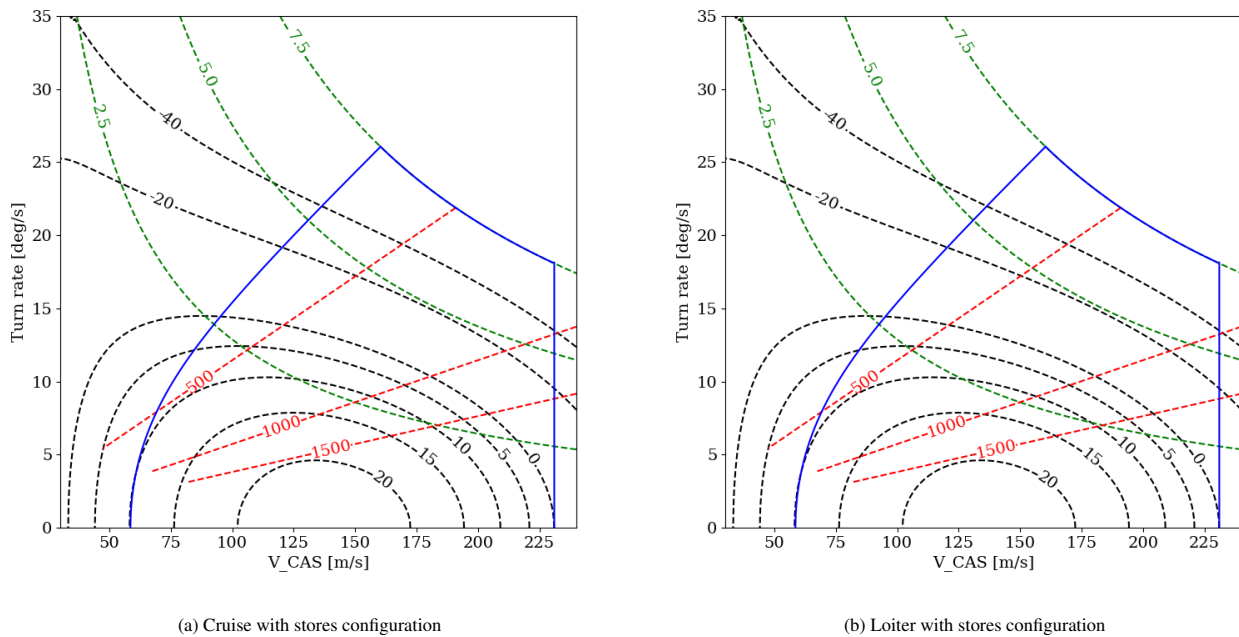


Figure 14.3: Turn rate diagrams

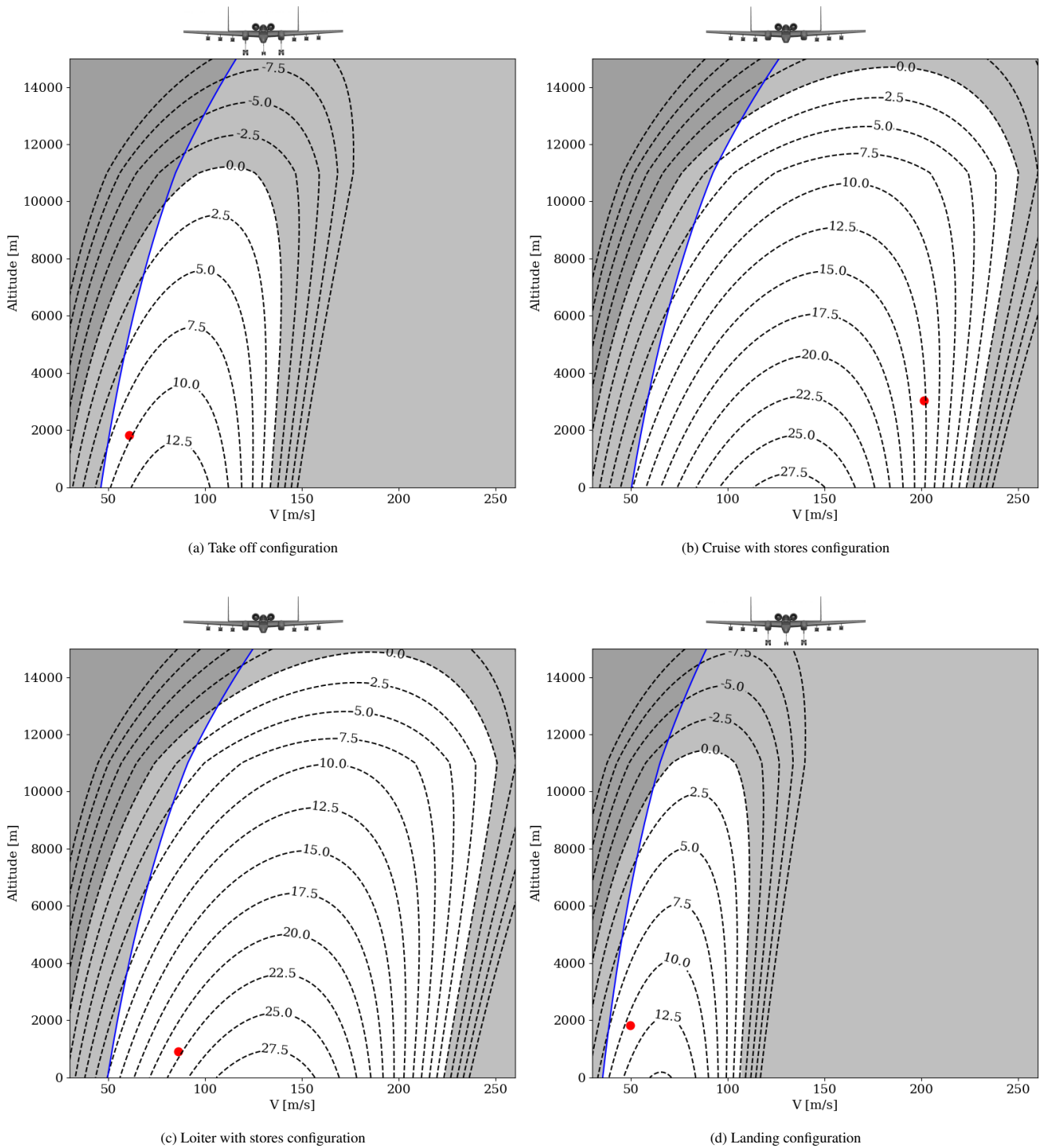


Figure 14.4: Specific excess power diagrams

15 Operations & Logistics Plan

In this chapter, the kind of operations and logistics that are considered throughout the project are discussed. The practicality of the aircraft, mentioning what values it offers to the air forces and what aspects of it make it a unique aircraft are covered.

15.1. Operations

Interviews with two fighter pilots gave insight on the kind of operations that are desired to be performed by the aircraft. These operations were one of the fundamental factors in the design of the aircraft. The A-20 is capable of "hot pit refueling and rearming". Hot pit refueling is a refueling method that occurs with engines still running and its operational purpose to have the aircraft ready to take off as soon as possible. In general, the time taken for hot pit refueling is 66% of refueling with engines turned off¹. On top of that, rearming is another operational performance which covers providing the aircraft with new supplies of ammunition for weapons. This depends on the type and quantity of the ammunition for the aircraft. In the interview with the F-35 pilot it was found out that the rearming process for an average fighter aircraft takes around 5 minutes per hard point. Given that the aircraft has 3 hard points per wing, this means that rearming the whole wing will take about 15 minutes.

15.2. Logistics Plan

One of the key challenges to operate from an austere field is logistics. To transfer the aircraft to operational locations, it is decided to dismantle the aircraft and fit inside shipping containers. This is the most cost effective method of transportation, since the infrastructure required already exists and no aerial refueling or intermediate stops are required. However, there are restrictions on the weight and dimensions of the cargo, due to the ratings and dimensions of ISO shipping containers used within the shipping industry. Therefore, the cargo is subjected to a dimension and weight below 16.2m x 2.6m 2.9m and 25 440 kg². These containers can also be transported by train or truck, this can further make use of readily existing infrastructure. In the event of quick deployment, specialized carriers such as the C-17 *Globemaster* or A400M *Atlas* are used, since the cargo bay of both aircraft can comfortably accommodate the container's dimension. Either way, the aircraft has to be disassembled and reassembled after arrival. Therefore, a modular design is required to reduce the assembly time. As a side benefit, maintenance on austere field can be simplified. Instead of fixing the broken part on site, the broken modular can be replaced by a spare and shipped back to the factory for maintenance.

For assembly and disassembly of the aircraft, the most important factors are first maintaining the structural integrity of the aircraft and then being able to fit those components inside the containers with the given dimensions. Furthermore, it needs to be mentioned that the assembly methods depend on the dimensions of the container, aircraft geometry and its structural

¹<https://www.airforce-technology.com/news/usaf-practises-hot-pit-refuelling-technique/>, conducted on [04-01-2021]

²<http://containertech.com/container-sales/53ft-high-cube-container-domestic/>, conducted on [13-01-2021]

integrity. The aircraft can be split into several parts which are shown in [Figure 15.1](#). During the assembly procedure, all of these components are bolted to each other. Below each of these parts is mentioned and the split lines are indicated:

- **Along the wings' span:** These lines are shown with the green color in [Figure 15.1](#). These lines are located on the leading edge spar. The front section of this cut includes the leading edge structure as well as the landing gear wheel well. The rear section includes the rest of the wing structure as well as the hard points and actuator systems for the main landing gear.
- **Wing connections inside the fuselage:** The white line in [Figure 15.1](#) shows the split line of the wing along the wing root.
- **Engine pylons:** The orange lines in [Figure 15.1](#) indicate the line of separation of the engine assembly.
- **Horizontal stabilizers:** These lines are shown with the yellow color on [Figure 15.1](#).
- **Vertical stabilizers:** The empennage itself can be split along the blue lines as indicated in [Figure 15.1](#). This allows to remove the vertical stabilizers.

According to the group's estimation, it would take 2 containers with dimensions mentioned above to fit in all of the aircraft's components. In total, 4 half wings can be stored in one container, when placing them diagonally. The other container includes the fuselage, engines, horizontal and vertical stabilizers. Thus, 2 aircraft can be shipped in 3 containers.

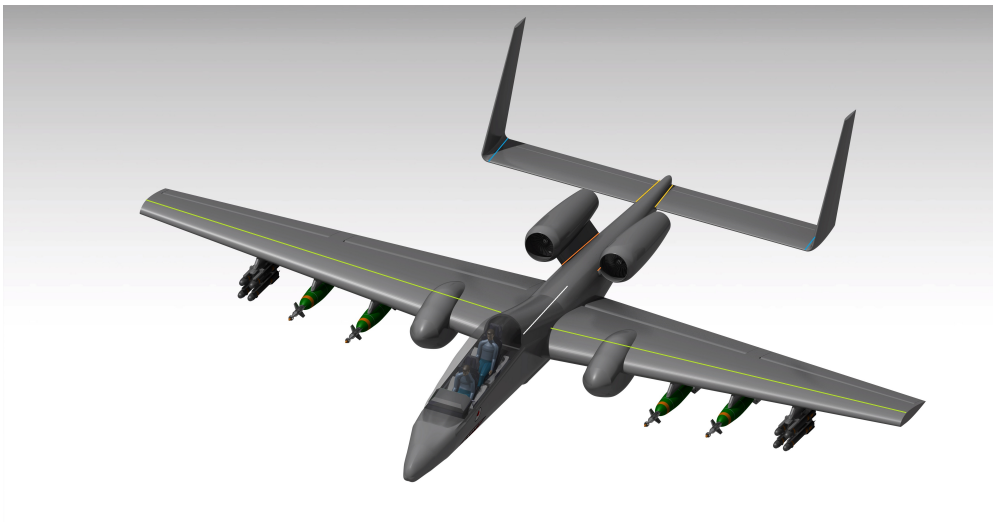


Figure 15.1: Top view of the aircraft with assembly and dismantling lines

16 Production Quantity and Cost Analysis

This chapter focuses on first finding the number of the aircraft to be made. Next based on this value and cost estimating methods, the costs of different design stages are found. These values add up together to estimate the unit cost of the aircraft. After that the operational, maintenance and transportation costs of the aircraft are found. At last it needs to be mentioned that this section also includes the cost distribution per subsystem.

16.1. Production Quantity

To estimate the production quantity, first the reference aircraft from [Table 3.1](#) that are still in service were selected. These aircraft were initially the A-10 Thunderbolt, Eurofighter, F-16, F-4 Phantom II and F-35A. However, after initial analysis, the Eurofighter was decided to be neglected as its unit price is drastically higher with respect to other aircraft¹.

It is found that out of 716 produced A-10s, 282 of them are still active today². These aircraft were manufactured at least 37 year ago and have received updates since. The USA, in which the A-10 is manufactured, has decided not to sell the A-10 to other countries, despite the success of the A-10. It was found that the US is planning to keep the A-10 in-service until late 2030, and is already looking for a replacement³. As a rough estimate for the production quantity, it considered to sell 100 aircraft to the U.S. airforce as a replacement for the A-10s in the current fleet.

The next reference aircraft is F-16, for which out of 4 600 aircraft, around 3 000 units are still active today⁴. As is presented in [section 16.2](#) the unit selling price of group's aircraft will be significantly lower than F-16. Additionally, the upgrade costs of F-16 is remarkably high; for instance the Greek air force has signed a contract of \$1.5 billion to upgrade 84 of its F-16 to the latest F-16V edition, which is the most advanced version⁵. This means an upgrade per F-16 aircraft is worth almost 18 million which is even more expensive than the fly away cost of the A-20, which is calculated in [section 16.2](#).

This budget logic not only applies to the F-16, but it is also true for F-35. For instance, UK has recently halved the number of its purchased F-35s⁶. Next to economical factors, political factors can also influence the customer's behavior as mentioned in [chapter 3](#). For instance, the Venezuelan air force is equipped with F-16s. However, due to current political tensions between Venezuela and the USA, maintenance of these aircraft will be challenging⁷. Because of the above reasoning, the group is

¹<https://www.reuters.com/article/us-aerospace-belgium/belgium-picks-lockheeds-f-35-over-eurofighter-on-price-idUSKCN1MZ1S0>, conducted on [04-01-2021]

²<https://www.airforcetimes.com/news/your-air-force/2019/08/13/a-10-re-winging-completed-will-keep-warhog-in-the-air-until-late-2030s/>, conducted on [04-01-2021]

³<https://www.defensenews.com/air/2019/10/25/air-force-officially-buying-light-attack-planes/>, conducted on [04-01-2021]

⁴<https://news.lockheedmartin.com/2018-06-25-Lockheed-Martin-Awarded-Contract-to-Build-F-16-Block-70-Aircraft-for-Bahrain>, conducted on [04-01-2021]

⁵<https://www.dw.com/en/lockheed-martin-to-upgrade-greeces-f-16-fighter-jets/a-51815309>, conducted on [04-01-2021]

⁶<https://www.pesmedia.com/f-35-tempest-fighter-jet-08092020/>, conducted on [04-01-2021]

⁷<https://www.state.gov/the-united-states-sanctions-maduro-aligned-officials-of-venezuelas-military-counterintelligence-agency>, conducted on [04-01-2021]

confident that it can replace at least 400 F-16s and even F-35 orders.

The next reference aircraft is the F-4 Phantom II. Looking at current countries with active F-4 phantoms in their air force⁸, it is estimated that there are 146 units of this aircraft are still in service. The manufacturing of the F-4 has stopped 40 years ago, so most customers are looking for a replacement of this aircraft. Currently, the F-15 Strike Eagle is known to be a replacement for F-4s. However, given the unit cost of F-15 Strike Eagle is at least \$80 million⁹, a replacement of 90 units was considered.

Next to replacing the above mentioned aircraft, it is also possible to sell the aircraft to new customers, as the light attack aircraft is able to take off and land from austere airfields with limited length. An example of potential new customers are countries that are economically weaker such as African, South American or Eastern European countries. A prediction of 200 aircraft to be sold to such customers is made. Adding all these target quantities up, that leads to an expected value of 830 aircraft to be sold to the fighter aircraft market.

16.2. Cost Analysis

This section describes the cost analysis method used to determine the price of the aircraft. Firstly, the costs of several engineering and design stages are estimated. Secondly, the break-even point and return on investment are discussed. Afterwards, the flight cost per hour is analyzed. Finally, the subsystems of aircraft are compared with each other in terms of cost.

To estimate the cost of the production of the aircraft, the method presented by Gudmundsson's was performed [30]. This method is based on the "Development And Production Costs of Aircraft", or DAPCA, method, specifically DAPCA-IV. . Furthermore, according to Raymer, the avionics for airliners cost about 5%-25% of the flyaway cost, depending on how sophisticated the system is [8]. Military avionics system are generally more advanced and the value for this aircraft is thus assumed to be 30%.

Since the values of DAPCA are from 1986, the costs should be adjusted to account for inflation. Gudmundsson already adjusted the values to 2012. However, since the designed aircraft will enter service in 2025, the values had to be adjusted to that year. Therefore, the Consumer Price Index, CPI, was used¹⁰. The average CPI growth over the period of 1982 to 2020 was calculated, and used to predict the CPI growth factor, which was approximately 1.39 for the period of 2012-2025.

In [Table 16.1](#) the outcome of the adjusted DAPCA-IV method is presented. The liability cost was estimated to be 15% of the production cost. Lastly a quantity discount factor, QDF, was included in the table, as also used in Gudmundsson [30]. A discount factor of 5% was assumed which resulted in the QDF for 830 unit being equal to 0.61. However, since this would be optimistic, the worst case scenario, where there would be no QDF, was considered.

It should be noted that the software is not taken into account for determining the cost estimation. This is due to the fact that the DAPCA-IV method is from 1986, which doesn't take into account the software development costs. As future recommendation,

⁸<https://nationalinterest.org/blog/buzz/its-hard-believe-f-4-phantom-still-flying-after-60-years-112186>, conducted on [04-01-2021]

⁹<https://www.airspacemag.com/military-aviation/shocking-resurrection-f-15-180974446/>, conducted on [04-01-2021]

¹⁰https://www.bls.gov/regions/mid-atlantic/data/consumerpriceindexhistorical_us_table.htm, conducted on [18-12-2020]

these values should also be included, in order to get a better understanding of the certification cost.

Table 16.1: Cost analysis as presented in the DAPCA-IV method

	Man-hours [h]	Rate [\$/hr]	Total cost [2025 US\$]	Cost per unit [2025 US\$]	
Engineering	2.8 million	90	740 million	890 thousand	
Development support			42 million	51 thousand	
Flight test operations			7.9 million	9.5 thousand	
Tooling	1.4 million	60	0.26 million	310 thousand	
Certification Cost			1.0 billion		
Manufacturing labour	10 million	50	1.5 billion	1.8 million	
Quality Control			210 million	250 thousand	
Materials/ Equipment			220 million	270 thousand	
Units Produced in 5 years				830	
Quantity discount factor				0.61	
				Without QDF	With QDF
Engines				2.9 million	1.8 million
Avionics				2.3 million	1.4 million
Liability cost				1.1 million	0.69 million
Total cost to produce				7.6 million	4.6 million
Min selling price				10 million	6.6 million

As can be seen in table [Table 16.1](#), a minimum selling price for the aircraft was calculated. The price was determined such that the break-even point is reached when all units produced in 5 years, are sold. From a business point of view, this induces a lot of risk and will not result in any profit. Therefore, it is useful to make an analysis of the break-even point and how it shifts with the increase of the selling price.

Table 16.2: Break-even point and ROI for different selling prices

Price per unit [mln 2025 US\$]	Break-even amount	ROI
9.96	830	0%
10.5	600	5%
11.0	470	10%
11.2	420	12.5%
11.5	380	15%

Finally a selling price had to be chosen. The selling price of the aircraft is \$10.96 million. With this selling price, the break-even point is at approximately 470 units. This covers risks involved with the market. For example, if the US government would not buy any to replace the A-10 fleet, the margin would still be big enough to make the sales profitable. Hence, even if the aircraft is performing worse than expected on the market, the break-even point will still be met. In case the full estimated volume gets sold, the profit would amount to \$830 million, which equals to a ROI of 10%.

Transportation by container was found to be a cheap method of transportation. It was found that transferring a container from New York to London will cost about \$2 500¹¹. This means that based on the dimensions of the containers which are mentioned in [Section 15.2](#) and given that two containers are required per aircraft, the transport cost of one aircraft would be \$5 000. On

¹¹<https://www.icontainers.com/>, conducted on [18-12-2020]

the other hand, the jet fuel of aerial refueling aircraft for the same distance is at least \$27 000¹². Given that affordability is an important factor in trade off and design of this aircraft, this cheap method of transfer gives an advantage to the product in terms of logistic cost.

An adapted DAPCA-IV method from Gudmundsson was used to estimate the maintenance cost [30]. The overhaul price of the engine was estimated to be 30% of the total cost of the engine. An estimated Time Between Overhauls, TBO, of 3 000 flight hours was assumed. For estimating the fuel cost, it was assumed that all of the fuel will be consumed during a flight. A typical flight is also assumed to equal 5.5 flight hours, with an average of 1 200 flight hours per year, which will meet requirement LAA-TIM-SER-1.2¹³. This means approximately 218 flights are performed per aircraft each year. Combined with the cost of JP-8 fuel, which was approximately \$0.78 per liter in 2020¹⁴, the fuel cost per year was calculated, as presented in Table 16.3. However, note that fuel prices fluctuate a lot, and that fuel prices on remote locations may drastically increase to up to \$100 per liter¹⁵. In comparison the Super Tucano costs \$1 000 per flight hour, an AT-6 roughly \$2 500 per flight hour, and the A-10 \$20 000 per flight hour¹⁶. This means the operational cost of this aircraft is relatively cheap.

Table 16.3: Operational and maintenance costs

Cost factor	Cost [2025 US\$]
Engine overhaul	880 thousand
Maintenance cost per year	43 thousand
Fuel cost per year	890 thousand
Total operational and maintenance cost per year	1.3 million
Total cost per flight hour	1100

Figure 16.1 represents the ratio of costs with respect to each subsystem of the aircraft. The source for the construction of this figure is a study that has gathered data and regression equations from several military aircraft [31]. Based on these data and equations, a model is made which produces the cost of each subsystem based on its weight.

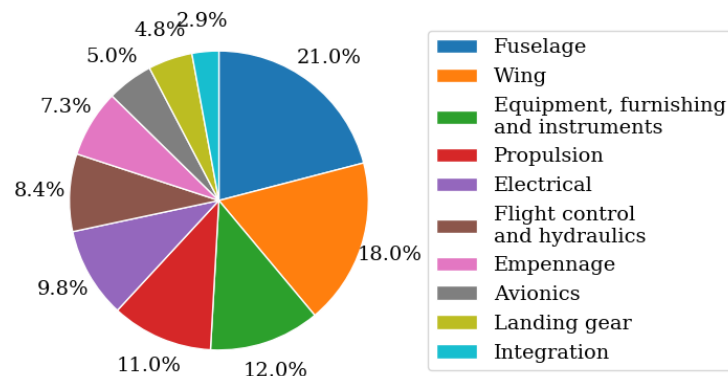


Figure 16.1: Cost breakdown per subsystem of the aircraft

¹²<https://thepointsguy.co.uk/guide/cost-of-fueling-an-airliner/>, conducted on [18-12-2020]

¹³LAA-TIM-SER-1.2: The aircraft shall have a service life of at least 15 000 flight hours over 25 years.

¹⁴https://www.dla.mil/Portals/104/Documents/Energy/Standard%20Prices/Petroleum%20Prices/E_2019Oct1PetroleumStandardPrices_190928.pdf?ver=2019-09-30-072433-663, conducted on [18-12-2020]

¹⁵<https://thehill.com/homenews/administration/63407-400gallon-gas-another-cost-of-war-in-afghanistan->, conducted on [18-12-2020]

¹⁶<https://www.csis.org/too-little-too-much-or-lot-little-air-force-oa-x-light-attack-program>, [conducted on 26-01-2021]

17 Next Design Steps

This chapter includes the layout for project design & development logic for the A-20 *Chimera* project. Project design & development logic represents the logical order of all major steps that should be done after this conceptual design stage.

17.1. Work Flow Diagram for future steps

Figure 17.1 represents the work flow diagram which illustrates the order of activities right after this conceptual stage. This figure is 3 levels deep. The most detail level is shown with the yellow colour. Yellow cells add up together to form blue cells. Furthermore blue cells form together to make red cells.

As can be seen from the step 6.1, the aircraft will be ready to enter service in 2025, hereby satisfying requirement LAA-TIM-SER-1.1¹.

¹LAA-TIM-SER-1.1: The aircraft shall enter service in 2025.

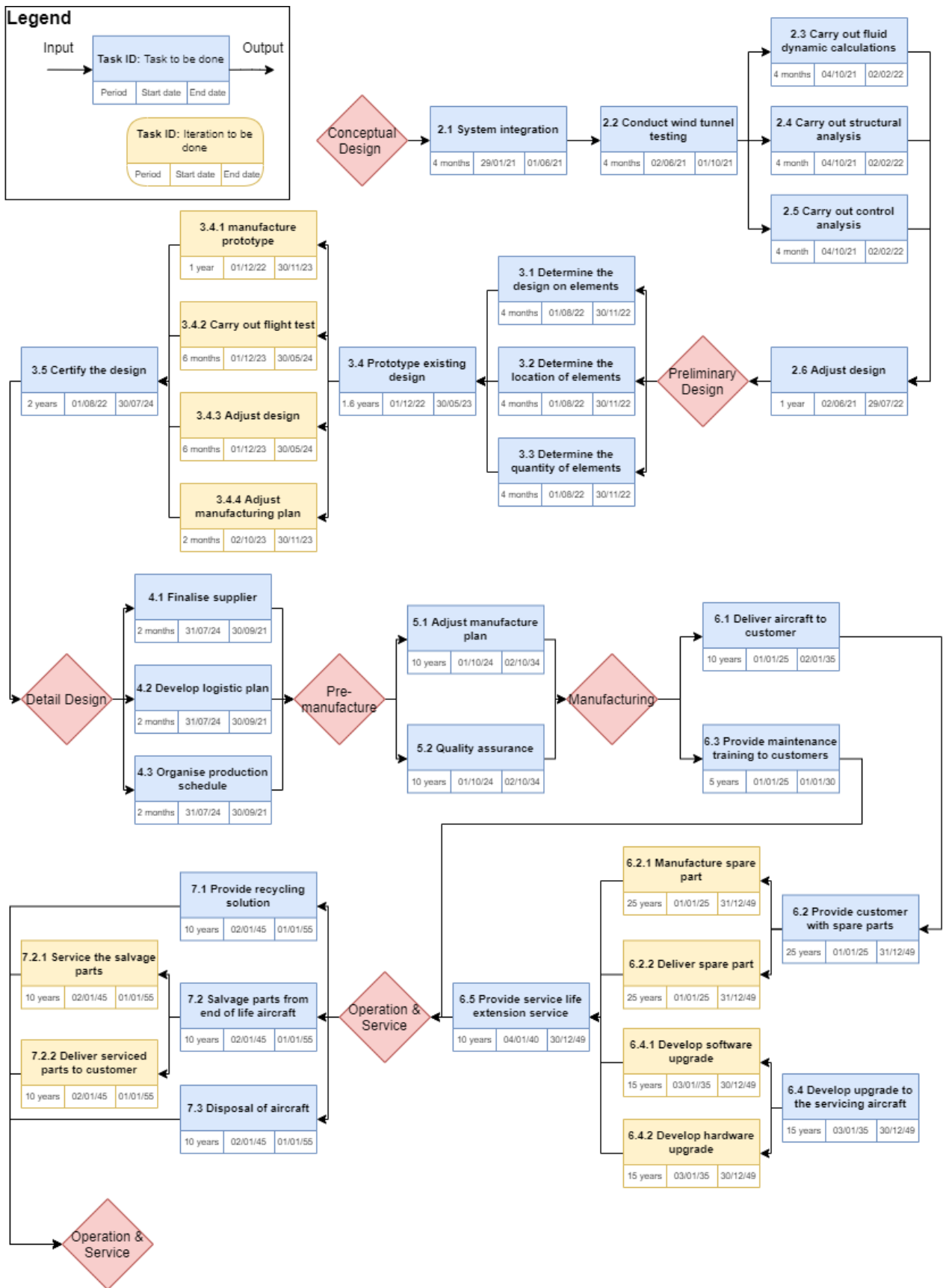


Figure 17.1: Work flow diagram of future development

18 Compliance to User Requirements & Future

Recommendations

In this chapter an overview is presented of the user requirements and if they have been complied with in [section 18.1](#). Furthermore, the future recommendations are described in [section 18.2](#).

18.1. User Requirements Compliance Table

The user, or AIAA, has setup several requirements that impact the design. These requirements are listed below in [Table 18.1](#) and ticked off whether the requirements are met. In the table also the subsection is given where the requirement is discussed.

Table 18.1: Compliance check of list of user requirements for the Light Attack Aircraft given by the AIAA

Requirement ID	Description	Method of compliance	Compliance check
Payload			
LAA-PAY-WTH-1.1	The aircraft shall be able to carry 3 000 lbs of armament.	section 2.6 , section 5.1	✓
Performance			
LAA-PER-SER-1.1	The aircraft shall have a service ceiling of at least 30 000 ft.	section 5.1 , subsection 14.3.2	✓
LAA-PER-FEM-1.1	The aircraft shall have a ferry range of at least 900 nmi at a cruise altitude of at least 18 000 ft.	subsection 7.2.1 , subsection 14.1.1	✓
LAA-PER-DSM-1.1	The aircraft shall be able to take off over a 50 ft obstacle within a distance of maximum 4 000 ft at a density altitude of up to 6 000 ft on runways with CBR 5.	section 9.2 , section 10.2	✓
LAA-PER-DSM-2.1	The aircraft shall have a cruise altitude of at least 10 000 ft.	subsection 7.2.1	✓
LAA-PER-DSM-2.2	The initial cruise of 100 nmi and following descent to 3 000 ft shall take no longer than 20 minutes.	subsection 14.1.2	✓
LAA-PER-DSM-3.1	After the initial cruise phase, the aircraft shall be able to loiter for 4 hours at an altitude of 3 000 ft, without dropping stores.	section 11.1	✓
LAA-PER-DSM-4.1	After a loiter period of 4 hours at an altitude of 3000 ft without dropping stores, the aircraft shall be able to climb to cruise altitude with following cruise of 100 nmi.	subsection 14.1.2	✓
LAA-PER-DSM-5.1	The aircraft shall be able to land over a 50 ft obstacle within a distance of maximum 4 000 ft at a density altitude of up to 6 000 ft on runways with CBR 5.	section 10.2	✓
LAA-PER-DSM-5.2	After landing, the aircraft shall have enough reserves for a climb to 3 000 ft with following loiter period of 45 minutes.	section 11.1	✓
Power and Propulsion			
LAA-PAP-DSM-1.1	Warm-up shall take no longer than 5 minutes.	section 11.3	✓
LAA-PAP-DSM-1.2	Shutdown shall take no longer than 5 minutes.	section 11.3	✓
Time			
LAA-TIM-SER-1.1	The aircraft shall enter service in 2025.	section 17.1	✓

Table 18.1: Compliance check of list of user requirements for the Light Attack Aircraft given by the AIAA

Requirement ID	Description	Method of compliance	Compliance check
LAA-TIM-SER-1.2	The aircraft shall have a service life of at least 15 000 flight hours over 25 years.	section 16.2	✓
Technology			
LAA-TEC-RDY-1.1	Critical technologies shall be above TRL 8 in 2020.	No untested/unproven systems were selected during the design process	✓
Structures			
LAA-STR-WPN-1.1	The aircraft shall feature a board canon to engage ground targets.	section 2.6	✓
LAA-STR-CRW-1.1	The aircraft shall be able to fit two crew members.	section 6.2	✓
LAA-SUR-SAF-1.1	The aircraft shall be fitted with two zero-zero ejection seats.	section 6.2	✓

18.2. Future Recommendations

In this section future recommendations will be given for the detailed design stages.

In the additional subsystems design, schematic diagrams were made for the fuel, hydraulic and electrical systems. These can be worked out in further detail in a later design stage. Next to this, the environmental control system was not designed, only a concept was thought of. In future design stages this system can be designed in more detail.

This also ties into the fuselage design. During future design stages, the subsystems should be integrated into the fuselage.

As stated in [chapter 12](#) it is recommended that the C_{D_0} of the flapped configuration should be checked for errors, as it seems that the trend line is off. It was also recommended that the drag analysis could be verified with a CFD analysis.

In order to make sure the aircraft has level 1 handling quality for all eigenmotions in all flight phases, a more complete PID controller has to be designed for the aperiodic spiral motion. The next step would be to add a sensor and to update the transfer functions.

To further improve the cost analysis, an estimation of the software development and certification cost should be included. This would give a more accurate approximation of the actual cost of the aircraft. Furthermore, more components can be included in the estimation of the maintenance cost for a more detailed analysis of that.

19 Conclusion

The goal of this report was to present the steps that have been taken in the conceptual design phase of a light attack aircraft which can operate from short austere fields. The aircraft was named the A-20 *Chimera*.

A concept was worked out with an iterative Class II component weight estimation, which was implemented in the existing Class I sizing. Different subsystems, mainly the fuselage, wings, empennage, propulsion unit and landing gear, were designed separately. For each subsystem it was concluded that it would comply with the set requirements. Additional subsystems, such as the fuel, hydraulic, and electrical system were designed with redundancy in mind, which makes the aircraft safer to operate in CAS missions.

From the design stages, it was concluded that the aircraft can take off and land on austere fields and arrive at the mission location at short notice.

In addition, the wing span provides enough space for six hardpoints next to two guns integrated within the fuselage, hence it was concluded that the A-20 is flexible when it comes to payload choice.

A challenge regarding the logistic plan was to come up with a way to transport the aircraft to mission location in a safe, efficient and cost effective way. It was concluded that the A-20 will be transported by delivery via a standard sized container, as this is the most cost effective way of transportation. Transport by other aircraft will only be used in the event of quick deployment.

From the stability and control analysis, it was concluded that the aircraft is statically stable. However, it is not fully dynamically stable. The phugoid motion and the aperiodic spiral motion in landing configuration did not comply with the desired level 1 handling qualities. Therefore, an auto-throttle and a PID controller had to be designed in order to counteract the phugoid motion and spiral motion, respectively.

Performance diagrams were made in order to evaluate the flight configurations and their respective performance, from the diagrams it was concluded that each flight configuration was within their respective positive specific excess power range. Next to this, the turn rate performance was analysed.

From the market and cost analysis a production quantity, and cost analysis was carried out. When producing 830 aircraft, a unit selling price of \$11 million results in a break-even point at 470 units. In comparison to competitive aircraft the A-20 *Chimera* was found to be relatively cheap.

In general, it was concluded that the A-20 *Chimera* is suitable to carry out missions from short, front-line, austere fields at short notice, while being affordable as the aircraft was in compliance with all set requirements.

References

- [1] TRADOC, *TRADOC Bulletin 3. Soviet RPG-7 Anti-Tank Grenade Launcher Capabilities and Countermeasures*, TRADOC, 1967.
- [2] AIAA, *AIAA 2021 Undergrad Team Aircraft Design RFP*, 2020.
- [3] Department of Defense (USA), *Joint Service Specification Guide: Air Vehicle*, Department of Defense, April 2004.
- [4] Intelligence, S. D., “The Global Military Fixed-Wing Aircraft Market 2015-2025,” 2015.
- [5] Smith, S., “The Global Military Fixed-Wing Aircraft Market 2015-2025,” January 2015.
- [6] FAA, *Airplane Flying Handbook*, U.S. Department of transport, 2016.
- [7] Roskam, J., *Airplane Design Part 1: Preliminary Sizing of Airplanes*, Design, Analysis and Research Corporation, 1985.
- [8] Raymer, D., *Aircraft Design: A Conceptual Approach*, AIAA, 2004.
- [9] Roskam, J., *Airplane Design Part 5: Component Weight Estimation*, Design, Analysis and Research Corporation, 1985.
- [10] Roskam, J., *Airplane Design Part 3: Layout Design of Cockpit, Fuselage, Wing and Empennage: Cutaways and Inboard Profiles*, Design, Analysis and Research Corporation, 1985.
- [11] Marx, J., Portanova, M., and Rabiei, A., “Performance of Composite Metal Foam Armors against Various Threat Sizes,” Tech. rep., North Carolina State University, November 2020.
- [12] Spick, M., *Great Book of Modern Warplanes*, Zenith Press, September 2000.
- [13] Sadraey, M. H., *Aircraft Design: A System Engineering Approach*, John Wiley & Sons, Ltd. publication, 2013.
- [14] Torenbeek, E., *Synthesis of Subsonic Airplane Design*, Delft University Press, 1982.
- [15] Bock, G., Gerlach, C., Beauvais, H., Sarnes, W., and Mörchen, W., “Operations from Unprepared & Semi-prepared Airfield,” Tech. rep., North Atlantic Treaty Organization Advisory Group for Aeronautical Research and Development, September 1960.
- [16] Gavel, H., “On Aircraft Fuel Systems, Conceptual Design and Modeling,” Tech. rep., Linköpings Universitet, 2007.
- [17] Lars P. Lauritzsen, J. P., “Pressure Breathing in Fighter Aircraft for g-Accelerations and Loss of Cabin Pressurization at Altitude A Brief Review,” *Canadian Journal of Anesthesia*, 2003.

- [18] J. Shetty, C.P. Lawson, A. S., "Simulation for Temperature Control of a Military Aircraft Cockpit to Avoid Pilots Thermal Stress," *CEAS Aeronaut Journal*, Vol. 6, 2015, pp. 319–333.
- [19] Reddy, P. K. P., "Environmental Control System of Military Aircraft, LCA," *International Journal of Engineering Research and Technology*, 2013.
- [20] Segvic, M., Krajcek, K., and Ivanjko, E., "Technologies for Distributed Flight Control Systems: A Review," *Faculty of Transport and Traffic Sciences*, 2015.
- [21] Department of Defense (USA), "MIL-STD-469B: Interface Standard for Radar Engineering Interface Requirements, Electromagnetic Compatibility," Tech. rep., 1996.
- [22] Roskam, J., *Airplane Design Part 6: Preliminary Calculation of Aerodynamic, Thrust and Power Characteristics*, Design, Analysis and Research Corporation, 1987.
- [23] in 't Veldt, A., "AE3212-I: Aerospace Flight Dynamics Reader," February 2019.
- [24] Department of Defense (USA), "MIL-F-8785C: Military Specification Flying Qualities of Piloted Airplanes," Tech. rep., November 1980.
- [25] Handa Xi, J. S., "Effects of Actuator Dynamics on Stabilization of High-Speed Planing Vessels with Controllable Transom Flaps," Tech. rep., University of Michigan, 2005.
- [26] Department of Defense (USA), "MIL-A-8861B: Military Specification Airplane Strength and Rigidity Flight Loads," Tech. rep., 1986.
- [27] Department of Defense (USA), "MIL-A-8860B: Military Specification Airplane Strength and Rigidity General Specification," Tech. rep., 1987.
- [28] Anderson, J. D., *Introduction to Flight*, McGraw-Hill Education, 8th ed., 2016.
- [29] Ruijgrok, G., *Elements of Airplane Performance*, Delft Academic Press (VSSD), 2nd ed., 2013.
- [30] Gudmundsson, S., *General Aviation Aircraft Design*, Butterworth-Heinemann, 2013.
- [31] J.L.Brikler and Large, J., "A Method for Estimating Cost of the Aircraft Structural Modification," *Journal of Cleaner Production*, 1981.
- [32] Krakkers, A., "Parametric Fuselage Design Integration of Mechanics and Acoustic & Thermal Insulation," Tech. rep., TU Delft, September 2009.
- [33] Swedberg, S. and Svalstedt, M., "Commercial Aircraft Wing Structure," Tech. rep., Examenarbete Inom Technology, Grundniva, 2020.

-
- [34] Kyungtae Kim, Y. C. J., "Adhesion Enhancement and Damage Protection for Carbon Fiber-Reinforced Polymer (CFRP) Composites via Silica Particle Coating," *Composites: Applied Science and Manufacturing*, 2018.
- [35] C.T. McCarthy, M. M., "Design and Failure Analysis of Composite Bolted Joints for Aerospace Composites," Tech. rep., Woodhead Publishing Series in Composites Science and Engineering, 2020.
- [36] Mohammad R.M. Jamir, Mohammad S.A. Majid, M. S. M., "Natural Lightweight Hybrid Composites for Aircraft Structural Application," Tech. rep., University Malaysia, 2020.
- [37] Gudmundsson, S., "Aircraft Structural Layout," *Applied Methods and Procedures*, 2014.

Appendix A: Drag Analysis and Dynamic Stability

Table 1: Input values for drag analysis.

Wing			Fuselage			Empenage			Nacelle		
S	49.0	[m ²]	S_{wet}	20.1	[m ²]	S_{wet_v}	5.8	[m ²]	N_l	2.8	[m]
$\Lambda_{0.25c}$	0	[rad]	l_f	15.0	[m]	S_{wet_h}	22.3	[m ²]	N_d	0.76	[m]
MAC	2.81	[m]	d_f	1.28	[m]	t/c	0.1	[-]	$S_{wet_{nac}}$	7.0	[m ²]
A	7	[-]	S_{fus}	2	[m ²]	MAC_v	1.04	[m]	S_{nac}	2.79	[m ²]
λ	0.4	[-]	$S_{b_{fus}}$	0.134	[m ²]	MAC_h	1.34	[m]	$S_{nac_{base}}$	0.80	[m ²]
e	0.84	[-]	$S_{fus_{plf}}$	13.316	[m ²]						
t/c	0.18	[-]									
L'	1.2	[-]									
S_{wet}	97.0	[m ²]									
Stores			Flaps			Landing gear			Fairing		
# of stores	6	[-]	S_{wf}	27.25	[m ²]	<i>Main</i>			F_l	2.75	[m]
S_{store}	0.86	[m ²]	b_{fi}	1.2	[m]	S_{front}	1.87	[m ²]	F_d	0.82	[m]
$S_{b_{store}}$	0.19	[m ²]	b_{f0}	9.8	[m]	width	0.64	[m]	S_{wet}	8.37	[m ²]
$S_{wet_{store}}$	0.13	[m ²]	b	18.8	[m]	height	1.25	[m]	$S_{fearing}$	1	[m ²]
K	1.3	[-]	K	0.23	[-]	<i>Nose</i>			$S_{fearin_{base}}$	0.34	[m ²]
			K_{int}	0.3	[-]	S_{front}	0.28	[m ²]			
						height	1.99	[m]			
						width	4.13	[m]			

Table 2 represents the derivative results described in section 13.3. Secondly Table 3 represents the derivative results described in section 13.4.

Table 2: Longitudinal stability derivative data A20-Chimera

Longitudinal derivatives	Cruise	Landing	Loiter
C_{X_α}	-0.0881	-0.7826	-0.3293
C_{X_u}	-0.0944	-0.7139	-0.4156
C_{Z_α}	-5.5977	-4.2101	-5.3566
$C_{Z_{\dot{\alpha}}}$	2.1398	2.6279	2.4657
C_{Z_q}	-12.3350	-9.8499	-11.7716
C_{Z_u}	-0.0875	-0.0443	-0.0398
C_{m_α}	-0.8945	-0.6992	-0.8560
$C_{m_{\dot{\alpha}}}$	-4.7902	-5.7146	-5.5197
C_{m_q}	-7.1895	-7.9098	-8.633
C_{m_u}	0.0044	0.0077	0.0063

Table 3: Lateral stability derivative data A20-Chimera

Lateral derivatives	Cruise	Landing	Loiter
C_{Y_β}	-0.4376	-0.4270	-0.4376
C_{l_β}	-0.0825	-0.0723	-0.0864
C_{l_p}	-0.4987	-0.5129	-0.4943
C_{l_r}	0.2202	1.7366	0.7355
C_{n_β}	0.1216	0.1310	0.1234
C_{n_p}	0.0000	-0.3365	0.0000
C_{n_r}	-0.1736	-0.2156	-0.1801